ACTIVITY-DEPENDENT PHOSPHORYLATION OF DYNAMIN 1 AT SERINE-857 IN MOUSE HIPPOCAMPUS

--Implications for Learning and Memory

by

WEN XIE

A dissertation submitted to the Graduate Faculty in Biology

in partial fulfillment of the requirements for the degree of

Doctor of Philosophy

The City University of New York

2007

UMI Number: 3284412

UMI Microform 3284412

ProQuest Information and Learning Company
300 North Zeeb Road
P.O. Box 1346
Ann Arbor, MI 48106-1346

This manuscript has been read and accepted for the Graduate Faculty in Biology in satisfaction of the dissertation requirements for the degree of Doctor of Philosophy.

Chair of Examining Committee

Dr. Andrzej Wieraszko, College of Staten Island

Executive Officer

Dr. Richard L. Chappell

Dr. Abdeslem El-Idrissi, College of Staten Island

Dr. Yu-Wen Hwang, Institute for Basic Research

Dr. David L. Miller, Institute for Basic Research

Dr. Ying-Ju Sung, Columbia University

Supervisory Committee

THE CITY UNIVERSITY OF NEW YORK

Abstract

ACTIVITY-DEPENDENT PHOSPHORYLATION OF DYNAMIN 1 AT SERINE-857 IN MOUSE HIPPOCAMPUS

--Implications for Learning and Memory

by

Wen Xie

Advisor: Professor Andrzej Wieraszko

Dynamin 1 (Dyn1) is a brain-enriched large GTPase which participates in endocytosis, a process required for synaptic vesicle recycling and receptor internalization. Dyn1 is a phospho-protein whose level of phosphorylation is dependent on cell membrane potentials. Thus, the function of Dyn1 phosphorylation in synaptic transmission has been proposed and studied. Dyn1 is primarily phosphorylated at Serine-857 (S857) by minibrain / dual specificity tyrosine phosphorylation regulated kinase 1A (Mnb/Dyrk1A), which is linked to mental retardation of Down syndrome (DS). Phosphorylation at S857 regulates the interactions of Dyn1 with many endocytic accessory proteins *in vitro*. I chose the system of neuronal transmission in the Schaffer collateral / commissural - CA1 pathway from mouse hippocampus to investigate the regulation of Dyn1 phosphorylation at S857 *in vivo*. I found that the phosphorylation / dephosphorylation of Dyn1 was a dynamic physiological event that correlated with neuronal activity. Dyn1 was highly phosphorylated in nonstimulated slices, while the level of phosphorylation changed in response to different types of

electrical stimulation. The dephosphorylation was Ca^{2+}/calcineurin dependent and was mediated by AMPA/kainate receptors. An immunohistochemical study revealed that the distribution pattern of phosphorylated Dyn1 was also dependent on neuronal activity. In addition, as the primary kinase phosphorylating Dyn1 at S857, Mnb/Dyrk1A was also activated by neuronal activity. Together, these studies demonstrate that the phosphorylation of Dyn1 at S857 by Mnb/Dyrk1A is dynamically regulated by synaptic connections in mouse hippocampus.

To explore the involvement of Mnb/Dyrk1A in the learning and memory deficits of DS, a potential Mnb/Dyrk1A inhibitor, (-)-Epigallocatechin-3-Gallate (EGCG), was evaluated for its ability to alter neuronal plasticity in mouse hippocampus. EGCG had a promoting effect on LTP induction in wild-type mouse. Most strikingly, EGCG restored the impaired LTP induction in Ts65Dn mouse, the most studied mouse model for DS. Ts65Dn mouse over-expresses a group of genes that are syntenic to those in human chromosome 21 including the gene of Mnb/Dyrk1A. Although the mechanism(s) underlying the effect are still missing, the study not only implicates Mnb/Dyrk1A in DS, but also demonstrates a possible pharmacological intervention for DS.

To Dad, Mom and Yong

Acknowledgements

First of all, I wish to express deep appreciation to two co-mentors: Dr. Andrzej Wieraszko and Dr. Yu-Wen Hwang, who brought me to this exciting project and helped me all the way along, for their inspirations and scientific wisdoms.

I would like to thank Ph.D. program in Biology at Graduate Center of the City University of New York and IBR/CSI Center for Developmental Neuroscience for moral and financial support. This project was supported by an OMRDD Fellowship from IBR/CSI CDN.

This work could not be brought to completion without numerous wonderful people. I would like to thank Mo-Chou Chen-Hwang for teaching me everything from the beginning; Dr. Adayev Tatyana for sharing her experience with me; Dr. Ahmed Zaghloul for his generous help; Dr. Ekkehart Trenkner who brought me to the program in the first place; Ms. Diane R. Cocozza and Ms. Joan A. Reid for their assistance and patience; Dr. Robert L. Freedland for his support to students; Dr. Noriko Murakami for her help; Dr. Robert B. Denman for his critical comments; all the members of supervisory committee for their guidance.

Finally, I want to thank once again my immediate family, my parents and husband Yong. They are always by my side whenever I need them. I would like to share this joyous moment with them.

Table of Contents

List of Tables and Figures

Abbreviations

AMPA	alpha-amino-3-hydroxy-5-methyl-4-isoxazolepropionic acid
AMPAR	AMPA receptor
APV	D-2-Amino-5-phosphonopentanoic acid
CA	cornu ammonis
CaMKII	calcium/calmodulin dependent kinase II
Cdk5	cyclin-dependent kinase 5
CICR	calcium induced calcium release
CME	clathrin mediated endocytosis
CNQX	6-cyano-7-nitroquinoxaline-2,3-dione
CRIS	calcium release from intracellular storage
DG	Dentate Gyrus
DN	dominant negative
DS	Down syndrome
DSCR	Down syndrome critical region
DSCR1	Down syndrome critical region 1
Dyn1	dynamin 1
Dyn1xa	Dyn1 1aa and 1ba isoforms
EC	Entorhinal Cortex
EGCG	(-)-Epigallocatechin-3-Gallate
ERK	extracellular signal-regulated kinase
ERK1/2	T202/Y204 ERK

GABA	gamma-aminobutyric acid
GED	GTPase effector domain
GluR	glutamate receptor
GPCRs	G-protein coupled receptors
Grb 2	growth factor receptor-bound protein 2
GTPase	guanosine triphosphatase
HFS	high frequency stimulation
HSA21	human chromosome 21
IP	immuno-precipitation
KAR	kainate receptor
KYA	kynurenic acid, 6,7-dinitroquinoxaline-2,3-dione
LFS	low frequency stimulation
LTP	long-term potentiation;
MAPK	mitogen-activated protein kinase
MAP-2	microtubule-associated protein 2
MEK	a.k.a. MAPKK, MAP kinase
mGluR	metabotropic glutamate receptor
MMU 16	mouse chromosome 16
Mnb/Dyrk1A	minibrain / dual specificity tyrosine phosphorylation regulated kinase 1A
NFAT	nuclear factor of activated T-cells
NGF	nerve growth factor
NMDA	N-methyl-D-aspartate

NMDAR	NMDA receptor
pCaMKII	phosphorylation of CaMKII at T286
pERK1/2	phosphorylation of ERK at T202/Y204
PH	pleckstrin-homology
Pi	free phosphate
PKA	cAMP-dependent protein kinase
PKC	protein kinase C
PP	perforant path
PPI	paired-pulse inhibition
PRD	proline-rich domain
pS857	phosphorylated S857
S857	serine-857
S795	serine-795
Sb	subiculum
SH3	Src homology 3
SO	stratum oriens
SP	stratum pyramidale
SR	stratum radiatum
T202	threonine-202
T286	threonine-286
VGCC	Voltage-gated calcium channel
Y204	tyrosine-204

CHAPTER 1

Introduction

Dynamin

Dynamin belongs to a large (about 100 kDa) GTPase family which participates in the endocytic pathways of eukaryotic cells (Praefcke and McMahon, 2004). Endocytosis, a process allowing extracellular materials to enter the cell, involves the invagination and pinching-off of pieces of the plasma membrane (Conner and Schmid, 2003). A type of endocytosis named clathrin-mediated endocytosis (CME) is initiated by the localized formation of clathrin coated pits on the cytoplamic side of the plasma membrane. The pits are internalized and then released into the cytoplasm by the fission of budding coated vesicles from the membrane (**Figure 1.1**). Endocytosis is crucial for intercellular communications. In the central nervous system, specifically, CME is required for the efficient recycling of synaptic vesicle membrane proteins after neurotransmission (Ryan, 2006) and modulating the efficacy of neurotransmission by controlling the trafficking of ion channels or transmitter receptors (Malinow and Malenka, 2002). CME is assisted by numerous accessory proteins (Brodin et al., 2000).

Three different dynamin genes exist in mammals. Dynamin 1 (Dyn1) is the dominant species in the mammalian brain; dynamin 2 is ubiquitous (Sontag et al.,

1994); and dynamin 3 is mostly present in testis (Nakata et al., 1993), but is also expressed in heart, brain and lung. Multiple isoforms of each dynamin gene have been found. Dyn1, for example, contains two alternatively spliced sites; one is in the middle of the protein (two splicing forms: a and b) and the other is at the C-terminus (four splicing forms: a, b, c, and d). Together, they give 8 splicing isoforms (Cao et al., 1998) (**Figure 1.2**). There are five identified domains in dynamin starting from its N-terminus. There is a GTPase domain, a middle domain, a PH (pleckstrin-homology) domain, a GED (GTPase effector domain) and a PRD (proline-rich domain) (**Figure 1.2**).

Dynamin-like family members can be found in many organelles across species (Praefcke and McMahon, 2004), indicating its fundamental role in cell function. In animal cells, in addition to clathrin-coated vesicles and caveolae at the plasma membrane, they are involved in the trans-Golgi network, endosomes, mitochondrial membrane, smooth endoplasmic reticulum, and in perixisomes. In plants, dynamin homologues are expressed in the cell-plate tubular network, plastids, and in chloroplasts.

Dyn1 was first purified from bovine brain before its recognition as part of the dynamin superfamily. Sequence analysis revealed that it is a homologue of the *Drosophila* shibire gene. A mutation in *shibire* results in the interruption of the synaptic vesicle endocytosis and neurotransmission, which causes paralysis (Schmid et al., 1998). The inhibition in endocytosis was also found in mammalian

cells when dominant-negative dynamin mutants were over-expressed (Conner and Schmid, 2003). These results suggest a role for Dyn1 in neurotransmission. During neurotransmission, exocytosis (neurotransmitter-filled synaptic vesicles fusing with the presynaptic membranes) and endocytosis must be well balanced to ensure the continuity of neurotransmission during the different phases of synaptic activity. In addition to its presynaptic function in synaptic vesicle recycling, Dyn1 also plays a role in the internalization of receptors (Carroll et al., 1999) and signal transduction (Kranenburg et al., 1999) postsynaptically.

Two models of Dyn1 function have been proposed: a mechanochemical enzyme or a regulatory protein (Song and Schmid, 2003). Under physiological conditions, Dyn1 spontanously self-assembles into rings or spirals around the neck of invaginated synaptic vesicles or pits in neuronal cells in the presence of GTP (Sever et al., 2000). In the mechanochemical model, it was postulated that GTP hydrolysis mediated by Dyn1's GTPase domain causes a force-generating conformational change, which leads directly to either constriction of the assembled structure or expansion of the helical pitch that pinches off the vesicles. On the other hand, Dyn1 may function as a classical GTPase with a regulatory role. In this model, Dyn1 recruits effectors to the coated pit, which in turn mediate coated vesicle formation. As the neck narrows and vesicle formation completes, Dyn1 triggers GTP hydrolysis to terminate its interaction with these effectors.

Dyn1 interacts with many proteins. The PRD of Dyn1, where up to one in every three amino acids is proline, binds to Src homology 3 (SH3) domains. SH3 domains can be found in many endocytic accessory proteins (such as amphiphysin, endophilin, syndapin, and intersectin), proteins associated with the cytoskeleton (such as actin binding protein1) and signal transduction related proteins (such as growth factor receptor-bound protein 2, Grb 2). The interactions with endocytic accessory proteins recruit Dyn1 to endocytic process on the plasma membrane. Amphiphysin I, for example, is the major Dyn1 binding partner in brain extracts (Grabs et al., 1997). Full-length amphiphysin I forms dimers *in vivo*. The dimers have a higher affinity for Dyn1 oligomers than does the monomeric isolated amphiphysin SH3 domain (Wigge et al., 1997). The dynamin-amphiphysin interaction stimulates Dyn1 GTPase activity (Yoshida and Takei, 2005). This interaction is inhibited by Dyn1 phosphorylation (Huang et al., 2004) and both proteins are dephosphorylated at the onset of exo/endocytosis (Cousin and Robinson, 2001).

Dyn1 belongs to a group of phospho-proteins whose state of phosphorylation depend on the cell membrane potential (Cousin and Robinson, 2001; Huang et al., 2004). This group also includes amphiphysin 1 and 2, synaptojanin, AP180, Epsin, Eps15 and AP2 (Cousin and Robinson, 2001). Dyn1 is phosphorylated in the resting state. Upon depolarization, it is rapidly dephosphorylated (in less than 2 s). Subsequently, the protein undergoes a slower rephosphorylation ($t_{1/2}$ ~40s) before it can respond to the next stimulation

(Robinson et al., 1987) (**Figure 1.3**). In cultured cells, such as PC12 cells, the dephosphorylation can be triggered by a high extracellular concentration of K^+ ion (Huang et al., 2004). Dephosphorylation of Dyn1 is calcium dependent and is mediated by calcineurin (Lai et al., 1999; Cousin and Robinson, 2001), a calcium-dependent phosphatase2B (Winder and Sweatt, 2001).

Additionally, Dyn1 has been shown to be phosphorylated on various sites by multiple kinases, such as minibrain / dual specificity tyrosine phosphorylation regulated kinase 1A (Mnb/Dyrk1A), Cyclin-dependent kinase 5 (Cdk5) and protein kinase C (PKC), in (**Table 1**).

Mnb/Dyrk1A primarily phosphorylates Dyn1 at serine-857 (S857) (Chen-Hwang et al., 2002). It is found to co-localize with Dyn1 in growing dendritic trees in chick embryo (Hammerle et al., 2003) and in differentiating hippocampal cell lines HN2-5 (unpublished data from Dr. Tatyana Adayev). The level of phosphorylation on this site changes with membrane potential in PC12 cells (Huang et al., 2004). This phosphorylation is the basis for regulating the interactions of Dyn1 with various endocytotic accessory proteins, such as amphiphysin 1, endophilin 1 and Grb 2 (Huang et al., 2004) (**Figure 1.4**). The interactions are essential for recruiting Dyn1 into the endocytotic complexes (McClure and Robinson, 1996). The S857 residue exists in only the 1aa and 1ba isoforms, thus the designation of Dyn1xa will be used to represent both isoforms throughout the text.

Sites	Kinase	Testing system	Functions
Serine 774 and 778	Cdk5 (cyclin-dependent kinase 5)	Synaptosomes	regulates the recruitment of syndapin I for synaptic vesicle endocytosis (Anggono et al., 2006)
Threonine 780	Cdk5	*in vitro*	blocks Dyn1 binding to amphiphysin (Tomizawa et al., 2003)
Serine 795	PKC (protein kinase C)	*in vitro*	prevents the association of Dyn1 with phospholipids (Powell et al., 2000)
	Mnb/Dyrk1A	*in vitro*	n/a
Serine 857	Mnb/Dyrk1A	PC12 cell (Huang et al., 2004) Rat brain extracts(Huang et al., 2004) Mouse hippocampus	regulates the binding of Dyn1 to amphiphysin 1 and Grb 2 (Huang et al., 2004)

Table 1. Dyn1 Phosphorylation sites. Phosphorylation sites in PRD domain. n/a: no function was found.

Cyclin-dependent kinase 5 (Cdk5) is another kinase which phosphorylates Dyn1. Cdk5 plays an inhibitory role in synaptic vesicle endocytosis, as it is evident that inhibition of Cdk5 enhances the electric stimulation–induced endocytosis in hippocampal neurons (Tomizawa et al., 2003). In synaptosomes, Dyn1 phosphorylation of serine-774 and serine-778 by Cdk5 (Tan et al., 2003) reduce Dyn1's binding to syndapin (Anggono et al., 2006) and endophilin (Anggono and Robinson, 2007). Furthermore, phosphorylation of threonine-780 by Cdk5 blocks Dyn1's binding to amphiphysin in a cell-free system (Tomizawa et al., 2003).

PKC also regulates dynamin-dependent endocytosis (Cousin et al., 2001). It phosphorylates Dyn1 at serine-795 (S795) *in vitro* and S795 phosphorylation abolishes Dyn1's binding to phospholipids (Powell et al., 2000). S795 is also a minor phosphorylation site of Mnb/Dyrk1A. In addition, Dyn1 can also be phosphorylated by extracellular signal-regulated kinase 2 (ERK2) *in vitro*, although the site has not been identified yet (Earnest et al., 1996). The phosphorylation weakens Dyn1's binding to microtubules and inhibits the GTPase activity of Dyn1.

Mnb/Dyrk1A and Down syndrome (DS)

DS is the most common cause of mental retardation. The incidence of DS is about 1 per 800-1000 live births (incidence, 2006). Besides cognitive impairment, patients with DS often suffer from characteristic physical features, congenital heart defects, high risk of leukemia, immune deficiencies, Alzheimer's disease, etc (Epstein, 1986; Epstein et al., 1991). DS is a genetic disorder caused by the presence of all or part of an extra chromosome 21 (HSA21) (Lejeune et al., 1959; Petersen et al., 1990). Its symptoms are generally thought to originate from a 1.5-fold increase in the dosage of genes within HSA21 (Epstein, 1986; Epstein et al., 1991). Based on the analysis of rare cases of partial trisomy 21, a segment around long arm (q22) of chromosome 21 has been designated as Down syndrome critical region (DSCR) (Shapiro, 1999). The Mnb/Dyrk1A gene is localized in the DSCR of HSA21 (Chen and Antonarakis, 1997). Mnb/Dyrk1A and many other genes located in DSCR are candidates for causing the neurobiological deficits associated with DS. A few HSA21 genes are listed in **Table 2**.

Mnb/Dyrk1A is the vertebrate orthologue of *Drosophila* minibrain kinase (Mnb), which is required for the proliferation of neuroblasts during post-embryonic neurogenesis (Tejedor et al., 1995). The name minibrain came from the fact that the Mnb mutation causes a reduction in brain size of adult flies. Similar to the

outcomes of Mnb mutation in Drosophila, mice with a single Mnb/Dyrk1A gene knock-out also display region-specific brain size reduction (Fotaki et al., 2002).

In addition to its role in embryonic neurogenesis, the expression of Mnb/Dyrk1A is persistent throughout adulthood in selected brain regions that are affected most severely in DS, including the entorhinal cortex, olfactory bulb, cerebellum and the hippocampus (Marti et al., 2003; Wegiel et al., 2004). The distribution of Mnb/Dyrk1A suggests it has an important role in the functioning of adult brains. The level of expression of Mnb/Dyrk1A is elevated in DS brains (Tassone et al., 1999; Dowjat et al., 2007). Several lines of transgenic mice expressing an extra copy of Mnb/Dyrk1A gene have been established to mimic the Mnb/Dyrk1A imbalance in DS. All lines show deficits in motor function, spatial memory and synaptic plasticity associated with learning (Branchi et al., 2004; Martinez de Lagran et al., 2004; Ahn et al., 2006). Those studies support the hypothesis that the abnormal expression of Mnb/Dyrk1A plays an important role in learning and memory impairments associated with DS.

Mnb/Dyrk1A is highly conserved among different organisms (Becker and Joost, 1999; Hämmerle et al., 2002; Raich et al., 2003). Besides a protein kinase domain, the protein contains a nuclear targeting signal sequence, a leucine zipper motif, and a 13-consecutive-histidyl residue sequence (Song et al., 1996). It can phosphorylate its own tyrosine residues (Kentrup et al., 1996). Toward exogenous substrates, however, Mnb/Dyrk1A phosphorylates exclusively at serine/threonine

residues (Becker and Joost, 1999). It prefers a site containing the sequence: Arginine(R)–Proline(P)-X-Serine(S) /Threonine(T)-Proline(P) (Himpel et al., 2000). The primary Mnb/Dyrk1A phosphorylation site of Dyn1, RPES(^{857})P, matches the preferred sequence.

On the cellular level, the endogenous Mnb/Dyrk1A can be found in both the nucleus and cytoplasm. Mnb/Dyrk1A has been shown to phosphorylate and regulate several transcription factors, such as CREB (Branchi et al., 2004), Gli 1 (Morita et al., 2006), and NFAT (Arron et al., 2006). In addition, it can phosphorylate some splicing factors indicating that it may be involved in the regulation of pre mRNA-splicing (de Graaf et al., 2006). On the other hand, cytoplasmic Mnb/Dyrk1A is mainly found in neuronal processes and synapses, implying a role for Mnb/Dyrk1A in synaptic functions (Hammerle et al., 2003). In fact, the majority of the kinase is found to associate with the cytoplasmic membrane fraction of the brains (unpublished observations), suggesting a membrane-associated functions such as recycling of the synaptic vesicles and the trafficking of neurotransmitter receptors.

The connection between Mnb/Dyrk1A and learning/memory in transgenic mice suggests that Mnb/Dyrk1A may play an important role in regulating synaptic activity. The identification of Dyn1xa as Mnb/Dyrk1A's substrate suggests a possible underlying mechanism.

Gene	Location	Functions in DS
APP (amyloid beta precursor protein)	21q21.3	Altered APP metabolism was found in Down syndrome (Kwak et al., 2006); High levels of Abeta1-42 peptide are associated with earlier onset of dementia in DS (Schupf and Sergievsky, 2002).
DSCR1 (Down syndrome critical region 1)	21q22.12	Interacts with calcineurin and inhibits calcineurin-dependent signaling pathways (Harris et al., 2005); Interacts with Mnb/Dyrk1A leading to reduced NFAT activity and many of the features of DS (Arron et al., 2006).
SIM2 (single-minded homolog 2 of Drosophila)	21q22.13	Encoded protein is a master regulator of fruit fly neurogenesis (Thomas et al., 1988); Expressed in human CNS development and in the region correspond to the altered structures in DS patients (Rachidi et al., 2005).
Mnb/Dyrk1A	21q22.13	Involved in signaling pathways regulating cell proliferation and brain development (Galceran et al., 2003; Kelly and Rahmani, 2005); Bridging between beta-amyloid production and tau phosphorylation in Alzheimer disease (Kimura et al., 2007); phosphorylation of amphiphysin I at serine-293 (Murakami et al., 2006) and Dyn1 at S857 (Chen-Hwang et al., 2002).
KCNJ6 (potassium inwardly-rectifying channel, subfamily J, member 6)	21q22.13 -q22.2	Expressed in the human cerebellum during development (Thiery et al., 2003).
KCNJ15 (potassium inwardly-rectifying channel, subfamily J, member 15)	21q22.2	Expressed in development in both mice and humans brain (Thiery et al., 2003); Interact with calcium-sensing receptor and decrease their currents (Huang et al., 2007).

Table 2. Genes in HSA 21. Some genes in long arm (q) of HSA 21 could be related to the mental retardation associated with DS.

Hippocampus

The hippocampus lies under the temporal lobe on each side of the mammalian brain. It forms a part of the limbic system and plays a part in memory and spatial navigation. In general, it has an essential role in forming declarative memory, which stores facts. Damage to the hippocampus usually results in profound difficulties in forming new memories, and also affects access to memories prior to the damage (Scoville and Milner, 1957).

The hippocampus consists of the dentate gyrus (DG), the cornu ammonis fields CA1-CA3 (and CA4, frequently called the hilus and considered part of the DG), and the subiculum (Sb) (**Figure 1.5**). Information flowing through the hippocampus proceeds from the DG to CA3 to CA1 to Sb, with additional input information at each stage and outputs at each of the two final stages (**Figure 1.5** and details below).

The perforant path is the major input to the hippocampus. The axons of the perforant path arise principally in layers II and III of the entorhinal cortex (EC), with minor contributions from the deeper layers IV and V. Axons from layers II/IV project to the granule cells of the DG and pyramidal cells of the CA3 region, while those from layers III/V project to the pyramidal cells of the CA1 and the Sb. The main output pathways of the hippocampus arise from the CA1 and Sb to the cingulum bundle and fimbria/fornix of EC.

There are two major pathways involving the two hippocampi from both hemispheres, the Mossy Fiber Pathway and the Schaffer Collateral/Commissural Pathway. The mossy fibers are the axons of DG granule cells. They extend from the dendate gyrus to CA3 pyramidal cells in the same hippocampus. On the other hand, the Schaffer Collateral/Commissural Pathway is derived from axons that project from the CA3 region to the CA1 region. The axons either come from CA3 neurons in the same hippocampus (Schaffer Collateral fibers) or from an equivalent structure in the opposite hemisphere (Commissural fibers). The hippocampus also receives a number of subcortical inputs, including the amygdala, the thalamus, the lateral preoptic and lateral hypothalamic areas, the raphe nuclei, etc. It is widely accepted that each of these regions has a unique functional role in the information processing of the hippocampus.

The Schaffer Collateral -CA1 pathway in mouse hippocampal slices is one of the most widely used model systems for studying neuronal functions. The efficiency of transmission in this pathway can be strengthened by a brief, high-frequency stimulation (Bliss and Lomo, 1973; Bliss and Collingridge, 1993) that mimics normal firing patterns (Douglas, 1977). This phenomenon was defined as Long-Term Potentiation (LTP). The long-lasting change in synaptic function is believed to be the cellular basis of learning and memory (Hebb, 1949; Alkon and Nelson, 1990; Kandel, 1997). Since the hippocampus is involved in the highest-order of memory, LTP in this structure is the most extensively characterized example of synaptic plasticity (Soderling and Derkach, 2000).

The neuronal activity in the Schaffer Collateral -CA1 pathway is mediated primarily by the activation of glutamate on two types of ionotropic receptors: AMPA (alpha-amino-3-hydroxy-5-methyl-4-isoxazolepropionic acid) and NMDA (N-methyl-D-aspartate) receptors. The AMPA receptor (AMPAR) opens in response to glutamate and mediates most of the rapid excitatory postsynaptic current (Isaac, 2003). The NMDA receptor (NMDAR) opens in response to glutamate only when the postsynaptic membrane is concomitantly depolarized and Mg^{2+} channel blocker is removed (Sheng and Kim, 2002). It is accepted that the triggering of LTP requires synaptic activation of postsynaptic NMDARs in Schaffer Collateral-CA1 pathway (Malenka and Nicoll, 1999).

Since the observation of LTP induction in brain slices, a debate whether LTP is expressed pre- or post-synaptically has ensued. The studies showing a decrease in the synaptic failure rate following the induction of LTP argue for an increase in the probability of transmitter release (Bekkers and Stevens, 1990). These presynaptic changes may include an increase in the number of vesicles released (Atwood and Karunanithi, 2002) or a change in the mode of glutamate release (presumably from kiss-and-run to full fusion) (Ryan, 2003). In pre-synaptic neurons, high rates of action potential firing during LTP induction require efficient machineries to recover a limited number of synaptic vesicles and replenish the vesicle pool in order to sustain the flow of information across the synapse over time. By studying the time course of synaptic vesicle fusion, three distinct types of pathways have been proposed (Aravanis et al., 2003; Gandhi and Stevens, 2003).

In the first, vesicles are recycled quickly (less than a second) in a dynamin-independent manner, which may represent pure membrane retrieval by simple fusion pore closure. It is referred as kiss-and-run. The second type of fusion is slower, with vesicles are recycled after 8-21 seconds. It is a dynamin-mediated but presumably non-clathrin-mediated retrieval pathway, referred as fuse-pinch-linger (Ryan, 2003). In the third, the vesicles remain fused with the membrane for more than 45 seconds and are recycled by CME. This is referred to as fuse-and-collapse. Since it is involved in both fuse-pinch-linger and fuse-and-collapse pathways, Dyn1 may function as a regulatory component in pre-synaptic portion of LTP.

However, other studies also implicate a post-synaptic modification for LTP expression, including receptor trafficking (Collingridge et al., 2004) and signal transduction pathways (Sheng and Kim, 2002). It is generally agreed that postsynaptic AMPAR function makes an important contribution to the expression of LTP. AMPAR is highly dynamic, as there is evidence showing that HFS induces the movement of AMPAR to the surface of the dendritic shaft and spines (Shi et al., 1999). Because AMPAR itself lacks a motor domain, the receptor must associated with protein partners that assist in its trafficking (Bredt and Nicoll, 2003). The removal of AMPARs from synapses, as part of trafficking, is regulated by dynamin-dependent endocytosis (Carroll et al., 1999). Furthermore, the ERK pathway is one of the most important signaling pathways regulating synaptic

plasticity (Thomas and Huganir, 2004). The process leading to ERK activation also requires dynamin-dependent endocytosis (Kranenburg et al., 1999).

Regardless of the debate between the pre- vs. post- synaptic LTP schools, Dyn1 dependent endocytosis could be involved in both parts. Thus, Dyn1 and other endocytosis-related proteins might be crucial factors in synaptic plasticity, such as LTP.

Objective of the study

Although the S857 phosphorylation of Dyn1 by Mnb/Dyrk1A has been studied *in vitro*, the effect of Dyn1xa S857 phosphorylation in a physiological process has not been determined. In this study, the synapses in the Schaffer Collateral-CA1 pathway of mouse hippocampal slices were chosen to assess how Dyn1xa S857 phosphorylation is regulated following different types of neuronal activity.

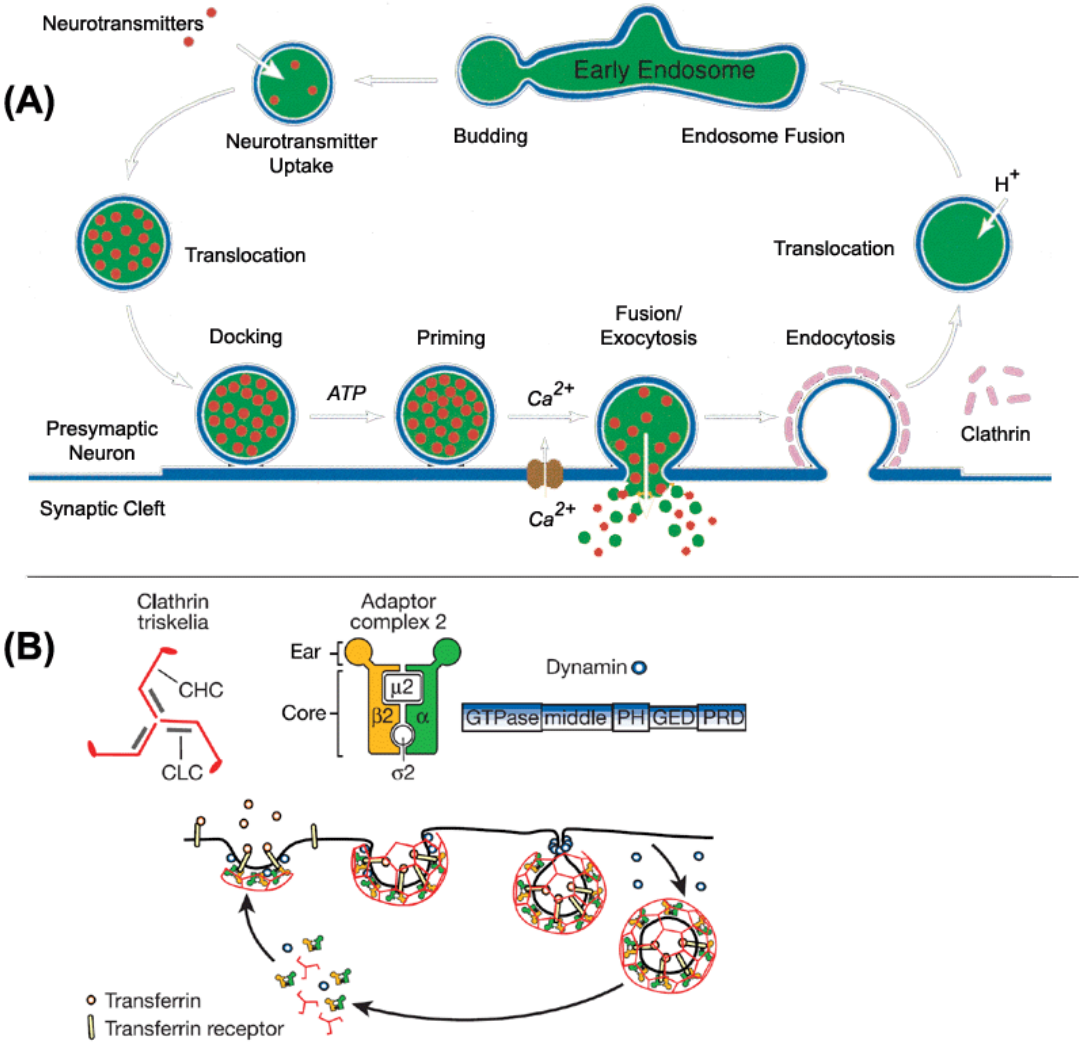

Figure 1.1 The involvement of dynamin in endocytosis. A. *Cartoon model of synaptic vesicle recycling in the presynaptic neurons* (Sudhof, 1995). After neurotransmitters are released from the presynaptic neurons upon the Ca^{2+} influx, the vesicle membranes are coated with clathrin and are internalized into the cytoplasm with the assistance of endocytic accessory proteins. The coated pits are then uncoated and are fused with endosomes. After modification in endosomes, the neurotransmitter loaded vesicles buds off and are ready for the

next round of neurotransmission. **B.** *The role of dynamin in vesicle internalization* (Conner and Schmid, 2003). Clathrin triskelions, composed of three clathrin heavy chains (CHC) and three clathrin light chains (CLC), assemble the budding membrane vesicle. Adaptor complexes 2 mediate clathrin assembly. Dynamin (blue open circles) is found around the neck of invaginated vesicles to mediate membrane fission.

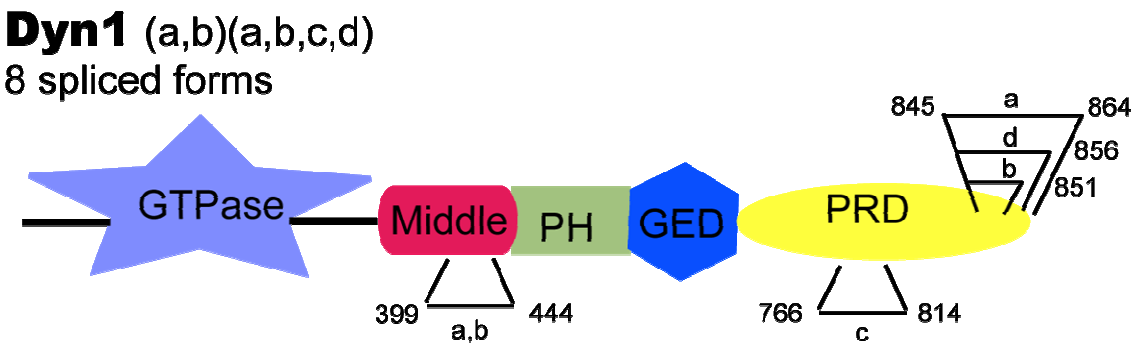

Figure 1.2 Structure and isoforms of Dyn1. GTPase domain binds and hydrolyses GTP providing energy for Dyn1 function. Middle domain and GED is involved in oligomerization and stimulation of GTPase activity. PH domain is responsible for interacting with lipids. PRD interacts with SH3 domains of other proteins. There are 2 variants (a,b) in the middle domain and 4 variants (a,b,c, and d) in the PRD domain. Together, they give rise to 8 splicing isoforms. Numbers indicate the locations of splicing sites. Alphabets, a, b, c and d, indicate splicing isoforms.

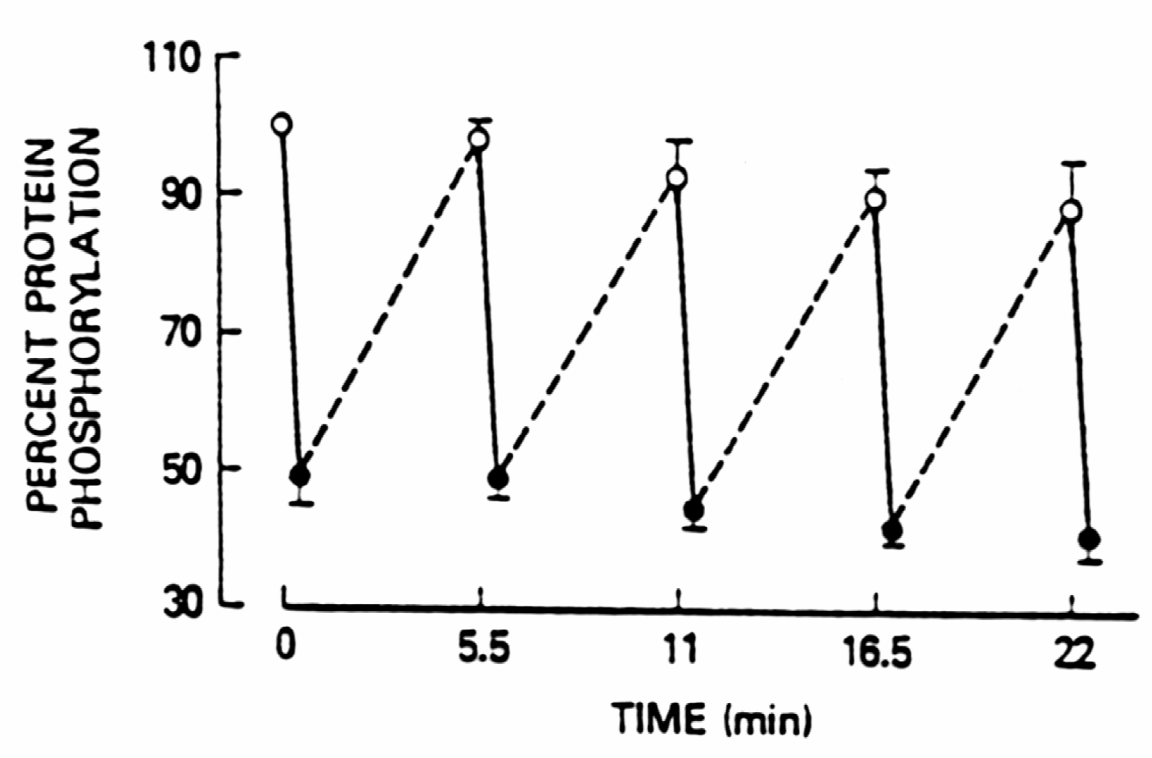

Figure 1.3 Phosphorylation cycle of Dyn1 in synaptosomes (Robinson et al., 1987). Synaptosomal Dyn1 shows a high level of phosphorylation upon polarization (open circles). The phosphorylation level (black circle) decreases quickly upon depolarization (solid line). After repolariztion, the phosphorylation level recovers (dash line).

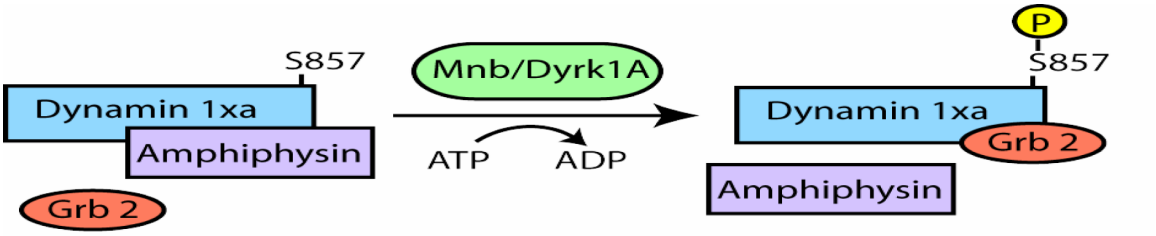

Figure 1.4. Model of the interaction of Dyn1 with its binding partners (Huang et al., 2004). The model depicts the regulation of Dyn1xa protein-protein interactions by Mnb/Dyrk1A phosphorylation. Unphosphorylated Dyn1xa could readily interact with endocytic accessory protein, amphiphysin. After S857 phosphorylation by Mnb/Dyrk1A, however, Dyn1xa is now having a higher affinity for binding growth factor receptor-bound protein 2 (Grb 2) than amphiphysin.

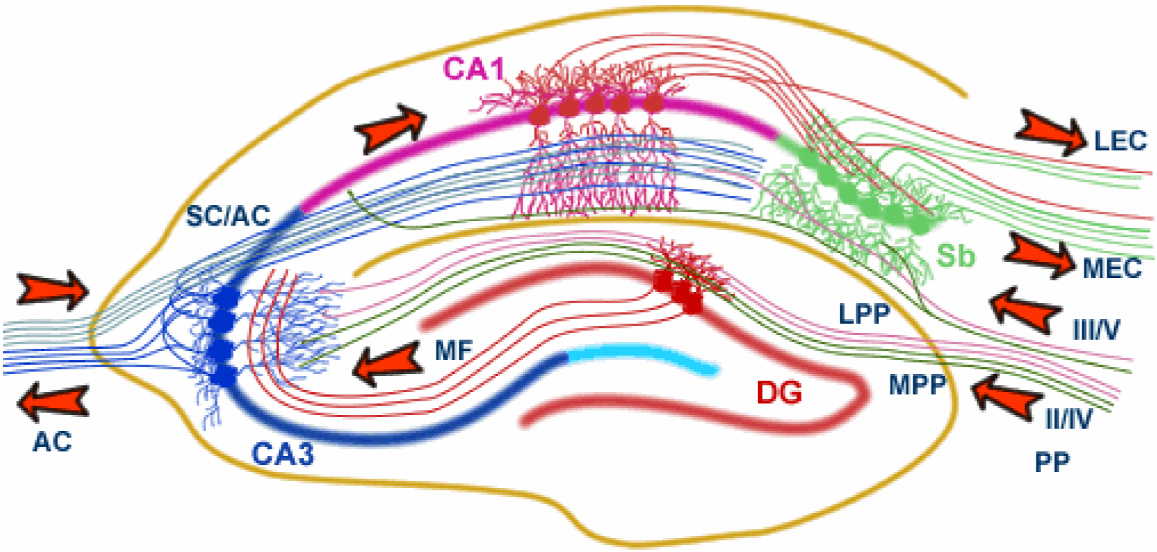

Figure 1.5 Pathways in hippocampus. Perforant Path (PP-split to lateral and medial path, LPP and MPP): input from Entorhinal Cortex (EC) to Dentate Gyrus (DG); Mossy Fiber path (MF): connection between axons of DG (mossy fibers) and CA3 pyramidal neurons; Schaffer Collateral/Association Commissural path (SC/AC): axons of CA3 pyramidal neurons coming from either an ipsilateral hippocampus (Schaffer Collateral) or a contralateral hippocampus (AC) to the CA1 pyramidal neurons; Entorhinal Cortex (EC) path: the pathway from CA1 pyramidal neurons to Subiculum (Sb) and out to the EC (EC-split to lateral and medial path, LEC and MEC).

CHAPTER 2

Materials and Methods

Reagents.

Cyclosporine A, Kynurenic acid (KYA), D-2-Amino-5-phosphonopentanoic acid (APV), 6-cyano-7-nitroquinoxaline-2,3-dione (CNQX), ethylenediamine tetraacetic acid (EDTA), NaCl, $MgCl_2$, okadaic acid, cypermethrin, sodium pyrophosphate, sodium orthovanadate, glycerol, bromine phenol blue, ethylene glycol tetraacetic acid (EGTA), NP-40, Triton X100, Tween 20 and paraformaldehyde were purchased from Sigma. BAPTA/AM and dithiothreitol (DTT) were purchased from Calbiochem. P81 membranes were purchased from Whatman International Ltd. Tris-HCl was purchased from Research Products International Corporation. Sodium dodecyl sulfate (SDS) was purchased from J.T. Baker. Complete EDTA-free phosphatase inhibitor cocktail tablets were purchased from Roche. Liquid-gel (acrylamide) was purchased from MP Biomedicals. Bovine serum albumin (BSA) was purchased from USB Corporation. Alkaline phosphatase-CDP-Star detection system was purchased from New England Biolabs. Calcineurin assay kit (catalog number: AK-816) was obtained from BioMol International. Ultralink protein A/G was purchased from Pierce. LipofectAMINE 2000 reagent, goat serum, and PBS were purchased from Invitrogen. QuikChange site-directed mutagenesis kik was purchased from

Stratagene. PVDF membranes (Immobilon P) were purchased from Millipore Corporation. Autoradiography film was purchased from Denville Scientific. TBS tissue freezing medium was obtained from Electron Microscopy Sciences.

Mnb/Dyrk1A clones.

pcMnb, a pcDNA3-based vector for expressing full-length wild-type Mnb/Dyrk1A was constructed as described previously (Chen-Hwang et al., 2002). Mnb/Dyrk1A containing the K188R and the D306N substitution was constructed by the QuikChange site-directed mutagenesis kit and subsequently spliced into the pcDNA3 vector as full-length mutant Mnb/Dyrk1A similarly as described (Huang et al., 2004; Adayev et al., 2006).

Antibodies.

Mouse anti-Dyn1xa pS857 monoclonal antibody (3D3) was produced as described previously (Huang et al., 2004). Rabbit anti-Dyn1xa isoforms antibody (R53) was raised by using conjugated unphosphorylated Dyn1xa-specific peptide (PSRSGQASPSR) as the antigen (**Figure 2.1**). Mouse anti-Mnb/Dyrk1A monoclonal antibody (7F3) was produced as described previously (Wegiel et al., 2004). Mouse anti-dynamin monoclonal antibody (Hudy-1) was purchased from Upstate Biotechnology Inc. Mouse anti-MAP-2 monoclonal antibody (MAP-2) and anti-actin monoclonal antibody (actin) were purchased from Sigma. Goat

polyclonal Mnb/Dyrk1A (G19), Dyrk2, and Dyrk3 antibodies were obtained from Santa Cruz Biotechnology. Sheep polyclonal anti-pS774 and pS778-Dyn1 antibodies were obtained from Zymed Laboratories Inc. Goat anti-mouse and anti-rabbit IgG (alkaline phosphatase conjugated) were obtained from Sigma. Donkey anti-sheep IgG (alkaline phosphatase conjugated) was obtained from Santa Cruz Biotechnology. Alexa fluor 488 Goat anti-mouse and anti-rabbit IgG were obtained from Invitrogen.

Determining the level of S857 phosphorylation.

Purified rat brain Dyn1 was phosphorylated with GST-Mnb/Dyrk1A at molar ratio of 4:1 (Dyn1: Mnb/Dyrk1A) for 40 min at 30 ^{o}C as described (Chen-Hwang et al., 2002). The progress of S857 phosphorylation was monitored at several time points by antibody 3D3 staining. The level of phosphorylation at S857 (pS857) reaches a plateau in about 10-15 min under the specified assay conditions. The “fully” phosphorylated Dyn1 was then mixed with the unphosphorylated Dyn1 to create a series of Dyn1 standards, with 20, 40, 60, and 80 % pS857. Unknown samples to be determined (lysate containing 10-20 µg Dyn1xa pre-estimated by R53 staining) were processed together with all four Dyn1 standards in the same blot. Two identical blots were prepared for each experiment, one each for staining with 3D3 and R53. The data for standards from the 3D3 stained blot were plotted and used to determine the apparent level of S857 phosphorylation for the

unknowns. These numbers were subsequently corrected for the difference in the level of Dyn1xa protein (from the R53 stained blot) to give the final values.

Slice preparation.

One- to three-month-old CD-1 mice were used in my investigations. The animals were kept on an automatic 12-hr light–dark cycle (lights on at 0600 h; lights off at 1800 h), with food and water ad libitum. Following decapitation, the brains were quickly removed and placed into ice-cold Ringer's solution. The Ringer's solution consists of 124 mM NaCl, 3.1 mM KCl, 1.3 mM KH_2PO_4, 1.3 mM $MgSO_4$, 3.1 mM $CaCl_2$, 25.2 mM $NaHCO_3$, and 10.0 mM Glucose (pH 7.4) and was oxygenated with a CO_2:O_2 (5 %:95 %) mixture prior to use. Both hippocampi were dissected out, placed into ice-cold Ringer's and sliced on a manual tissue chopper into 350 μm individual slices. The slices were pre-incubated for at least 1 hr in oxygenated Ringer's buffer at 33 ^{o}C before recording. All protocols for animal care and use were approved by the Animal Welfare Committees of the College of Staten Island and the City University of New York. NIH guidelines were followed for all protocols.

Electrophysiological recordings.

A single hippocampal slice was placed in an interface recording chamber (containing 1.5 ml of Ringer's) maintained at 33 ^{o}C with constant oxygenation. A

bipolar, stimulating electrode was placed on the Schaffer Collateral/Commissural fibers and the extracellular recording electrode was placed in the stratum pyramidal cell layer under a dissecting microscope (Olympus SZ-40) (**Figure 2.2**). To measure neuronal excitability, expressed as the magnitude of the population spike, the slices were stimulated electrically with a frequency of 0.033 Hz throughout the entire experiment except during brief periods of high-frequency stimulation (HFS) (100 Hz for 1 sec, 3 times every 10 sec) used to induce LTP. The amplitude of the population spike was measured on-line with the LTP Program. The strength of the stimulation was adjusted to give approximately 50 % of the maximal response. The baseline recording was usually followed for at least 10 min before applying HFS. Five sweeps taken immediately prior to HFS were averaged and used as the baseline for all chemically and electrically induced changes in the amplitude of the population spike. The potential after LTP induction was followed for 10 min after HFS. An amplification of the potential by at least 15 % was accepted as LTP (El-Sherif et al., 2003).

Hippocampal slice extract preparation.

Extracts from hippocampal slices were prepared by homogenizing a single hippocampal slice in a disposable micro tissue grinder attached to a motor driver in a lysis buffer containing 50 mM Tris-HCl (pH 8.0), 20 mM EDTA, 150 mM NaCl, 0.05 % SDS, 1X Roche Complete protease inhibitor cocktail, 0.2 μM okadaic acid, 4 μM cyclosporine A, 5 μM cypermethrin, 2.5 mM sodium pyrophosphate, and 1

mM sodium orthovanadate. After removing cell debris by centrifugation (12,000 Xg for 6 min), the supernatant was mixed with sample buffer (8 % SDS, 40 % glycerol, 0.25 M Tris-HCl pH 6.8, 40 mM DTT, 0.05% bromine phenol blue) and boiled for 5 min before using for Western blotting. The protein concentration in each sample was determined by the Bradford dye assay (Bradford, 1976).

Western blotting.

All samples were separated in 8 % SDS-PAGE gel (1 M Tris-HCl pH 8.45, 0.1 % SDS, and 8 % liquid-gel acrylamide) at 90 V for 90 min. The proteins were then transferred onto PVDF membranes at 70 mA / gel for 100 min with a semi-dry transfer device. All membranes were processed as follows: (a) incubate the membrane with blocking buffer (5 % BSA or 2 % milk, 1 X PBS, and 2.5 mM Tween 20) at room temperature for 1 hr; (b) incubate the membrane with primary antibodies diluted in the same blocking buffer at 4 ^{o}C overnight; (c) wash the membrane with PBST (1 X PBS and 2.5 mM Tween 20) 20 min with three changes; (d) incubate the membrane with secondary antibodies diluted in 2 % milk blocking buffer for 1 hr at room temperature; (e) wash the membrane with alkaline buffer (10 mM Tris-HCl pH 9.5, 10 mM NaCl and 10 mM MgCl2) for at least 1 hr with multiple changes. Protein detection was then visualized on X-ray film using the chemiluminescent reagent CDP-Star. Quantification of the scanned X-ray film images was performed using NIH image 1.6 software.

Drug treatment.

Cyclosporine A was dissolved in ethanol to obtain a stock solution of 40 mM; BAPTA/AM was dissolved in DMSO to obtain a stock solution of 5 mM; KYA was dissolved in water to obtain a stock solution of 50 mM; APV was dissolved in water to obtain a stock solution of 12.5 mM; and CNQX was dissolved in water to obtain a stock solution of 5 mM. All drugs were diluted to the desired concentrations in Ringer's solution (2 μM for Cyclosporine A, 10 μM for BAPTA/AM, 2.5 mM for KYA, 50 μM for APV, and 50 μM for CNQX) and used immediately. Half of the prepared slices were picked up randomly and transferred into a separated but adjacent holder containing the drug in Ringer's solution in the same incubation chamber. After at least 1 hr incubation with drugs, each slice was placed in an interface-recording chamber containing the same concentration of drug in Ringer's solution and recorded as described in **Electrophysiological recordings**.

Calcineurin activity assay.

Phosphatase assays were performed by following the supplier's instructions briefly as described below. Hippocampal slices were homogenized on ice in lysis buffer containing 50 mM Tris (pH 7.5), 0.1 mM EDTA, 0.1 mM EGTA, 1 mM DTT, 0.2 % NP-40 and 1X Roche Complete protease inhibitors cocktail. After sedimentation at 150,000 Xg in centrifuge at 4^{o}C for 45 min, the supernatant was

collected and passed through a re-hydrated resin column to remove free phosphate and nucleotides. The prepared lysate was then incubated with calcineurin substrate, a peptide derived from cAMP-dependent protein kinase (PKA) regulatory subunit type II (RII) with the sequence Asp(D) – Leu(L) – Asp(D) – Val(V) – Pro(P) – Gly(G) – Arg(R) – Phe(F) – Asp(D) – Arg(R) – Arg(R) – Val(V) – pSer(S) – Val(V) – Ala(A) – Ala(A) – Glu(E) (MW=2192.0), at 30 ^{o}C for 30 min. The detection of free-phosphate (Pi) released by calcineurin is based on a Malachite green assay read at OD 620 nm. The enzymic activity was expressed in nmol Pi released / min / mg protein from the substrate. The protein concentration in each sample was determined by the Bradford dye assay (Bradford, 1976). To minimize individual animal variation, an entire set of experiments including nonstimulated control, HFS and LTP-induced slice was prepared from the same animal.

Immunofluorescence staining.

After recording, the slices were fixed in 4 % paraformaldehyde for 12 hrs. Then the slices were embedded in tissue freezing medium on dry ice and sectioned into 25 μm pieces on a cryostat microtome (Vibratome UltraPro 5000) at -20^{o}C. The sections were processed as follows: (a) block in 2 % non-fat dry milk, 0.2 % Triton X100 and 10 % goat serum at room temperature for 1 hr; (b) incubate with primary antibody (3D3, Hudy-1 or MAP-2) in 2 % non-fat dry milk and 2 % goat serum at 4 ^{o}C overnight; (c) rinse with PBS 3 times for 10 min each

time; (d) block in 2 % non-fat dry milk and 2 % goat serum at room temperature for 1 hr; (e) incubate with secondary antibody in 2 % non-fat dry milk and 2 % goat serum at room temperature for 1 hr; (f) rinse with PBS 3 times for 10 min each time; (g) mount the sections on gelatin coated slides and cover with cover-slips. Fluorescence from images was detected with a NIKON PCM 2000 dual laser-scanning confocal microscope (Nikon, Melville). Sequences of 30-40 sections in 0.6 μm steps were taken using successive (z) scans. The maximum projections from the z-stack of images were analyzed by AutoDeblur V93 plus AutoVisualize U93 software.

Time-course phosphorylation assay.

Extracts from mouse hippocampus were prepared from the fractions of hippocampi in lysis buffer containing 50 mM Tris-HCl (pH 8.0), 150 mM NaCl, 0.9 % Triton X100, and 1X Roche Complete protease inhibitor cocktail. After removing cell debris by centrifugation (12,000 Xg for 6 min), aliquots (40 μl per reaction) of the supernatant were incubated in phosphorylation mixtures containing 5 mM ATP and phosphatase inhibitors (0.2 μM okadaic acid and 4 μM cyclosporine A) at 30 ^{o}C. The reactions were terminated at 0, 20, 40, 60, and 90 min by adding sample buffer to the reaction mixtures and boiling them for 5 min. The reaction samples along with a sample of unphosphorylated hippocampal extract were then subjected to immunoblotting against antibodies 3D3 and R53.

Immunodepletion.

Antibody coating was prepared by mixing 75 µl of Ultralink protein A/G with 200 µg of G19, Dyrk2 or Dyrk3 antibody overnight at 4 ^{o}C. The antibodies coated protein A/G were then blocked with 2 % BSA for 2 hrs. Mouse hippocampi were homogenized in buffer containing 50 mM Tris-HCl, (pH 8.0), 150 mM NaCl, 0.9 % Triton X100, and 1X Roche Complete protease inhibitor cocktail. The lysates were incubated with either protein A/G or the immobilized antibody at 4 ^{o}C for 3 hrs. The mixtures were sedimented and the recovered supernatants were incubated with 5 mM ATP and phosphatase inhibitors (0.2 µM okadaic acid and 4 µM cyclosporine A) at 30 ^{o}C to promote the phosphorylation. After 30-min reaction (as described in **Time-course phosphorylation assay**), phosphorylation was terminated by adding sample buffer to the reaction mixture and boiling them for 5 min. The immunodepleted samples with and without phosphorylation were subjected to immunoblotting against antibodies 3D3 and R53.

Kinase activity assay.

(a). Mnb/Dyrk1A activity in HN2-5 cells was determined as follows. HN2-5 cells were first transfected with pcDNA3, pcMnb/Dyrk1A (WT), pcMnb/Dyrk1A (K188R), pcMnb/Dyrk1A (D306N) or a mixture of pcMnb/Dyrk1A WT (1:3 ratio) with either pcMnbK/Dyrk1A (188R) or pcMnb/Dyrk1A (D306N) by using the

Lipofectamine 2000 reagent. Transfection was performed by adding the mixture consisting of 3-4 µg total DNA and Lipofectamine 2000 (1 µg DNA per 2.5 µl reagent) directly to $1x10^6$ undifferentiated HN2-5 cells in suspension. The cells were then placed in a 6-well plate immediately, incubated for 5 hrs, followed by a media change. The transfected cells were allowed to recover for 24 hrs and differentiated by treating with 5 µM retinoic acid for an additional 24 hrs. Cells were lysed directly in well with 200 µl freshly prepared buffer containing 50 mM Tris pH 8.0, 20 mM EDTA, 150 mM NaCl, 1 % NP-40, and 1 mM EGTA supplemented with 1XRoche Complete protein inhibitor cocktail and phosphatase inhibitors (0.2 µM okadaic acid, 4 µM cyclosporine, and 1 mM sodium orthovanadate). A clear lysate was obtained from the homogenate by centrifugation at 12,000 Xg for 5 min. Mnb/Dyrk1A was immunoprecipitated with 1 µg immobilized Mnb/Dyrk1A antibody G19 from 1 µg cell lysates (total protein) for 1.5 hrs. The precipitated kinase was washed once with the kinase buffer (25 mM HEPES pH 7.5, 100 mM NaCl, and 5 mM $MgCl_2$) and then subjected to kinase reaction. Kinase reactions were performed in a 30 µl reaction mixture containing the kinase buffer, 4 µCi ^{32}P-ATP (specific activity 0.33 mCi/mmole), 1 µg dynatide 3 (a Dyn1 C-terminal peptide containing the sequence ASPSRPESPRPP), and IP pellets similarly as described (Huang et al., 2004). The reaction was allowed to proceed at 30 ^{o}C for 30 min with shaking. Phosphorylated dynatide 3 was measured by P81 phophocellulose membrane binding as described previously (Huang et al., 2004).

(b). For measuring hippocampal Mnb/Dyrk1A activity in hippocampus, hippocampal slices from control, HFS, or LTP-induced group were homogenized on ice in buffer containing 50 mM Tris-HCl (pH 8.0), 150 mM NaCl, 0.9 % Triton X100, 1X Roche Complete protease inhibitor cocktail, 0.2 µM okadaic acid, 4 µM cyclosporine A, and 5 µM cypermethrin. A clear lysate was obtained from homogenate by centrifugation at 12,000 Xg for 5 min. Mnb/Dyrk1A was immunoprecipitated from clear lysates with antibody G19 coated protein A/G for 1.5 hrs at 4 ^{o}C. After washing with kinase buffer (25 mM HEPES pH 7.5, 100 mM NaCl, 5 mM $MgCl_2$, and 5 mM $MnCl_2$), the immunoprecipitation complexes were incubated in a 50 µl reaction mixture containing a kinase buffer, 1 µg dynatide 3, 6 µCi of ^{32}P-ATP and 2 µg ATP. The reactions were allowed to proceed at 30 ^{o}C for 35 min. A 10 µl aliquot of the reaction mixure was withdrawn and the extent of ^{32}P incorporation was determined by P81 phophocellulose membrane binding.

Synaptosome preparation.

Synaptosomes were prepared from CD1 mice hippocampus according to a published procedure (Muzzolini et al., 1997). Briefly, both hippocampi were homogenized in ice-cold 0.32 M sucrose buffer at pH 7.4 supplemented with 1 mM $MgSO_4$. The homogenate was centrifuged at 900 Xg for 10 min at 4^{o}C. The synaptosomal fraction was obtained by centrifuging the supernatant at 12,000 Xg for 20 min. The pellets were then re-suspended in oxygenated (CO_2:O_2, 5 %:95 %) Ringer's solution. Aliquots of synaptosomes were either lysed immediately

(marked as time 0) or incubated in Ringer's solution maintained at 33 ^{o}C with constant oxygenation for 15 min or 1 hr. Those synaptosomes were lysed in sample buffer and boiled for 5 min before using for western blotting.

Statistics.

For all experiments, data were presented as mean±SEM. n representes the number of slices or independent trials analyzed in a given experiment. In comparisons between two groups with equal n numbers, the student's t test was used. In all other comparisons, one-way ANOVA followed by a post-hoc multiple comparisons Student-Newman-Keuls test was used. P values less than 0.05 were considered significant.

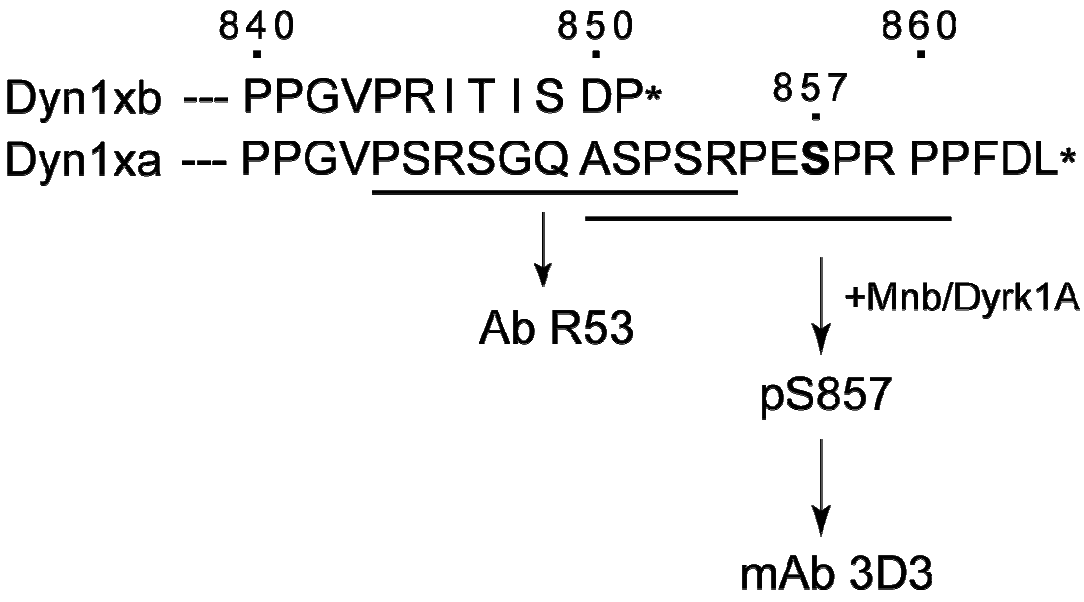

Figure 2.1 Dyn1xa antibodies. The peptides (sequence underlined) used for raising antibodies R53 and 3D3 were derived from the C-terminal sequences of Dyn1xa. To raise 3D3 antibody, a pS857-specific antibody, the antigenic peptide was extensively phosphorylated by Mnb/Dyrk1A *in vitro* before using for antibody preparation.

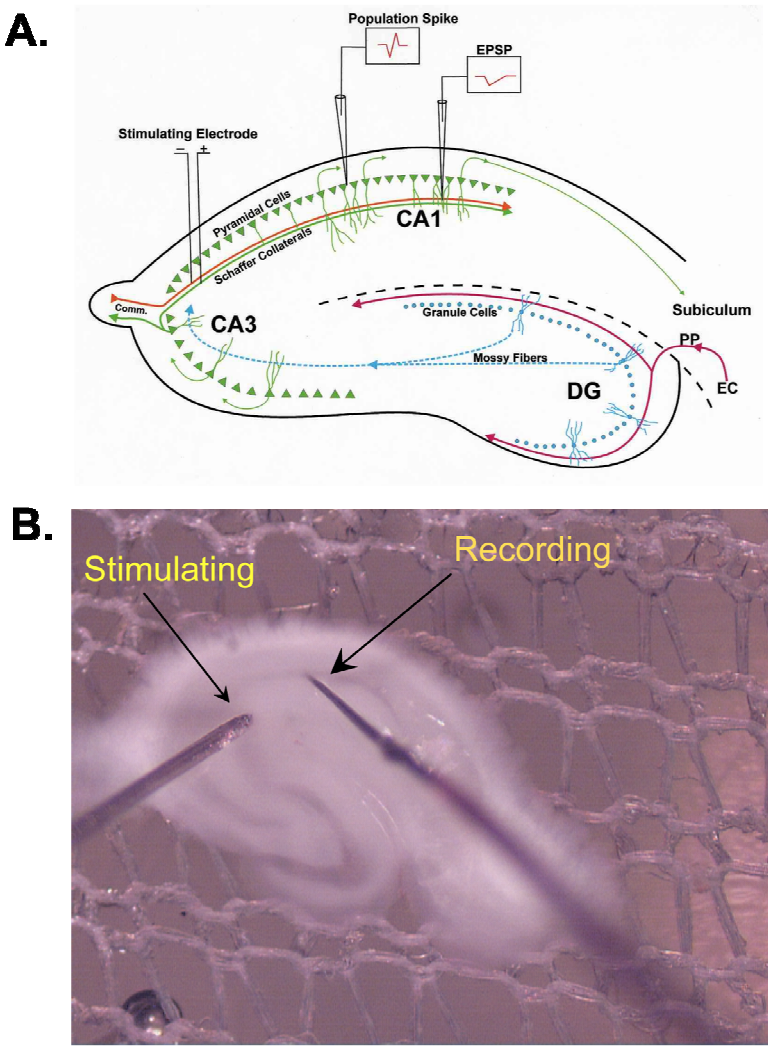

Figure 2.2 Stimulation and recording in hippocamal slices. A. *Schematic cartoon shows the position of the electrodes*. Population spikes are recorded if the recording electrode is placed in pyramidal cell layer and excitatory postsynaptic potentials (EPSPs) are recorded if the recording electrode is place in Schaffer Collateral/Commissural fibers. DG, Dentate Gyrus; EC, Entorhinal Cortex; PP, Perforant Path. **B**. *Stimulating and recording positions in an actual slice (40 X).* The recording electrode is guided into pyramidal cell layer seen in the picture as a darker line. The bipolar, stimulating electrode is located on the fibers of Schaffer Collateral/Commissural located further towards the center of slice.

CHAPTER 3

Results

Dyn1xa is highly phosphorylated at S857 in nonstimulated hippocampal slices.

To determine the level of phosphorylated S857 (pS857) Dyn1xa in hippocampal slices, a semi-quantitative method for measuring the level of phosphorylation was developed. Briefly, purified rat brain Dyn1 was phosphorylated extensively with Mnb/Dyrk1A until the level of phosphorylation reached a plateau (**Figure 3.1 A**). Phosphorylation at this stage was considered to be 100 % if the reaction was performed with high Mnb/Dyrk1A to Dyn1 ratio (Chen-Hwang et al., 2002). Then 100 % pS857 Dyn1 was mixed with known amounts of un-phosphorylated Dyn1 (0 %) to create a series of pS857 Dyn1xa standards ranging from 20-80 %. Unknown samples (crude hippocampal lysates) were immuno-blotted together with these standards and probed with a Dyn1 pS857-specific antibody, 3D3. The level of pS857 was calculated based on the pS857 standard curve (**Figure 3.1 C**) and corrected for the amount of total Dyn1xa used in the assay as determined in a second immunoblotting using antibody R53, which is not sensitive to S857 phosphorylation. According to this method, S857 of Dyn1xa in nonstimulated control hippocampal slices was estimated to be 66.8 ± 5.4 % (n = 5) phosphorylated (**Figure 3.1 B**). This result

indicates that the endogenous Dyn1xa S857 phosphorylation is high in hippocampus.

Phosphorylation of Dyn1 at S774 and S778 was previously studied in the synaptosomes (Tan et al., 2003; Tomizawa et al., 2003; Anggono et al., 2006). Synaptosomes are isolated synapses obtained after the homogenization and fraction of nerve tissues. They contain the molecular machinery necessary for the uptake, storage, and release of neurotransmitters. They are commonly used as a model for studying pre-synaptic function. However, synaptosomes exhibited weak S857 phosphorylation even afer a prolonged incubation in oxygenated buffer (**Figure 3.2** S1: 9.3 ± 2.0 %; S2: 12.5 ± 1.2 %; S3: 15.2 ± 3.9 %). The inability to support substantial S857 phosphorylation as compared to hippocampal slices disqualified synaptosomes as a suitable system for studying the physiological consequences of Dyn1xa phosphorylation at S857.

The level of pS857 Dyn1xa changes with neuronal activities.

Hippocampal slices were divided into four groups and treated accordingly: the nonstimulated (control) group, the low frequency stimulation (LFS) group, the high frequency stimulation (HFS) group and LFS/HFS group (**Figure 3.3**). In the LFS group, stimulation was applied to each slice every 30 sec (0.033 Hz) for 20 min. In the HFS group, each slice received only the HFS stimulations (3 times 100 Hz stimulations for 1 sec with 10 sec interval). In the LFS/HFS group, each slice

was first stimulated every 30 sec for 10 min to get a stable baseline potential. Then, after applying HFS, each slice underwent another 10 min of 0.033 Hz stimulation to determine whether LTP was induced.

The state of phosphorylation in the LFS group remained essentially the same as that in the control group (0.96 ± 0.13, n = 6, p > 0.5, LFS slices vs. control slices) (LFS in **Figure 3.4 B**). However, a drastic reduction in pS857 (0.29 ± 0.05, n = 6, p < 0.0001, HFS slices vs. control slices) was observed in the slices taken for analysis immediately (less than 2 sec) after the application of HFS (HFS in **Figure 3.4 B**). In the LFS/HFS group, where LTP could be induced, the level of pS857 was also reduced (0.69 ± 0.05, n = 17, p < 0.0001, LFS/HFS slices vs. control slices) (LFS/HFS in **Figure 3.4 B**). These results show that the level of pS857 Dyn1xa is regulated by electrical stimulation. Interestingly, the reduction of pS857 did not directly correspond to the duration of stimulation as the level of pS857 Dyn1xa in the LFS/HFS group was significantly higher than that in the HFS group, which received a less stimulation than the LFS/HFS group.

LFS/HFS is intended to induce LTP; however, not every slice in the LFS/HFS group displayed LTP (defined as at least a 15 % enhancement of potential over the base line 10 min after HFS). To determine whether the actual LTP induction affected the level of pS857 Dyn1xa, slices in the LFS/HFS group were separated into two sub-groups based on whether or not LTP was induced. In the sub-group of slices which demonstrated LTP, the pS857 level was found to be

significantly higher than in the non-LTP induced group (0.77 ± 0.06, n = 10 vs. 0.58 ± 0.06, n = 7, $p < 0.05$) (**Figure 3.5**). This indicates that LTP induction may induce the change in pS857 levels.

Dephosphorylation of Dyn1xa at S857 is dependent on Ca^{2+}/calcineurin.

Calcium and calcineurin (protein phosphatase 2B, a calcium-dependent phosphatase) have been implicated in the dephosphorylation of Dyn1 (Lai et al., 1999; Cousin and Robinson, 2001). To determine the specific involvement of Ca^{2+}/Calcineurin in S857 Dyn1xa dephosphorylation in hippocampus, slices were pre-incubated with either cyclosporine A (calcineurin inhibitor) or BAPTA/AM (membrane permeable calcium chelator) for 1 hr and then stimulated with HFS. The pS857 level in the cyclosporine A - treated slices was the same as in those nonstimulated controls (0.90 ± 0.10, n = 7, $p > 0.5$ vs. nonstimulated slices treated with cyclosporine A) (cyclosporine A in **Figure 3.6**). A similar result was also found in the BAPTA/AM - treated group (1.07 ± 0.21, n = 7, $p > 0.5$ vs. nonstimulated slices treated with BAPTA/AM) (BAPTA/AM in **Figure 3.6**). These results indicate that the HFS - stimulated Dyn1xa dephosphorylation at S857 is dependent on Ca^{2+}/Calcineurin.

The activity of calcineurin doesn't change upon HFS.

If calcineurin is involved in HFS or LFS/HFS induced Dyn1xa dephosphorylation, its activity might be regulated by the stimulation. To determine the calcineurin activity directly, I measured enzymatic dephosphorylation of a calcineurin substrate in slice homogenates. The inorganic phosphate (Pi) released from the labeled calcineurin substrate by the nonstimulated slices homogenates remained the same as those that had received HFS (1.041 ± 0.152, n = 6) and expressed LTP induction (1.075 ± 0.120, n = 6) (**Figure 3.7**). The results indicate that the overall calcineurin activity is not significantly altered by these different stimulations.

Dyn1xa dephosphorylation at S857 is mediated by AMPA/Kainate glutamate receptors.

The synaptic activity in the Schaffer collaterals-CA1 region of hippocampus is mediated through glutamate receptors. To investigate whether glutamate receptors are involved in Dyn1xa dephosphorylation, slices incubated with KYA (a general glutamate receptor antagonist) were subject to LFS/HFS stimulation. Those slices display no potential at all. The S857 phosphorylation level of Dyn1xa remained unchanged compared to the control (1.10 ± 0.08, n = 6, vs. the nonstimulated slices treated with KYA, $p > 0.25$) (KYA in **Figure 3.8**). This

suggests that the dephosphorylation of Dyn1xa S857 is mediated by glutamate receptors.

There are two main subtypes of ionotropic glutamate receptors: NMDA and AMPA/Kainate receptors. Postsynaptic NMDA receptors are activated during LTP induction, while AMPA/Kainate receptors mediate basal synaptic activity. To further distinguish which sub-type of glutamate receptor is responsible for pS857 dephosphorylation in the LTP group, two selective ionotropic glutamate receptor blockers were tested: APV (a selective antagonist for NMDA receptors) and CNQX (a selective antagonist for AMPA/Kainate receptors). Slices treated with APV displayed basal potential but failed to induce LTP, while slices incubated with CNQX displayed no potential at all. In the APV treated slices, the level of pS857 Dyn1xa was significantly reduced by the HFS/LFS (0.48 ± 0.13, n = 5, vs. the nonstimulated slices treated with APV, $p < 0.02$) (APV in **Figure 3.8**). However, the CNQX treated slices had nearly the same pS857 as the control (1.17 ± 0.17, n = 6, vs. the nonstimulated slices treated with CNQX, $p > 0.3$) (CNQX in **Figure 3.8**). This result suggests that the dephosphorylation of S857 Dyn1xa during LTP is mediated through AMPA/Kainate glutamate receptors.

The distribution of pS857 Dyn1xa changes with neuronal activity.

To investigate the cellular distribution of pS857 Dyn1, hippocampal slices were immuno-stained with Dyn1xa pS857-specific antibody (3D3). 3D3 appeared

to stain most pyramidal neurons, especially in the CA1 region (**Figure 3.9**). A similar staining pattern was also observed for MAP-2 antibody in the CA1 region (**Figure 3.10**). Since MAP-2 is a dendritic marker, the result of 3D3 staining indicates that 3D3 recognizes the pyramidal neurons. 3D3 staining showed that pS857 Dyn1xa was evenly distributed in both CA1 pyramidal cell bodies and the entire length of apical dendrites in nonstimulated hippocampus (control in **Figure 3.11 A**). Some sections also showed basal dendrite staining (data not shown).

Upon HFS, the number of pS857 positive neurons was drastically reduced compared to the control slices. However, the pattern of pS857 staining in a few stained neurons was similar to the control slices (HFS in **Figure 3.11 A**). This observation is consistent with the significantly reduced pS857 levels observed in slices stimulated with HFS (HFS in **Figure 3.4 B**). This indicates that most neurons in the CA1 area are globally dephosphorylated upon HFS.

Interestingly, LTP induction produced a drastically different pS857 Dyn1xa distribution. The staining in the distal parts of apical dendrites disappeared. As the result, pS857 Dyn1xa was restricted to cell bodies and to the proximal regions of apical dendrites (LTP-induced in **Figure 3.11 A**). To quantify the results, the number of pS857 Dyn1xa positive neurons in three different regions, somas of the pyramidale cell layer (SP), dendrites in the proximal and distal parts of apical dendrites (pSR and dSR) were counted (**Figure 3.11 B**). The numbers in the three areas decreased upon HFS, while the LTP-induced slices displayed a

distance-dependent reduction in staining number. The largest reduction in number occurred in dSR.

The change in the pS857 Dyn1xa staining pattern in LTP-induced slices could be due either to regional dephosphorylation of pS857 Dyn1xa in the distal area of apical dendrites or to a redistribution of Dyn1 from the distal apical dendrites toward the soma. Further immunohistochemical staining with an anti-Dyn1 antibody Hudy-1, which is not sensitive to S857 phosphorylation, showed the same staining pattern among control, HFS, and LTP-induced slices (**Figure 3.12**). This indicates that the change in pS857 Dyn1xa in the LTP-induced slices is caused by a regional dephosphorylation in the distal part of apical dendrites rather than the redistribution of Dyn1. The result also suggests that Dyn1xa is re-phosphorylated at S857 in the cell bodies and the proximal apical dendrites during the transition from HFS to LTP.

The Mnb/Dyrk1A is the primary enzyme phosphorylating Dyn1xa at S857.

Previous work done by Dr. Tatyana Adayev in Dr. Yu-Wen Hwang's lab has shown that Mnb/Dyrk1A is the primary enzyme phosphorylating Dyn1xa at S857 in hippocampal cell lines. I will describe their work on dominant negative (DN) Mnb/Dyrk1A briefly below. Briefly, two types of DN Mnb/Dyrk1A mutants that can inhibit endogenous Mnb/Dyrk1A were constructed and used. The DN property of a kinase-deficient Mnb/Dyrk1A mutant, K188R, has been described

(Yang et al., 2001). The second potential DN mutant, D306N, was constructed based on the analogy of Mnb/Dyrk1A to other kinases (van den Heuvel and Harlow, 1993). These two mutants inhibit the activity of wild-type Mnb/Dyrk1A specifically when co-expressed (**Figure 3.13**).

Subsequently, the consequences of expressing the DN mutants on pS857 in endogenous Dyn1xa was examined in HN2-5 cells, a hippocampal cell line (Banerjee et al., 1993). Transfection of WT Mnb/Dyrk1A produced a large elevation in Mnb/Dyrk1A levels (**Figure 3.14 A**) but only a moderate increase in the level of pS857 (**Figure 3.14 B**). This is understandable, because endogenous Dyn1xa is already highly phosphorylated at S857 (approximately 70 % in HN2-5 cells according to the pS857 Dyn1xa standards). The introduction of either the K188R or the D306N mutant also led to an increase in the level of Mnb/Dyrk1A (**Figure 3.14 A**), but both mutants caused a significant reduction in pS857 (**Figure 3.14 B**). This result demonstrates that Mnb/Dyrk1A is the major enzyme responsible for phosphorylating Dyn1xa S857 in HN2-5 cells. It should be pointed out that neither the K188R nor the D306N mutant affects neuronal differentiation of HN2-5 cells under present assay conditions. (The results described in **Figures 3.13 and 3,14** are unpublished data kindly provided by Dr. Tatyana Adayev).

Mouse hippocampal extracts prepared without phosphatase inhibitors could regain some level of S857 phosphorylation after incubating with ATP and phosphatase inhibitors (**Figure 3.15**). The level of pS857 Dyn1xa reached 37.2 ±

3.1% (n = 3) after 60 min phosphorylation. To demonstrate the involvement of Mnb/Dyrk1A in the phosphorylation of Dyn1xa at S857 in mouse hippocampal extracts, an extract was immunodepleted of Mnb/Dyrk1A by incubating with immobilized anti-Mnb/Dyrk1A antibody. Then its ability to phosphorylate Dyn1xa was evaluated. As controls, hippocampal extracts were also mixed with protein A/G, immobilized antibodies against Dyrk2 and Dyrk3 (all are goat polyclonal antibodies from the same supplier). The hippocampal extract adsorbed with anti-Mnb/Dyrk1A antibody produced lower levels of pS857 than the extracts absorbed with immobilized protein A/G, anti-Dyrk2 or anti-Dyrk3 (**Figure 3.16**). Together with the result of DN mutant in the HN2-5 cell line, these finding indicate that Mnb/Dyrk1A is the primary, if not the only kinase, phosphorylating Dyn1xa at S857 *in vivo*.

Mnb/Dyrk1A is activated by neuronal activities.

Since Mnb/Dyrk1A is the primary kinase phosphorylating Dyn1xa at S857, I examined whether the elevation in pS857 in LTP-induced slices was due to an increase in Mnb/Dyrk1A activity. To examine the kinase activity, Mnb/Dyrk1A was immunoprecipitated from slices and used to phosphorylate a substrate peptide in a direct kinase assay (Huang et al., 2004). The LTP-induced slices showed an increase in Mnb/Dyrk1A activity (150.7 ± 18.0 %, n = 5, $p < 0.05$ vs. the control slices) (LTP-induced in **Figure 3.17**). However, slices stimulated with HFS also exhibited an increase in Mnb/Dyrk1A activity (185.5 ± 19.2 %, n = 4, $p < 0.03$ vs.

the control slices) (HFS in **Figure 3.17**), despite the fact that the HFS group has the lowest pS857 level among all treated slices (HFS in **Figure 3.4 B**). The result indicated that Mnb/Dyrk1A activity was elevated at the beginning of HFS and was apparently not specifically related to LTP-induction. Furthermore, the increase in activity was not due to an increase in the total amount of Mnb/Dyrk1A protein (**Figure 3.18**). This result suggests that the elevation of Mnb/Dyrk1A activity is due to enzymatic activation rather than protein expression.

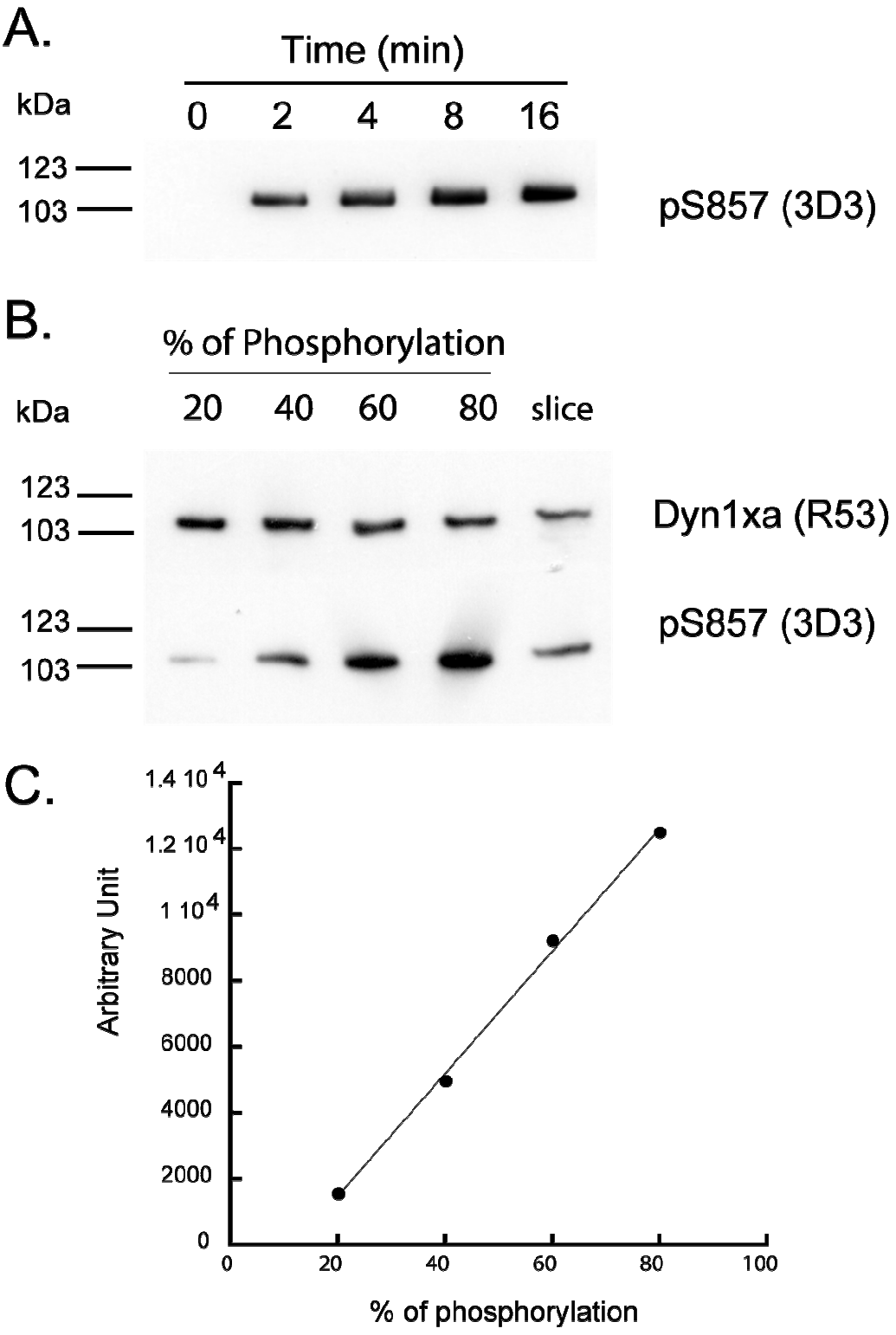

Figure 3.1 Measurement of pS857 Dyn1xa levels. A. *Time-course phosphorylation of purified Dyn1 at S857 by Mnb/Dyrk1A*. Dyn1 was

phosphorylated by Mnb/Dyrk1A as described in Materials and Methods. The reaction was initiated by adding Dyn1 and allowed to proceed at 30 ^{o}C. At the indicated times, an aliquot (50 ng Dyn1 per lane) of the reaction mixture was withdrawn and analyzed for S857 phosphorylation (3D3). **B**. *Analysis of the pS857 level*. Extracts prepared from the nonstimulated control slices (slices) were processed together with four standards with known pS857 level (20-80%). The pS857 level of the unknown was calculated by first deriving the value from the standard curve (3D3) and then corrected for the total level of Dyn1xa (R53). **C**. *Phosphorylation standard curve.* Curve was plotted from the values of pS857 standards. The pS857 levels in the sample (slice in **B**) to be analyzed was calculated based on this curve.

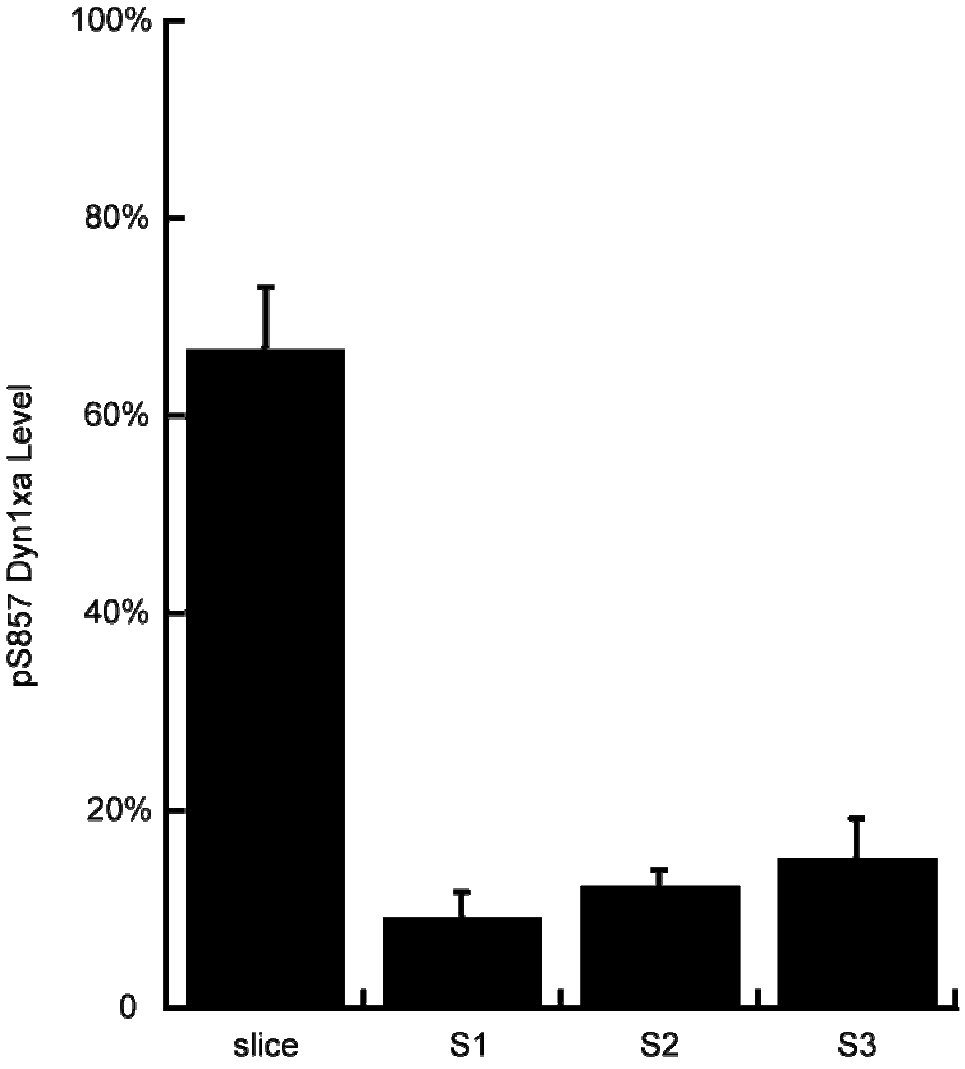

Figure 3.2 pS857 Dyn1xa levels in hippocampus. Extracts (slice) from nonstimulated control slices were prepared in the presence of phosphatase inhibitors as described. Extracts from Synaptosomes incubated in Ringer's solution either without oxygenation (S1) or with oxygenation for different times (S2: 15 min and S3: 60 min) were prepared as described in Materials and Methods. pS857 Dyn1xa levels were determined as described in Figure 3.1. Data represented the average (±SEM) from the total numbers (n) of slices or independent trials. Slice (n=5); S1 (n=3); S2: (n=3); S3: (n=3).

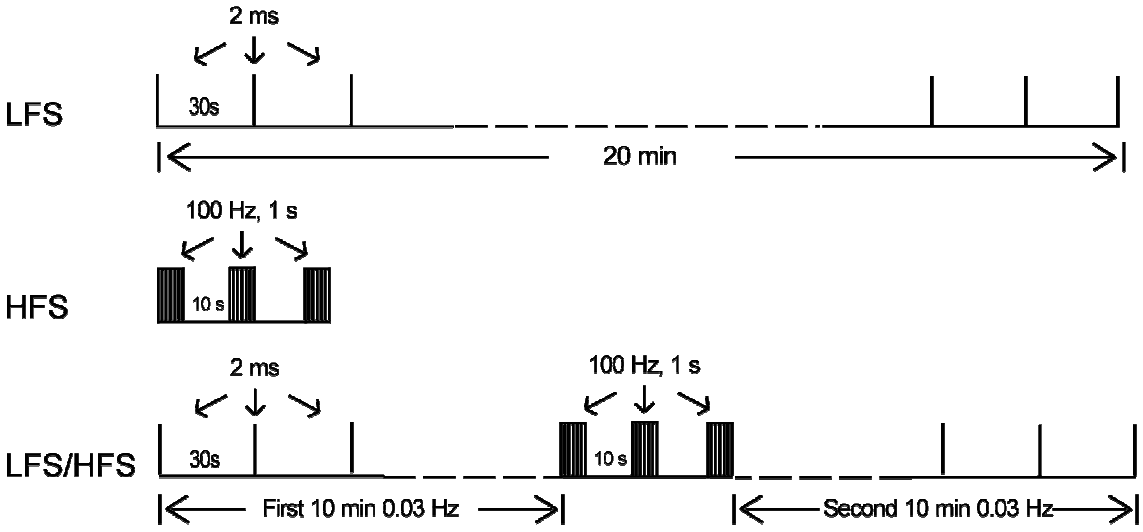

Figure 3.3 Different types of stimulation. The drawings (not to the scale) depict the frequency and duration for each of the stimulations. LFS, 2 ms stimulation was delivered at 30 sec interval for 20 min. HFS, three trains of 100 Hz stimulation for 1s with 10 sec interval. LFS/HFS, two sets of 10 min LFS were sandwiched by one set of HFS.

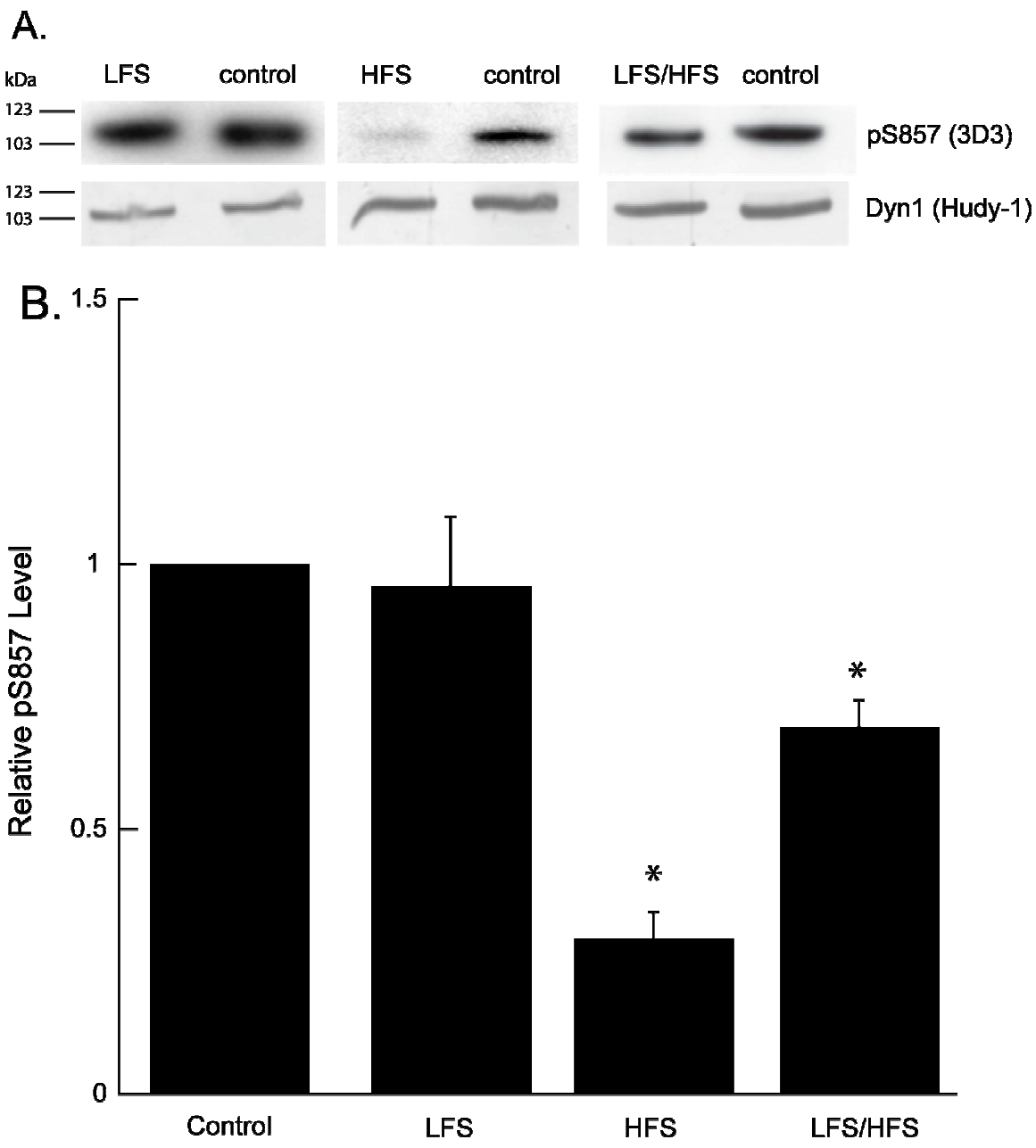

Figure 3.4 Dephosphorylation of pS857 in hippocampal slices upon stimulation. **A** *Typical blots from each assay in B are shown*. **B** *The relative levels of pS857 Dyn1xa in stimulated slices*. Hippocampal extracts from each stimulation group and nonstimulated (control) slices were prepared in the presence of phosphatase inhibitors as described. S857 phosphorylation in each

stimulated slice was determined as a pair with a nonstimulated (control) slice. The relative level of pS857 was then determined by setting the level of pS857 in the control as one. Data represent the average (±SEM) of the total number (n) of slices. LFS (n=6), HFS (n=6) and LFS/HFS (n=17). Star, $p<0.05$.

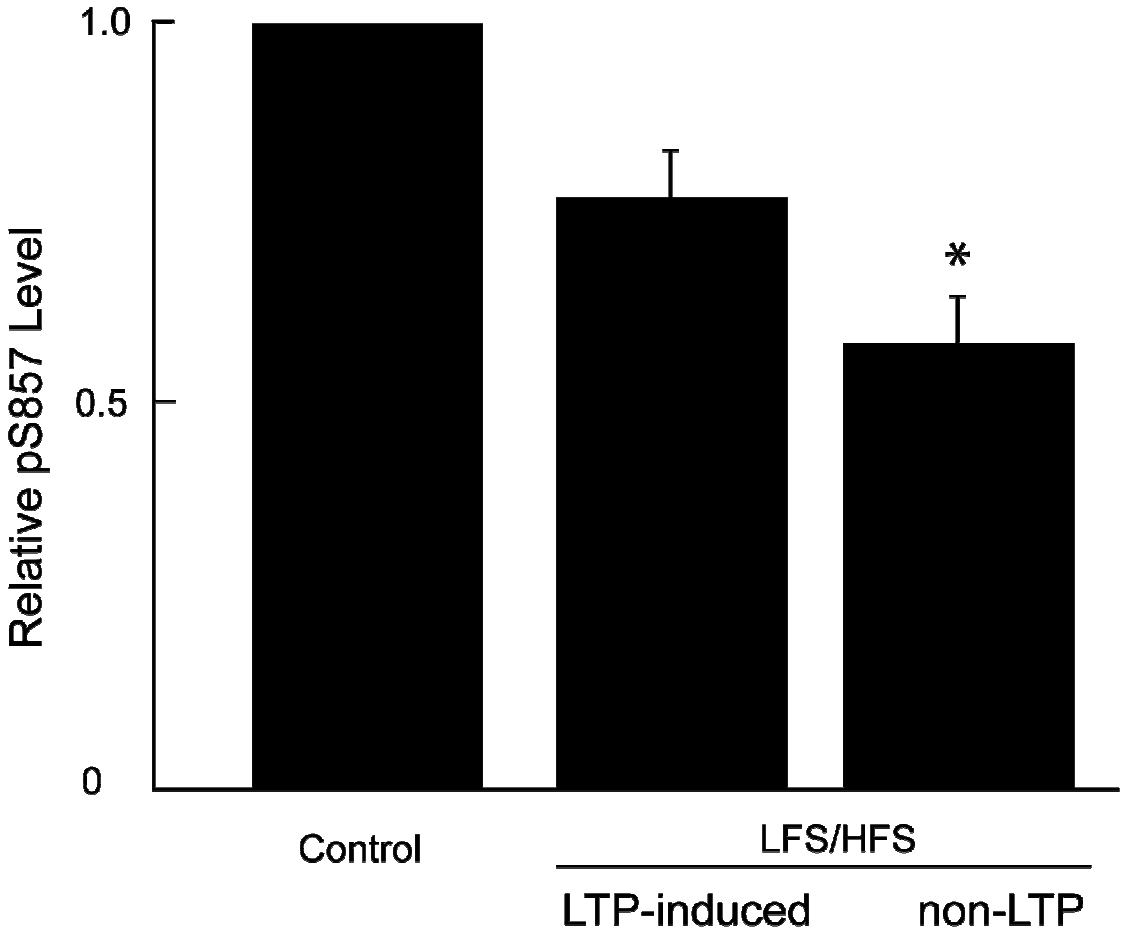

Figure 3.5 Dephosphorylation of pS857 in hippocampal slices upon LTP induction. The LFS/HFS group as shown in Figure 3.4 was sub-divided based on the presence of LTP induction. Data represent the average (±SEM) of the total number (n) of slices. LTP-induced group (n=10) and non-LTP induced group (n=7). Star, $p<0.05$.

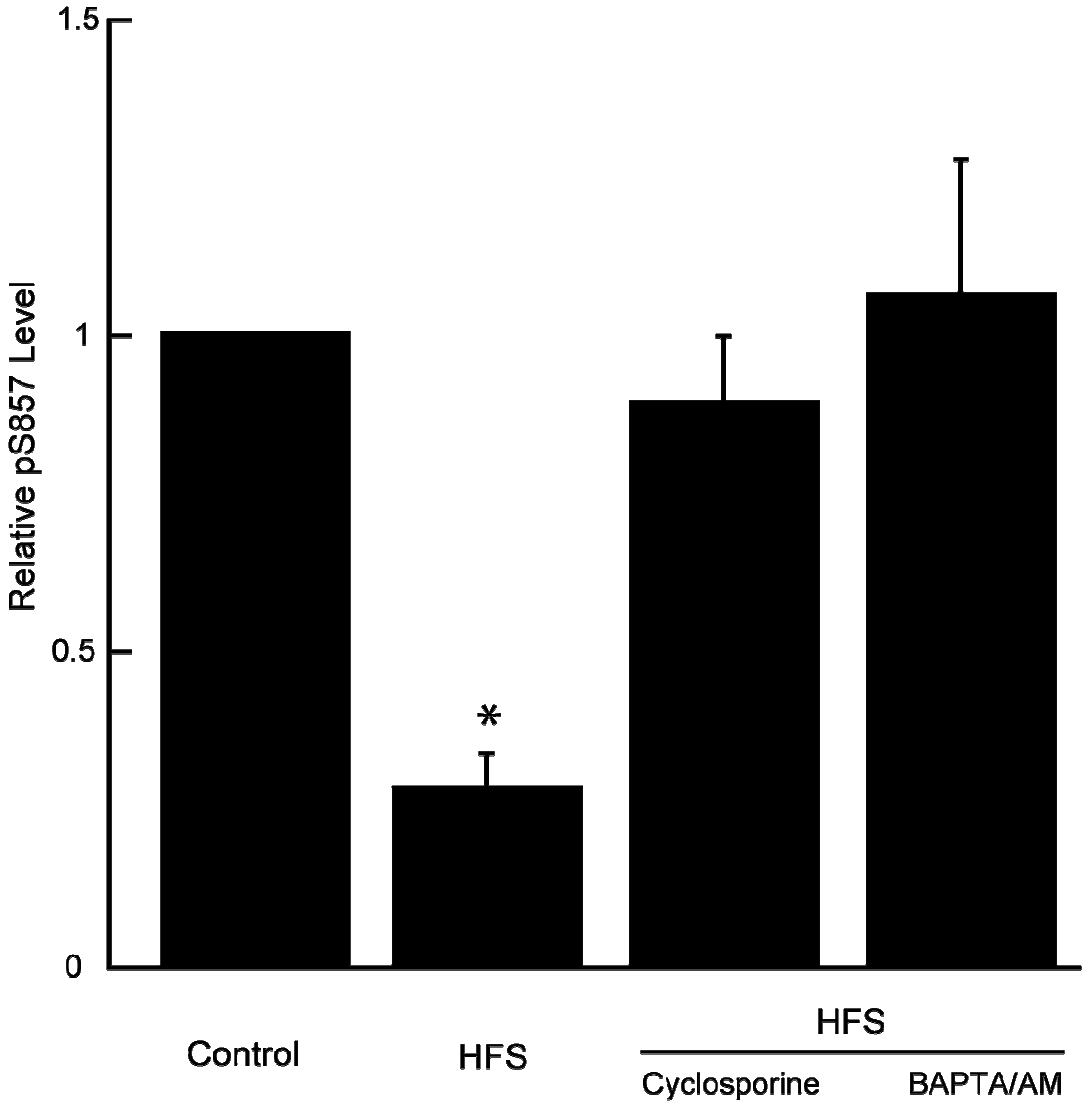

Figure 3.6 Dephosphorylation of pS857 requires Ca^{2+}/Calcineurin. Slices were incubated with the indicated chemical (2 μM cyclosporine or 10 μM BAPTA/AM) in oxygenated Ringer's solution at 33 ^{o}C for 60 min and then stimulated with HFS as described in Figure 3.3. S857 phosphorylation in each group was determined as a pair with a chemical-treated nonstimulated (control) slice. The control was set to one. Data represent the average (±SEM) of the total number (n) of slices. Cyclosporine (n=7) and BAPTA/AM (n=7). HFS was the same data as in Figure 3.4 re-plotted for comparison. Star, $p<0.05$.

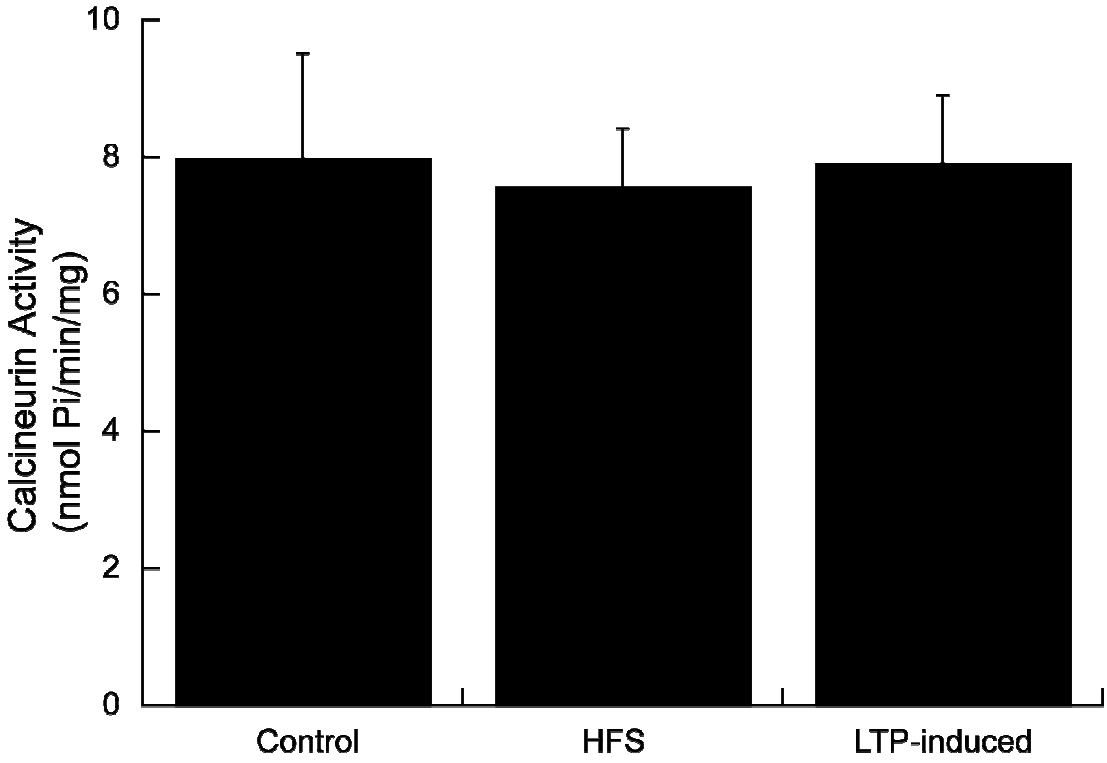

Figure 3.7 Calcineurin activity in slices exposed to different stimulations. Pi-labeled PKA-RII peptide, a calcineurin substrate, was dephosphorylated by hippocampal slice extracts prepared from nonstimulated group (control), HFS group (HFS) and LTP-induced group (LTP-induced). The amount of Pi released in each group was determined by the malachite green assay. Data represent the average (±SEM) of the total number (n) of slices. Control (n=6), HFS (n=6), and LTP-induced (n=6).

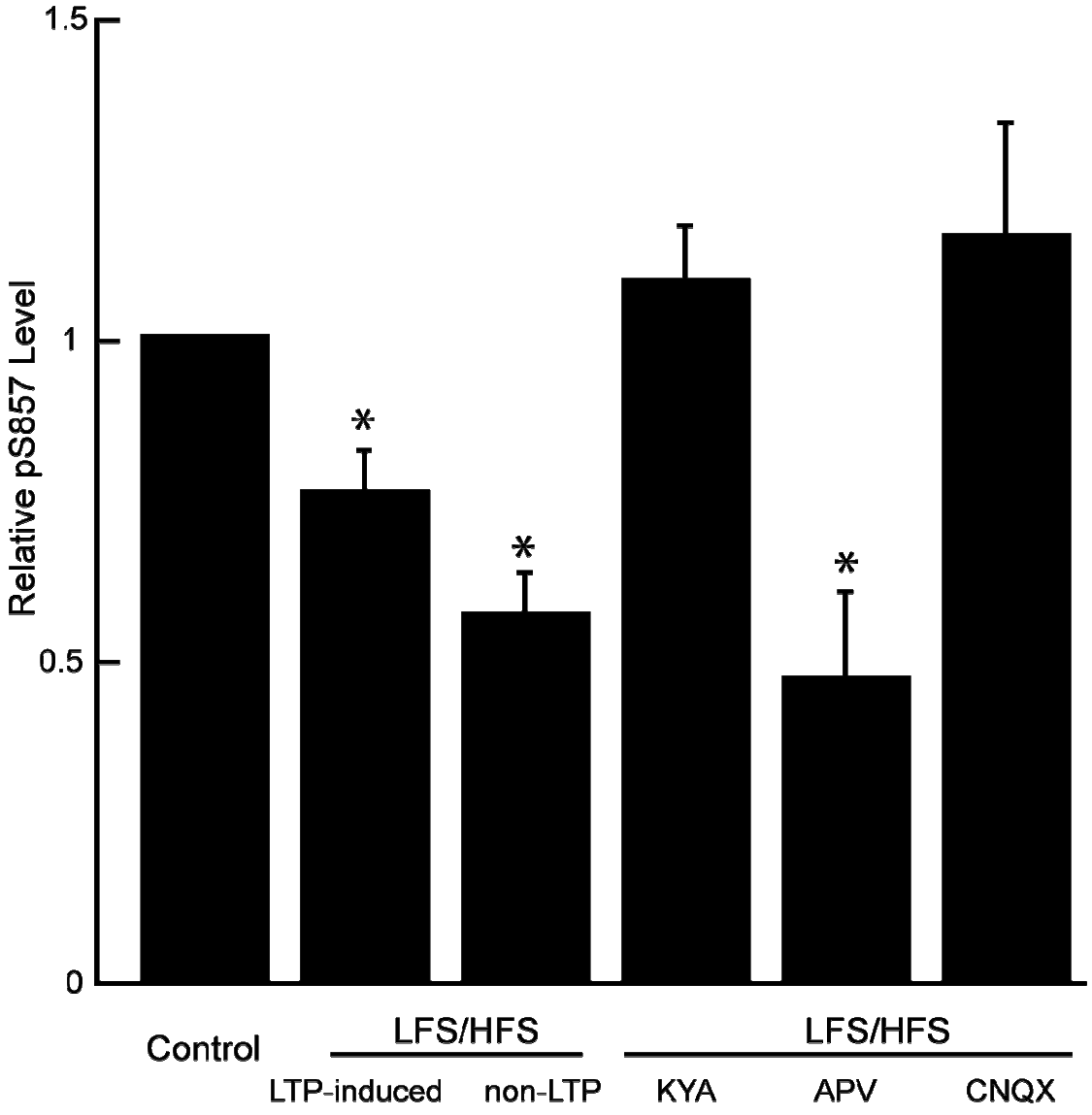

Figure 3.8 Dephosphorylation of pS857 Dyn1xa is mediated by ionotropic glutamate receptors. Slices were treated with the indicated chemicals (2.5 mM for KYA, 50 μM for APV, or 50 μM for CNQX) in oxygenated Ringer's solution at 33 ^{o}C for 60 min and then stimulated with LFS/HFS as described in Figure 3.3. S857 phosphorylation in each group was determined as a pair with a control slice; the control was set to one. Data represent the average (±SEM) of the total

number (n) of slices. KYA (n=6), APV (n=5), and CNQX (n=6). LTP-induced and non-LTP induced groups were the same data as in Figure 3.5 re-plotted for comparison. Star, $p<0.05$.

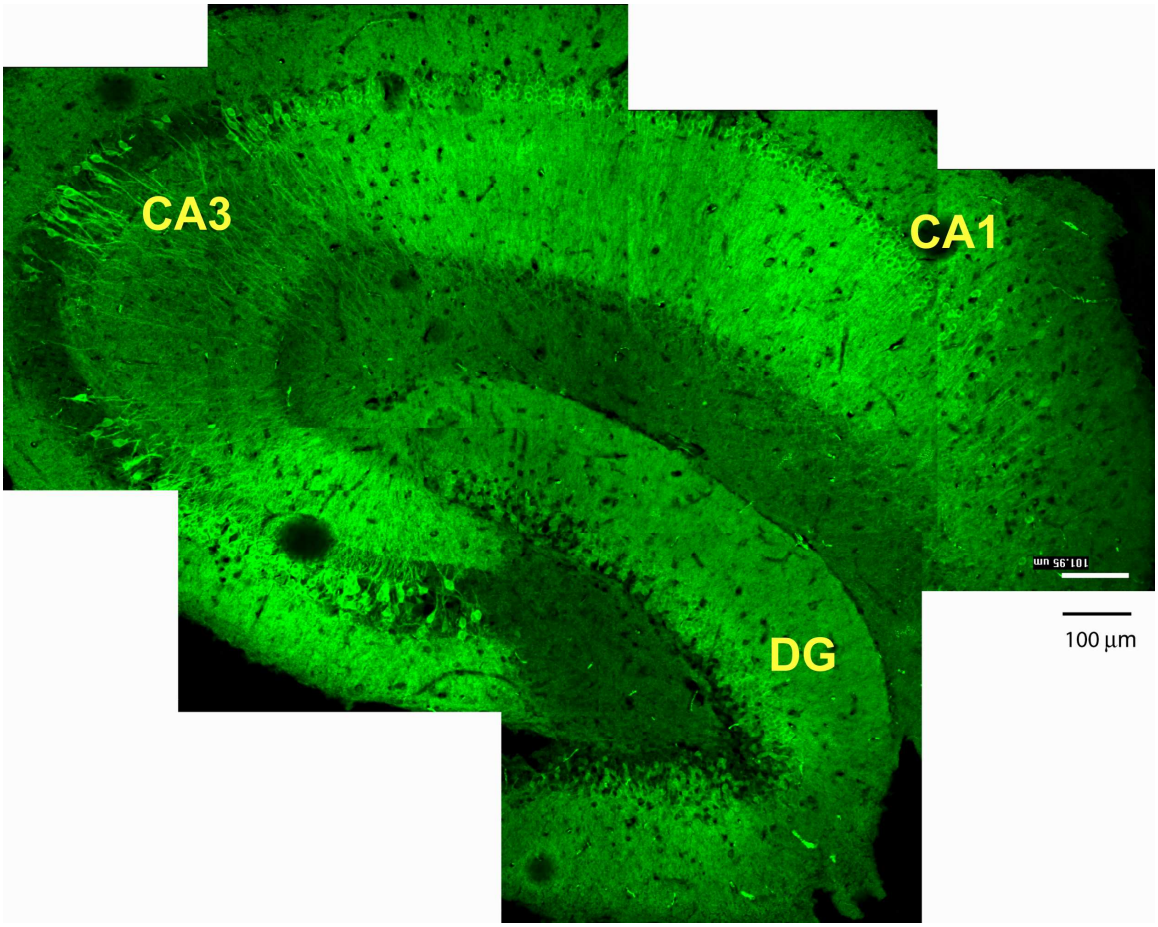

Figure 3.9 Distribution of pS857 Dyn1xa in hippocampus (200 X). A control slice was probed with pS857 Dyn1xa antibody (3D3). A composite of six images taken from different regions of a slice is shown. 3D3 stained both the pyramidal cell bodies and their dendrites. DG, Dentate Gyrus; CA1 and CA3 regions are marked.

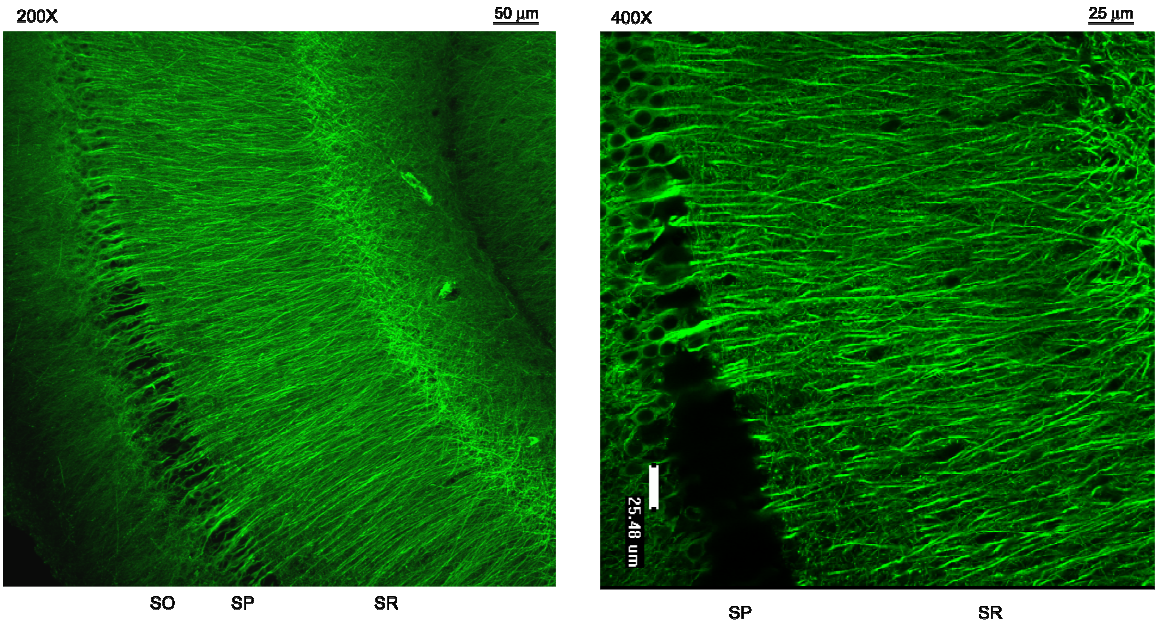

Figure 3.10 Distribution of MAP-2 in the CA1 region of the hippocampus. A control slice was probed with anti-MAP-2 antibody. MAP-2 stained both the pyramidal cell bodies and their dendrites in the CA1 region. Left, 200 X; right, 400 X. SR, stratum radiatum; SP, stratum pyramidale; SO, stratum oriens.

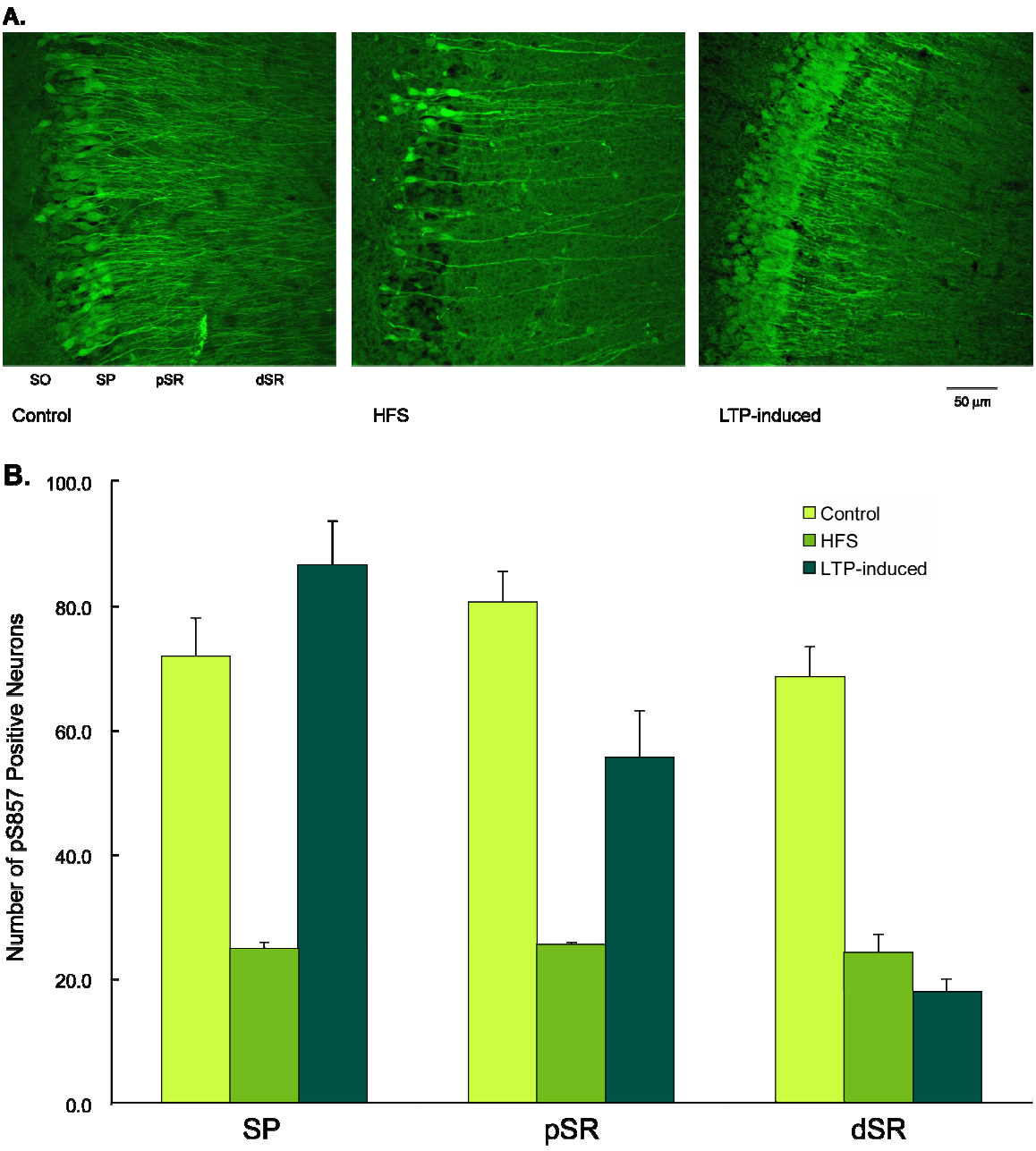

Figure 3.11 Distribution of pS857 Dyn1xa in the CA1 region. A *Pattern of pS857 Dyn1xa distribution*. Slices were stimulated as indicated and then probed with 3D3 to reveal the distribution of pS857 Dyn1xa. Pictures shown are the CA1 region of those slices. Control, nonstimulated slices; HFS, slices with HFS; LTP-induced; slices with LTP induction. SO: stratum oriens; SP: stratum

pyramidale; pSR: proximal portion of stratum radiatum; dSR: distal portion of stratum radiatum; **B** *Quantitative analysis*. The number of pS857 positively staining neurons in the SP area and pS857 positively staining dendrites in proximal and distal portions of apical dendrites (pSR and dSR) was counted in a 90000 μM^2 area of the CA1 region from control, HFS, and LTP-induced groups. Data represent the average (±SEM) of three slices from each group.

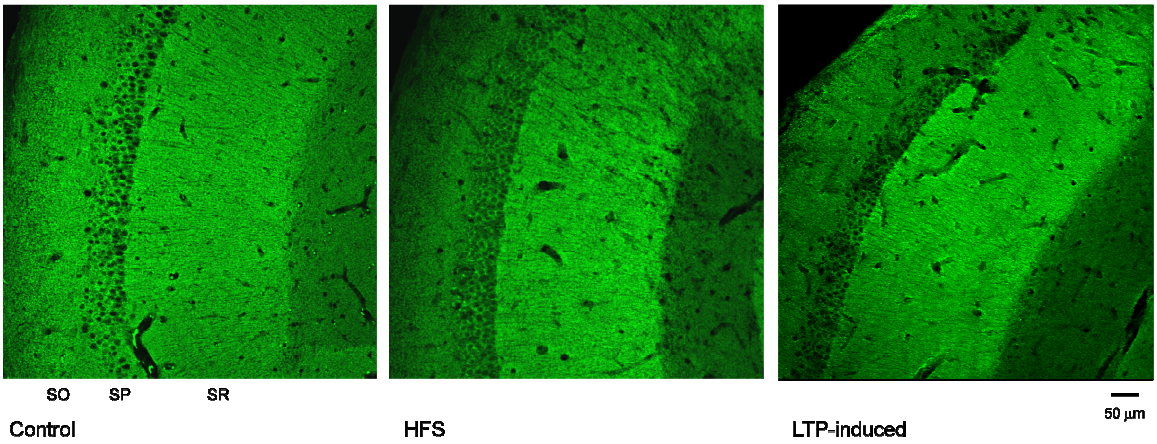

Figure 3.12 Distribution of total Dyn1 in the CA1 region. Slices were stimulated as indicated and then probed with Hudy-1 to reveal the distribution of Dyn1. Pictures shown are the CA1 region of those slices. Control, nonstimulated slices; HFS, slices with HFS; LTP-induced; slices with LTP induction. SR, stratum radiatum; SP, stratum pyramidale; SO, stratum oriens.

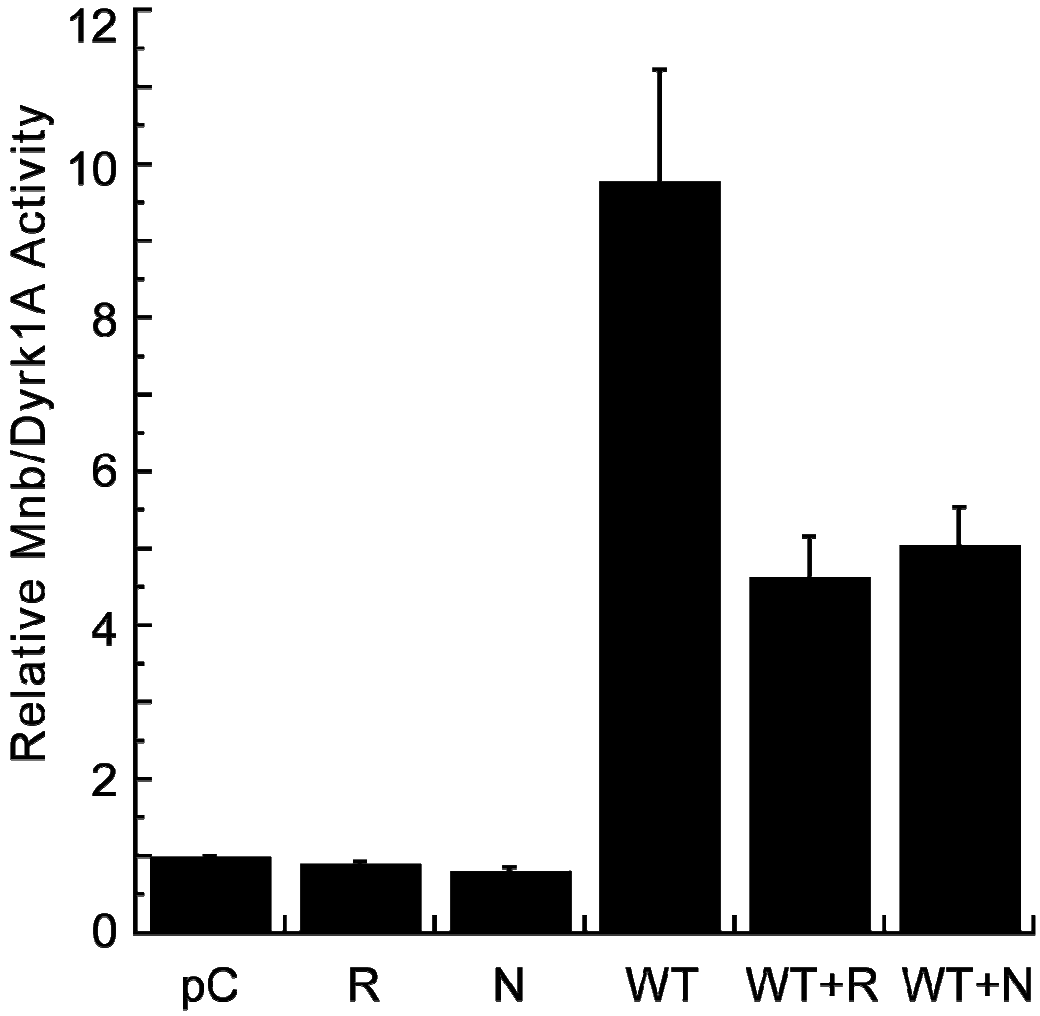

Figure 3.13 Specificity of the Mnb/Dyrk1A DN mutants. Two different Mnb/Dyrk1A DN mutants (K188R and D306N) were constructed. HN2-5 cells were transfected with the plasmids as indicated. The relative Mnb/Dyrk1A activity (normalized to vector transfection, pC) was determined in the transfected cells as described. Data represent the average (±SEM) of three independent trials. DN, dominant negative; pC, pCDNA3, the cloning vector; R, Mnb/Dyrk1A-K188R; N, Mnb/Dyrk1A-D306N; WT, Wild-type Mnb/Dyrk1A.

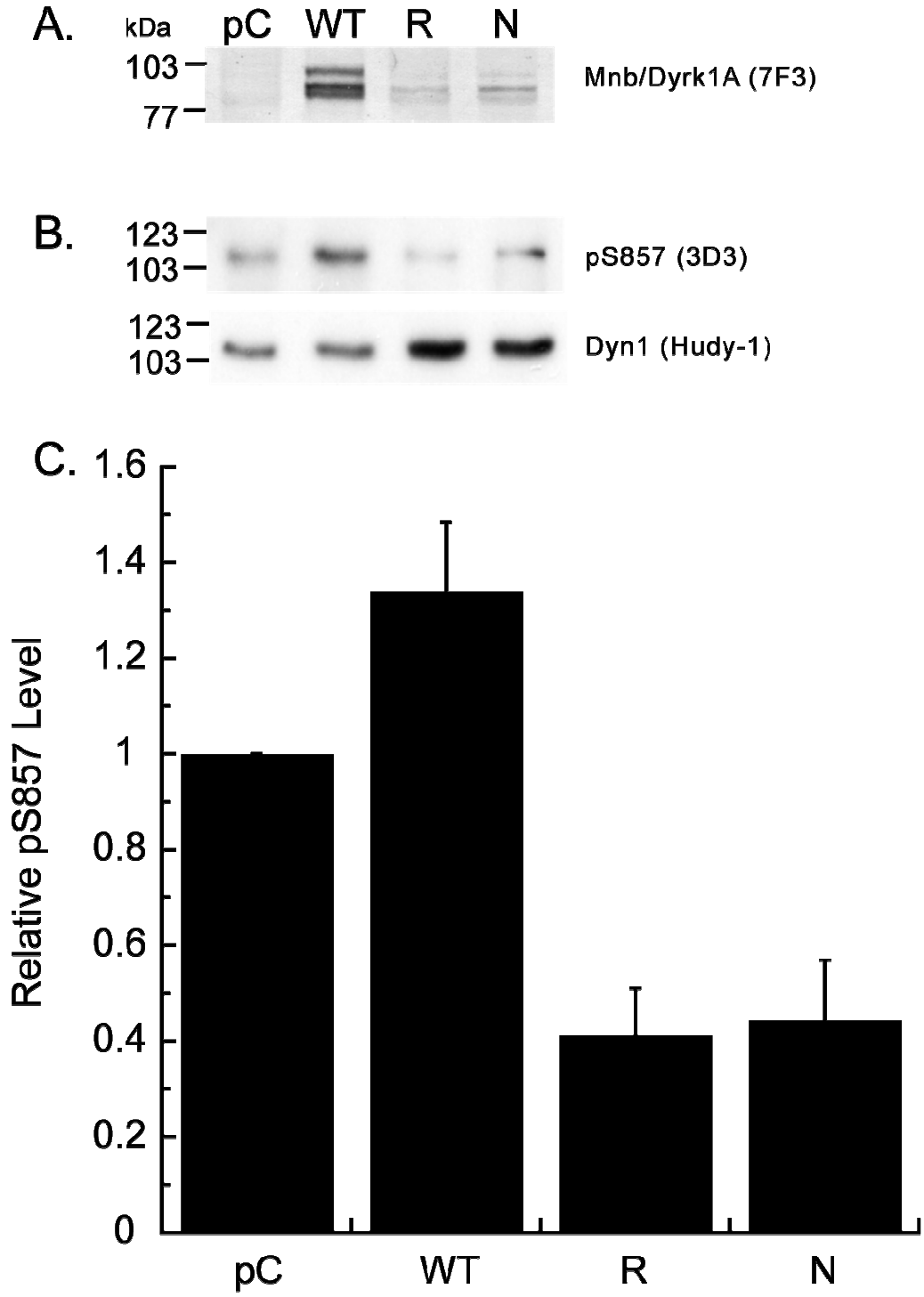

Figure 3.14 Inhibition of endogenous S857 Dyn1xa by Mnb/Dyrk1A DN mutants in HN2-5 cells. **A** *Mnb/Dyrk1A expression*. HN2-5 cells were

transfected with the plasmids as indicated and then analyzed for the level of Mnb/Dyrk1A in Western blotting against antibody 7F3. **B** *Analysis of Dyn1*. Endogenous Dyn1 was immunoprecipitated from extracts of transfected cells and the levels of pS857 Dyn1xa (3D3) and total Dyn1 (Hudy-1) were determined as described. **C** *Relative pS857 Dyn1xa level*. Data represent the average (±SEM) of three independent trials. DN, dominant negative; pC, pCDNA3; R, Mnb/Dyrk1A-K188R; N, Mnb/Dyrk1A-D306N; WT, Wild-type Mnb/Dyrk1A.

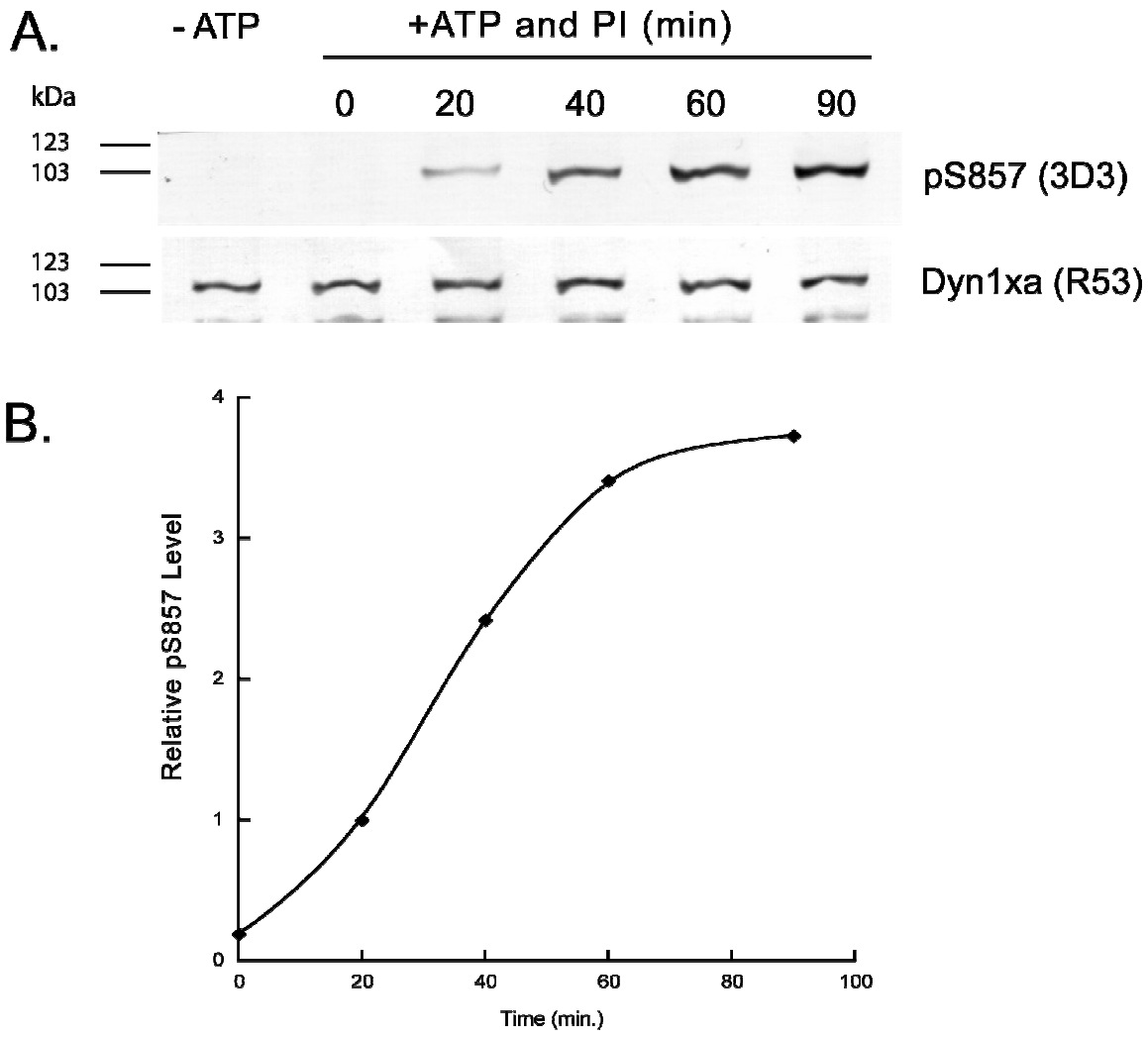

Figure 3.15 Time-course *in vitro* phosphorylation in hippocampus. A. *S857 Dyn1xa phosphorylation.* Hippocampal extracts prepared without phosphatase inhibitors were incubated either without ATP (-ATP) or with ATP and phosphatase inhibitors (+ATP and PI). The phosphorylation level at different times (0, 20, 40, 60, 90 min) was determined using pS857 Dyn1xa antibody 3D3. The same samples were also immuno-blotted with Dyn1xa antibody R53 as loading controls. **B.** *Time course phosphorylation curve*. The relative level of pS857 Dyn1xa (normalized to time 20) was shown.

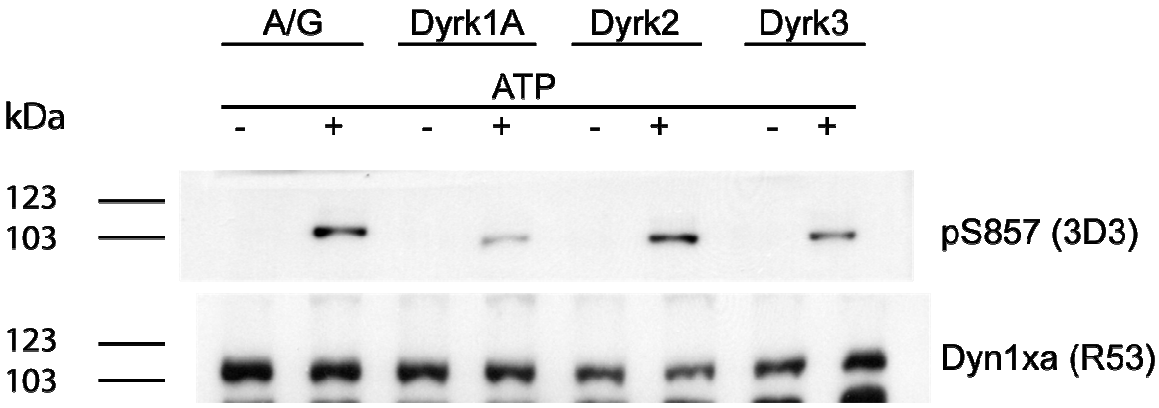

Figure 3.16 Immunodepletion of Mnb/Dyrk1A in hippocampus reduces the level of S857 phosphorylation. Hippocampal extracts prepared without phosphatase inhibitors were first absorbed with antibody coated protein A/G (Mnb/Dyrk1A, Dyrk2 or Dyrk3). Extracts absorbed with immobilized protein A/G (A/G) were used as an absorption control. Each immunodepleted sample was split in half. One half was incubated with ATP and phosphatase inhibitors (+ATP) to initiate *in vitro* phosphorylation and the other half was incubated without ATP and phosphatase inhibitors (-ATP) as the negative control. The level of pS857 Dyn1xa and total Dyn1xa was determined with antibodies 3D3 and R53, respectively.

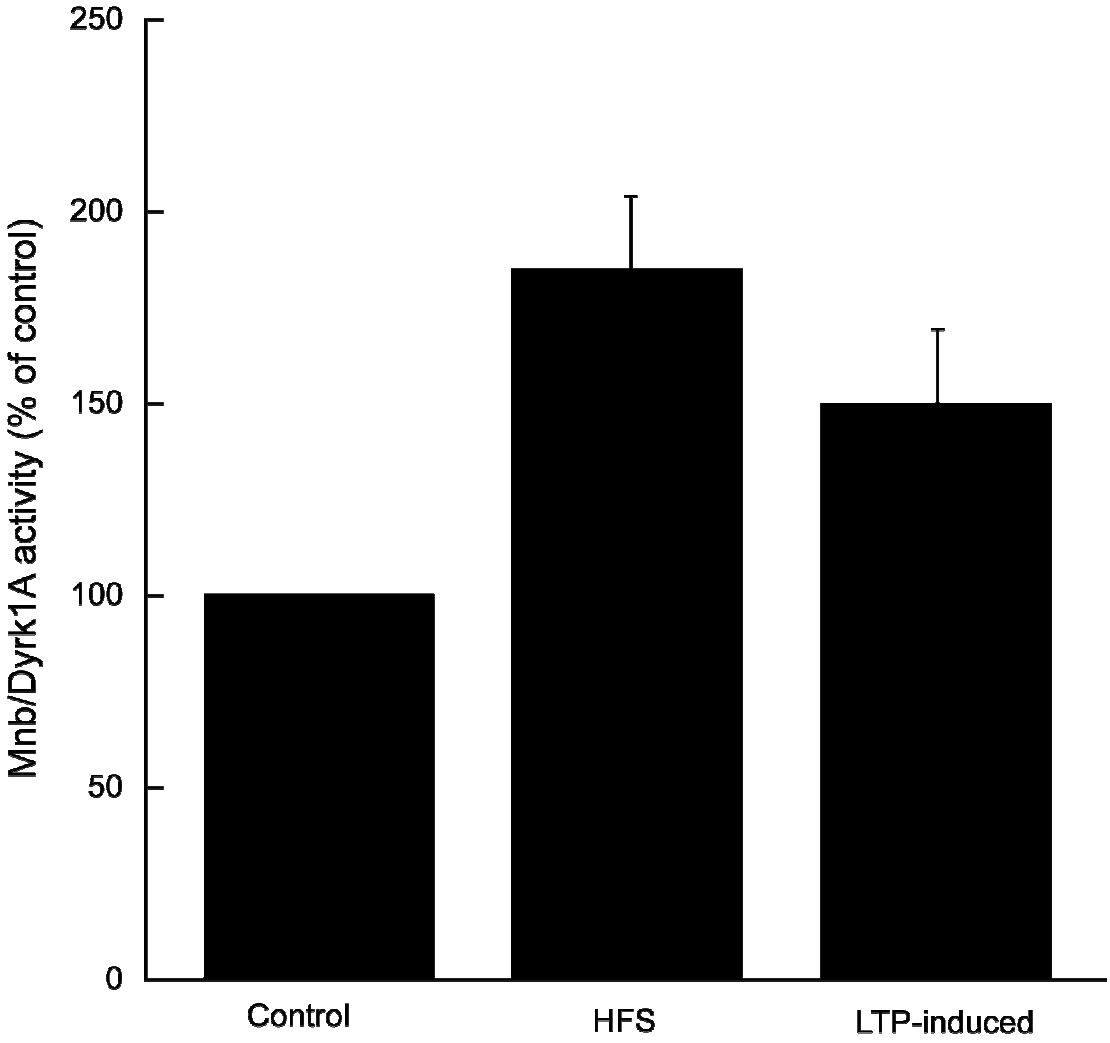

Figure 3.17 Mnb/Dyrk1A activity in slices exposed to different stimulations. Slices were stimulated as described. Mnb/Dyrk1A was then immunoprecipitated from slice extracts and used to phosphorylate dynatide 3. The relative activity of Mnb/Dyrk1A (normalized to the control slices) was determined in HFS and LTP-induced group. Data represent the average (±SEM) of total number (n) of slices. HFS (n=4) and LTP-induced (n=5).

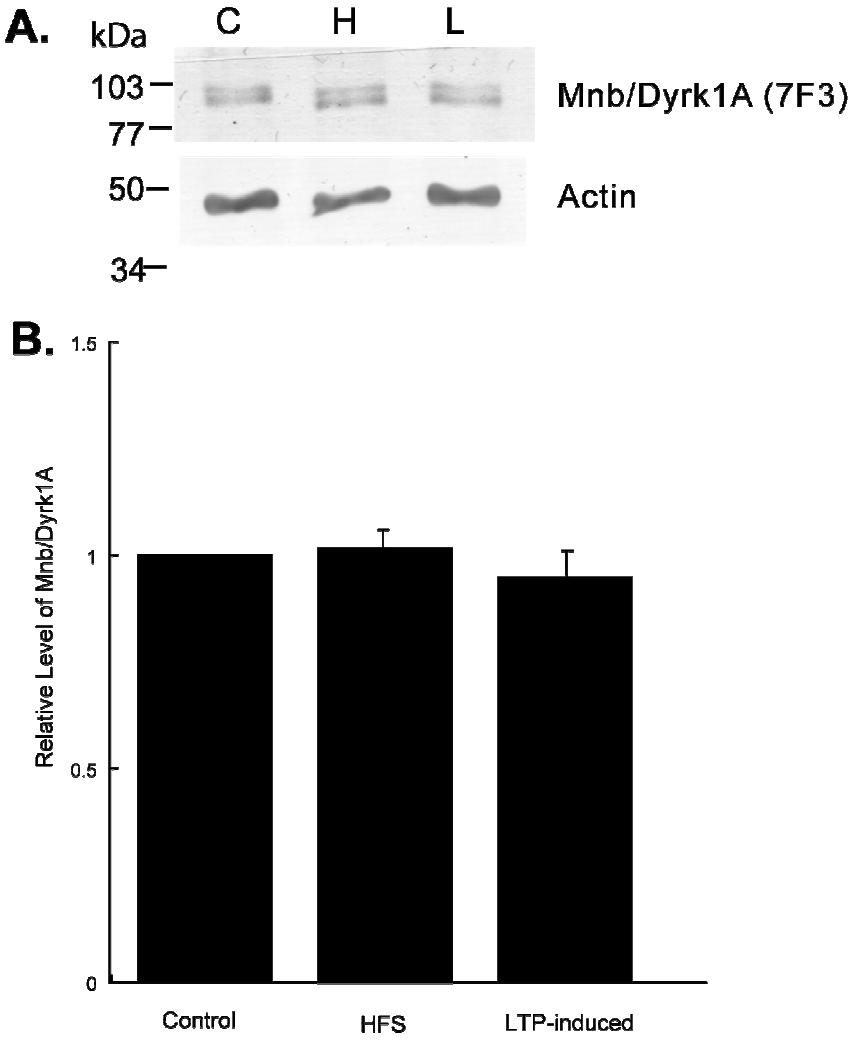

Figure 3.18 Expression level of Mnb/Dyrk1A in slices exposed to different stimulation. **A**. *Mnb/Dyrk1A expression in stimulated slices.* Extracts from Control, HFS and LTP-induced slices were probed with Mnb/Dyrk1A antibody 7F3. The same extracts were also probed with actin antibody as a loading control. C, control slice; H, HFS slice; L, LTP-induced slice. **B**. *The relative levels of Mnb/Dyrk1A*. The relative Mnb/Dyrk1A level (normalized to the control slices) was determined in the HFS and LTP-induced group. Data represent the average (±SEM) of three slices from each group.

CHAPTER 4

Discussion

Dyn1 cycles between phosphorylation and dephosphorylation states in response to membrane potential (Robinson et al., 1987; Huang et al., 2004). Together with its function in endocytosis (Praefcke and McMahon, 2004), a role of Dyn1 phosphorylation in synaptic activity is suggested. This study focused on the S857 found only in Dyn1xa isoforms (Chen-Hwang et al., 2002), one of several Dyn1 phosphorylation sites identified *in vitro* and *in vivo*. It was shown previously that the level of S857 phosphorylation changed with membrane potential in a neuronal cell line (Huang et al., 2004). Here, I determined the regulation of Dyn1xa S857 phosphorylation in hippocampal neurons.

Dyn1xa S857 is highly phosphorylated in the hippocampal slices (**Figure 3.1-2**). The pS857 level is dependent not only on electrical stimulation (**Figure 3.4**) but also on neuronal activity (**Figure 3.5**). S857 dephosphorylation upon stimulation requires calcium/calcineurin (**Figure 3.6**) and is mediated through AMPA/Kainate glutamate receptors (**Figure 3.8**). The immunohistochemical study confirms the HFS-promoted dephosphorylation and reveals a redistribution of pS857 in response to LTP induction (**Figure 3.11-12**). S857 of Dyn1xa is primarily phosphorylated by Mnb/Dyrk1A (**Figure 3.13-16**). The activity of Mnb/Dyrk1A is also regulated by neuronal activity (**Figure 3.17-18**).

Choice of Synapses:

Synapses in CA3-CA1 regions of mouse hippocampus were chosen for the study. This pathway is a well characterized and widely used model system for investigating the mechanisms of learning and memory at molecular level. The hippocampal slice has a stereotyped circuit diagram in which these connected areas are easy to spot under microscope (**Figure 2.2 B**). Although the depolarization areas on the slices are tiny, the stimulation can actually evoke action potentials all the way along the pyramidal cell line. This wide ranging effect makes the biochemical detection of the whole slices possible. In addition, a much higher pS857 level is found in hippocampal slices compared to other systems such as synaptosomes (**Figure 3.2**), making the slices a better system for investigating the phosphorylation / dephosphorylation of Dyn1. Although slice transfer from the electrical stimulation chamber to dry ice or fixation buffer for the further biochemical processing may take some time, this delay (within 5 second) is much shorter than the time of Dyn1 rephosphorylation (more than 1 minute) (Robinson et al., 1987). The relative slow rephosphorylation allows the accurate detection of Dyn1 dephosphorylation upon stimulation.

Specificity of antibodies:

In this study, pS857 Dyn1xa was recognized by mouse monoclonal antibody 3D3. 3D3 was produced (Huang et al., 2004) (**Figure 2.1**) by using

Mnb/Dyrk1A-phosphorylated Dynatide 3, a peptide containing S857 of Dyn1xa, as the antigen. 3D3 is highly selective for the Mnb/Dyrk1A-phosphorylated dynatide 3 and Dyn1xa. It has no reactivity against un-phosphorylated dynatide 3 and Dyn1xa. Immunocytochemical staining of a hippocampal cell line showed the staining of 3D3 co-localizes with that of Hudy-1, a well-characterized anti-Dyn1 antibody (unpublished observation by Dr. Tatyana Adayev).

The Dyn1xa isoform of Dyn1 was also recognized by rabbit antibody R53. R53 was raised using an non-phosphorylated Dyn1xa-specific peptide (PSRSGQASPSR) (**Figure 2.1**) as the antigen. Antibody R53 is specific for Dyn1xa and its reactivity with Dyn1xa is not affected by S857 phosphorylation (unpublished observation by Dr. Yu-Wen Hwang).

S857 phosphorylation in resting stage:

S857 of Dyn1xa is highly phosphorylated in resting hippocampal slices with approximately 70 % of total (endogenous) Dyn1xa containing pS857. The determination of this value was achieved by a combination of two immunoblots with pre-determined phosphorylation standards. So far, this is the first time that the near-absolute level of dynamin phosphorylation (at any given site) *in vivo* has been assessed. Immunohistochemical staining also reveals that pS857 Dyn1xa is present in most neurons of hippocampal slices. The involvement of a large

majority of endogenous Dyn1xa suggests that S857 phosphorylation is a physiological event.

S857 phosphorylation during neuronal activity:

The physiological significance of S857 phosphorylation is further strengthened by the finding that pS857 is dynamically regulated by neuronal activity. LFS, which excites the pre-synaptic neurons and subsequently depolarizes the post-synaptic neurons in the CA3-CA1 pathway, doesn't change the level of S857 Dyn1xa phosphorylation. While this finding seems to contradict the result that Dyn1 is dephosphorylated upon depolarization, is should be remembered that each stimulation in LFS lasts for only 2 millisecond. Thus, LFS is probably not intense enough to induce a detectable dephosphorylation in the whole slice. Also since the dephosphorylation is transient and lasts less than 2 seconds (Robinson et al., 1987), a slow but full rephosphorylation during the 30-sec interval between stimulations in LFS probably keeps the phosphorylation seemingly unchanged.

HFS causes short-term, intense membrane depolarization. This type of stimulation, which is used to induce LTP, immediately causes a 70 % reduction in pS857 levels in tissue lysates and a drastic decrease in total number of pS857 Dyn1 positive neurons. Ca^{2+}/calcineurin are required for Dyn1 dephosphorylation. The involvement of Ca^{2+}/calcineurin is consistent with previous findings. One, a

rapid elevation of Ca^{2+} from the proximal to the distal parts of apical dendrites was observed upon HFS (Regehr and Tank, 1992); and second, calcineurin is expressed in CA1 region, especially in the apical dendrites of pyramidal neurons (Morioka et al., 1997). Therefore, this overall dephosphorylation probably occurs via a Ca^{2+} influx throughout the pyramidal neurons and a subsequent activation of calcineurin over a wide area.

The pS857 level in LFS/HFS exposed slices was significantly greater than that in HFS slices. This was particularly evident for slices expressing LTP and indicates that it is not the electrical stimulation itself, but the neuronal activity induced by LFS/HFS which correlates with the state of S857 phosphorylation. In addition, since all LTP-induced slices were previously exposed to HFS (**Figure 3.3**), it is reasonable to assume that the pS857 Dyn1xa in LTP-induced slices represents a progression from that of slices stimulated only by HFS.

Similar to the results of immunoblotting, the results from the immunohistochemistry studies further confirm that there are higher levels of pS857 in the LTP-induced slices than that in the HFS-stimulated slices. The distribution pattern of pS857 Dyn1xa in the LTP-induced slices sharply contrasts to that of resting and HFS slices. Since there is no evidence to support that Dyn1 redistributes, the patterns of pS857 Dyn1xa in the LTP-induced slices must result from Dyn1xa rephosphorylation with the exception of those proteins located in the

distal apical dendrites, the region forming synapses with the impinging axons of the CA3 neurons.

Mnb/Dyrk1A and S857 phosphorylation:

Although it has not been directly demonstrated, the results obtained from comparable systems, hippocampal cell lines and phosphorylated (hippocampal) extracts, indicate that Mnb/Dyrk1A is likely the primary enzyme phosphorylating Dyn1xa S857 in the hippocampus (**Figure 3.13-16**).

Mnb/Dyrk1A is activated upon HFS and remains activated during LTP, even though Dyn1xa shows an overall reduction in pS857 in both HFS and LTP-induced slices. In HFS-stimulated slices, the reduction of pS857 despite Mnb/Dyrk1A activation is most likely due to a much quicker activation of calcineurin as a result of a transient and large amount of Ca^{2+} influx. Although the increased Mnb/Dyrk1A activity is maintained during a subsequent progression from HFS to LTP, the level of increase (~ 50%) is small and is probably not sufficient to solely account for the large scale rephosphorylation if cytoplasmic Ca^{2+} is not dissipated. Thus, it is most likely that the apparent distribution pattern of pS857 Dyn1xa during LTP reflects the elevation of Mnb/Dyrk1A activity as well as the re-distribution of cytoplasmic Ca^{2+}.

Ca^{2+}/Calcineurin and S857 dephosphorylation:

S857 dephosphorylation depends on both Ca^{2+} and calcineurin (**Figure 3.6)**. It is interesting that the Ca^{2+} accumulation upon HFS is not evenly distributed in the apical dendrites (Regehr and Tank, 1992) The areas showing greater Ca^{2+} elevation spatially match the areas where pS857 Dyn1xa is dephosphorylated during LTP. Since the rise and fall of cytoplasmic Ca^{2+} in response to stimulation is extremely rapid and may only takes a few seconds (Alford et al., 1993), it is likely that a relative slow rephosphorylation of Dyn1 in LTP-induced slices reflects the previous cytoplasmic distribution of Ca^{2+} in apical dendrites.

The transient activation of calcineurin that occurs during the Ca^{2+} influx upon HFS has been documented (Lu et al., 2000). However, I was unable to detect a change in calcineurin activity in slices exposed to different stimulations. This failure is probably due to limitations of the technique. Since the activation of calcineurin is transient and highly dependent on Ca^{2+}, the best way to monitor calcineurin activity is in live neurons. The method used in this study actually measured the total amount of calcineurin from each slice. The results only suggest that no additional calcineurin is delivered or synthesized upon HFS and LTP induction.

Receptors and S857 dephosphorylation:

Since LTP induction in the Schaffer Collateral-CA1 pathway is triggered by post-synaptic Ca^{2+} elevation, Dyn1xa dephosphorylation at S857 could be one of the downstream processes of calcium signaling for the induction and maintenance of LTP. NMDAR mediated Ca^{2+} influx into post-synaptic neurons is believed to be the main source of synaptically evoked Ca^{2+} transients. However, the finding that dephosphorylation of Dyn1xa S857 during LTP is not affected by an NMDAR antagonist but is mediated by AMPA/Kainate receptors indicates the involvement of mechanism(s) other than the NMDAR participation. There are several possible mechanisms (**Figure 4**).

1. AMPAR hypothesis: Ca^{2+} influx through AMPARs activates calcineurin and dephosphorylates S857.

Increasing evidence shows that LTP is expressed as an increase AMPAR response to HFS, which is part of postsynaptic modifications. AMPARs, which are permeable to Na^{+} and K^{+}, mediate fast synaptic transmission at excitatory synapses in the CNS, including hippocampal circuits. An increase in the number of synapses labeled with AMPAR, but not with NMDAR, is found in the adult rat hippocampus after HFS-induced LTP (Moga et al., 2006). The activity-dependent changes in AMPAR function after LTP induction may also include changes of

each channel conductance (Benke et al., 1998) or changes of the receptor number (Andrasfalvy and Magee, 2004).

AMPARs are tetrameric assemblies of subunits GluR1–4, which are encoded by separate genes and differentially expressed throughout the CNS (Dingledine et al., 1999). It has been shown that AMPARs containing GluR2 are impermeable to Ca^{2+}, while AMPARs lacking GluR2 are permeable to Ca^{2+} (Jonas et al., 1994). Since the principal neurons in the hippocampus express GluR2-containing Ca^{2+} impermeable AMPARs (Geiger et al., 1995), the S857dephosphorylation in LTP-induced slices seems unlikely to be mediated by a Ca^{2+} influx through AMPARs. However, the subunit composition and Ca^{2+} permeability of AMPARs are not static but dynamically remodeled in response to neuronal activity. LTP in CA1 pyramidal neurons has been shown to cause an immediate switch from GluR2-containing Ca^{2+} impermeable AMPARs to GluR2-lacking Ca^{2+} permeable AMPARs upon HFS and the existence of Ca^{2+} permeable AMPARs can last for about 25 minutes (Plant et al., 2006).

In addition, AMPAR distribution along the apical dendrites corresponds to the distribution of pS857 Dyn1xa after LTP-induction. It has been shown that AMPARs expression in CA1 pyramidal neurons is higher in the distal part than in the proximal part of apical dendrites, while synaptic NMDARs expression does not change with distance from soma (Nicholson et al., 2006). In addition, HFS can induce the movement of AMPAR to the surface of dendritic shafts and dendritic

spines (Shi et al., 1999). Together, Ca^{2+} influx through AMPARs, specifically the Ca^{2+} permeable AMPARs, which are physiologically expressed during LTP, could be the one of the pathways leading to S857 dephosphorylation in LTP. Also the dynamic distribution of AMPAR during LTP is consistent with the distribution pattern of pS857 in LTP-induced slices.

2. VGCC (Voltage-Gated Calcium Channel) hypothesis: Ca^{2+} influx through VGCC activates calcineurin and dephosphorylates S857.

VGCCs mediate calcium influx in response to membrane depolarization and regulate various intracellular processes including neurotransmission and synaptic plasticity. There are several different types of VGCC in neurons, muscle and endocrine cells, which are classified based on their response to specific antagonists (Dolphin, 2006). In the hippocampus, VGCC and NMDAR coexist and account for different types of LTP (Grover and Teyler, 1990; Huang and Malenka, 1993). For instance, LTP induced by a tetanic stimulation, 200 Hz trains for 0.5 s with 5 s interval (Little et al., 1995) (which is quite different from the HFS using in this study), requires an increase of intracellular post-synaptic calcium concentration (Grover and Teyler, 1990). This L-type VGCC dependent LTP turns out be NMDA independent (Huber et al., 1995).

Therefore, it is possible that VGCC could be activated by depolarization mediated through AMPA/Kainate receptors with blocked NMDAR, even though

Ca^{2+} influx through VGCC is unable to induce LTP. In contrast, no Ca^{2+} channel would open in the presence of AMPA/Kainate receptors antagonist. This would explain the unchanged pS857 level following the blocking of AMPA/Kainate receptors.

3. CRIS (Calcium release from Intracellular Storage) hypothesis: Ca^{2+} released from intracellular storage activates calcineurin and dephosphorylates S857.

The endoplasmatic reticulum (ER) which forms a continuous network in dendritic shafts as well as dendritic spines, is one of the sites for neuronal calcium storage. The release of calcium from the ER can be triggered by the activation of two classes of receptors: the ryanodine receptor (RyR) and the inositol 1,4,5-trisphosphate (IP_3)-gated receptor (IP_3R) (Rose and Konnerth, 2001). At excitatory synapses, the RyR is activated by calcium influx through ionotropic glutamate receptors or VGCCs (Calcium Induced Calcium Release, CICR) and releases calcium. IP_3Rs are activated by IP_3 produced with the binding of glutamate to metabotropic receptors (mGluRs).

In NMDAR antagonist treated slices, calcium influx through channel(s) other than NMDAR or activation of mGluR could induce calcium release from calcium stored in the ER and keep calcineurin activated during stimulation. This would explain the S857 dephosphorylation upon blocking of NMDAR. The calcium

concentration contributed by CRIS will still be below the threshold to induce LTP. It is consistent with the finding that calcium release from storage does not contribute significantly to synaptic calcium transients in dendrite spines of acute hippocampal slices (Mainen et al., 1999). In AMPA/Kainate receptors antagonist treated slices, however, no calcium influx or release from intracellular storage is induced without basal synaptic transmission. Thus the S857 phosphorylation remains unchanged. Further, calcium release in CA1 pyramidal neuron spines and dendrites probably occurs through different mechanisms because of the differential distributions of RyRs and IP_3Rs. The ER in dendritic shafts is equipped with both receptor types, whereas dendritic spines are devoid of IP_3Rs but possess RyRs (Svoboda and Mainen, 1999). This might account for the distribution pattern of pS857 in LTP-induced slices.

4. KAR (Kainate receptors) hypothesis: regulation of post-synaptic Ca^{2+} concentration by KARs is responsible for the S857 dephosphorylation.

Similar to AMPARs, KARs can also be found throughout the CNS (Huettner, 2003), including hippocampal circuits. There are five types of KAR subunits, GluR5-7 and KA1-2 (Hollmann and Heinemann, 1994), which can be arranged in different combinations to form tetramers. All those subunits share a weak sequence homology with subunits of AMPAR and NMDAR. In hippocampal slices, both pre-synaptic and post-synaptic actions of KARs were shown in the CA1, CA3 or interneurons (Chittajallu et al., 1996; Castillo et al., 1997; Clarke et

al., 1997; Frerking et al., 1998). So far, only pre-synaptic actions of KARs were found in the Schaffer collaterals-CA1 pathway (Chittajallu et al., 1996). The neurotransmitter release modulated by pre-synaptic KARs could affect the Ca^{2+} influx in the post-synaptic neurons and indirectly mediate the dephosphorylation of Dyn1xa at S857.

S857 phosphorylation and learning and memory:

In summary, this study confirms the existence of S857 phosphorylation in synapses and its regulation by synaptic plasticity. Studies *in vitro* have shown that S857 phosphorylation regulates the interactions of Dyn1xa with several endocytic accessory proteins (Chen-Hwang et al., 2002; Huang et al., 2004). The regulation of the pS857 levels could control the recruitment of Dyn1 into endocytic complexes (McClure and Robinson, 1996). Therefore, further determination of these complexes and their components in synapses will shed light on the mechanism of Dyn1 function in learning and memory.

The phosphorylation of Dyn1xa at S857 in synapses is a dynamic process resulting from the balancing of Mnb/Dyrk1A-mediated phosphorylation and calcineurin-mediated dephosphorylation. Mnb/Dyrk1A is known to be one of the candidates for the neurobiological impairments in Down syndrome (Chen and Antonarakis, 1997). Calcineurin may be also involved in DS indirectly via interaction with the Down syndrome critical region 1 (DSCR1), a calcineurin

inhibitor (Harris et al., 2005). Interestingly, the increase in Mnb/Dyrk1A and DSCR1 expression produces development impairments in mice similar to DS (Arron et al., 2006; Gwack et al., 2006). In those studies, Mnb/Dyrk1A was shown to work together with calcineurin in regulating the nuclear factor of activated T-cells (NFAT) pathway (Arron et al., 2006; Gwack et al., 2006), which is required for vertebrate development and organogenesis (Graef et al., 2001). Therefore, similar to the NFAT pathway in development, the S857 phosphorylation of Dyn1xa could also be regulated together by Mnb/Dyrk1A and calcineurin, which subsequently controls synaptic plasticity. Further studies in transgenic mice mimicking the genetic background of DS will help to determine the function of Dyn1xa S857 phosphorylation in learning and memory.

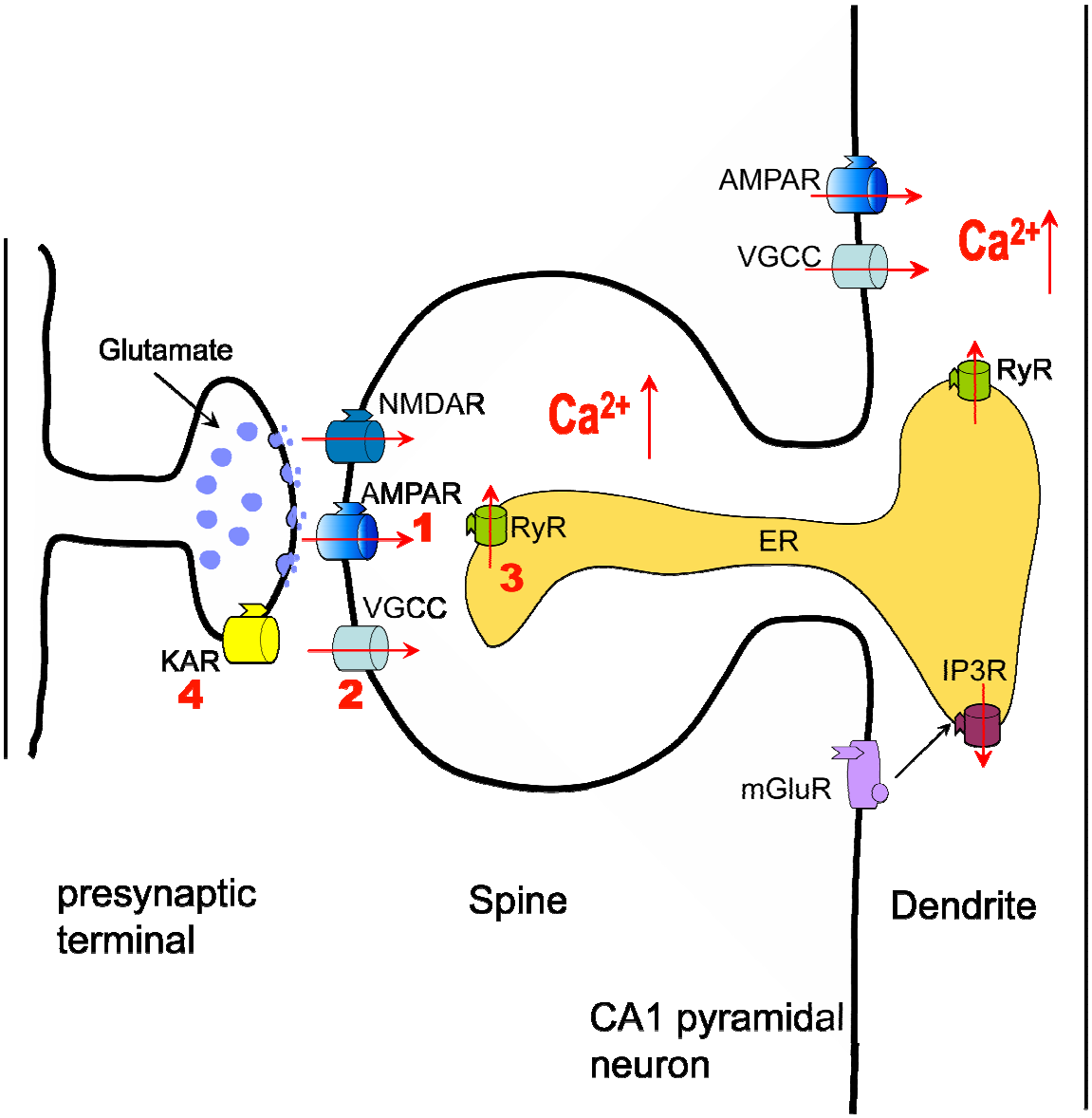

Figure 4 Model of calcium flux during LTP. Intracellular calcium increase (shown in red arrows), activating calcineurin and de-phosphorylating S857 Dyn1xa, might come from different sources. **1**. AMPAR hypothesis: calcium influx through Ca^{2+} permeable AMPAR; **2**. VGCC hypothesis: calcium influx from VGCC activated by depolarization through AMPAR; **3**. CRIS hypothesis: calcium release from intracellular storage; **4**. KAR hypothesis: calcium influx regulated by

pre-synaptic glutamate release. KAR, kainate recepto; NMDAR, N-methyl-D-aspartate receptor; AMPAR, alpha-amino-3-hydroxy-5-methyl-4-isoxazolepropionic acid receptor; VGCC, Voltage-Gated Calcium Channel; RyR, ryanodine receptor; ER, Endoplasmatic reticulum; mGluR, metabotropic glutamate receptor; IP3R, inositol 1,4,5-trisphosphate (IP_3)-gated receptor.

CHAPTER 5

Supplemental study

To correlate Mnb/Dyrk1A function with the learning and memory deficits in DS, I also evaluated the neuronal plasticity of a DS mouse model in the presence of a potential inhibitor to Mnb/Dyrk1A.

Introduction

Ts65Dn mouse

DS is caused by the presence of all or part of an extra chromosome 21 (Lejeune et al., 1959; Petersen et al., 1990). Since 80 % of HSA21 and mouse chromosome 16 (MMU 16) were syntenic (Hattori et al., 2000), several mouse models mimicking DS with various length of partial trisomic MMU 16 have been created (**Figure 5.1**) (Antonarakis et al., 2004). One widely studied model is the Ts65Dn mouse (Reeves et al., 1995). The extra MMU16 region encompasses about 130 genes (Baxter et al., 2000; Akeson et al., 2001) and includes the Mnb/Dyrk1A gene (Galdzicki and Siarey, 2003).

The Ts65Dn mouse survives into adulthood and displays multiple phenotypic abnormalities that are similar to DS. Specific skeletal malformations corresponding directly to the craniofacial dysmorphogenesis in DS (Richtsmeier et al., 2000) are presen. Other phenotypic abnormalities in the Ts65Dn mouse include reduced birth weight, postnatal developmental delay, muscular trembling and male sterility (Reeves et al., 1995; Baxter et al., 2000; Richtsmeier et al., 2000). Ts65Dn mice can perform simple learning tasks as shown in DS patients in spite of their low IQ (Caycho et al., 1991). However, Ts65Dn mice are impaired in the Morris water, radial arm mazes and passive avoidance tests. This is consistent with the fact that DS patients have difficulties with more complex cognitive tasks, particularly when spatial cues need to be used (Seregaza et al., 2006). Deficits in learning and memory spatial tasks suggest a dysfunction in the hippocampus (Escorihuela et al., 1998).

Hippocampal impairment has been further demonstrated using electrophysiological measurements. Hippocampal LTP is reduced while LTD is elevated in the Ts65Dn mice (Siarey et al., 1997; Siarey et al., 1999; Kleschevnikov et al., 2004; Costa and Grybko, 2005). Kleschevnikov et al. show that the enhanced GABA (Gamma-aminobutyric acid) -ergic inhibitory circuitry in the dentate gyrus may contribute to the abnormal synaptic transmission (Kleschevnikov et al., 2004). This hypothesis has been strengthened by the finding that both the altered synaptic plasticity and behavior deficits in Ts65Dn mice can be reversed by the administration of a GABA antagonist (Kleschevnikov

et al., 2004; Costa and Grybko, 2005). In addition, many signal transduction pathways that have shown to be involved in synaptic plasticity are also altered in the Ts65Dn hippocampus (Siarey et al., 2006). Therefore, the Ts65Dn mouse is one of the best models for investigating neuronal circuitry and behavior patterns that can underlie the more complex neurological and cognitive dysfunction found in DS individuals.

EGCG

(-)-Epigallocatechin-3-Gallate (EGCG) (**Figure 5.2**), the most abundant polyphenolic compound in tea (Yang et al., 2002), has been suggested to efficiently inhibit the activity of Mnb/Dyrk1A (Adayev et al., 2006), although it can also inhibit many other kinases (Bain et al., 2003). Its anti-oxidative and anti-inflammatory properties have been implicated in preventing cancer and cardiovascular disease (Lin et al., 1999; Yang et al., 2002; Higdon and Frei, 2003; Mandel et al., 2004; Mandel et al., 2005). Behavioral studies on both aged wild-type mice and a mouse model with an accelerated brain senescence have shown that long-term consumption of EGCG exhibits various neuroprotective effects (Mandel et al., 2004; Mandel et al., 2005) and, most interestingly, improves cognitive learning (Haque et al., 2006; Kuriyama et al., 2006). Especially, the enhanced spatial memory and delayed memory regression can be directly attributed EGCG enhancement of hippocampus-dependent learning and memory.

Despite its potential neuro-pharmacological benefits, the mechanisms of EGCG are still unknown. Many factors and signal transduction pathways that play the essential roles in gene expression, cell growth and apoptosis have been suggested as the targets of EGCG (Lin et al., 1999; Yang et al., 2002; Mandel et al., 2004).

Signal transduction pathways

To study the mechanism of learning and memory, hippocampal slices was used as a model to study neuronal plasticity. Several signaling pathways are involved in the induction and expression of synaptic plasticity. The mitogen-activated protein kinase (MAPKs) cascade plays a key role in cellular responses to external stimuli. The core of this signal cascade consists of three evolutionarily conserved and sequentially activated protein kinases. The activation of MAPK requires phosphorylation on conserved tyrosine and threonine residues by a dual-specificity MAPK kinase (MAPKK), and the MAPKK itself is in turn activated by phosphorylation on conserved serine and threonine residues by an upstream MAPKK kinase (MAPKKK). One of the best characterized MAPK cascades, the extracellular signal-regulated kinase (ERK) pathway consisting of Raf (MAPKKK) – MEK (MAPKK) – ERK (MAPK), was originally associated with cell growth and differentiation (Chang and Karin, 2001).

The MAPK pathway has now emerged as one of the most important signal pathways for regulating synaptic plasticity (Thomas and Huganir, 2004). In general, the stimulation of NMDAR triggers ERK activation (English and Sweatt, 1996) and ERK inhibitors have shown to impair not only synaptic plasticity but also memory and learning (Selcher et al., 1999; Selcher et al., 2003). A functional ERK pathway has been found in both presynaptic and postsynaptic neurons.

Active ERK is present in dendrites, indicating that the ERK cascade controls phosphorylation of targets close to synapses (Thomas and Huganir, 2004). In addition, serotonin induced long-term facilitation in Aplysia requires the activation of MAPK in presynaptic neurons (Hu et al., 2004).

The process leading to ERK activation requires dynamin-dependent endocytosis, as a dominant-negative dynamin mutant (harboring the K44A mutation) was shown to disrupt ERK activation promoted by numerous receptors such as the nerve growth factor (NGF) receptor and many G-protein coupled receptors (GPCRs) (McPherson et al., 2001). The dynamin-dependent step appears to be localized between MEK and ERK (Kranenburg et al., 1999). Recently, Mnb/Dyrk1A was shown to function as a negative regulator modulating the flow of signals from receptor to ERK and, intriguingly, the site of Mnb/Dyrk1A action was apparently localized between MEK and ERK (Adayev, T., et al, manuscript in preparation).

Besides the ERK pathway, calcium/calmodulin-dependent kinase II (CaMKII) is another key component that regulates LTP (Lisman et al., 2002). CaMKII is found in high concentrations in the postsynaptic density (Kennedy, 1997). Inhibitors of CaMKII or genetic deletion of a critical CaMKII subunit block the induction of LTP. Additionally, synaptic transmission is enhanced and LTP is occluded by increasing the concentrations of active CaMKII. These experiments showed that CaMKII plays a direct and causal role in LTP (Malenka and Nicoll,

1999). An important property of CaMKII is its autophosphorylation, which occurs on threonine 286. This autophosphorylation occurred after the triggering of LTP and replacing endogenous CaMKII with a form of CaMKII containing a point mutation at threonine 286 blocked LTP (Giese et al., 1998). The discovery of other CaMKII substrates, such as the AMPA receptor, NMDA receptor and K+ channel, also indicate the involvement of CaMKII in LTP (Malenka and Nicoll, 1999).

Objective of the study

Neuronal plasticity in hippocampal slices, such as LTP, is a widely used model to study memory and learning. To investigate a possible connection between Mnb/Dyrk1A and memory deficits in DS, I used the synapses between Schaffer collateral/commissural axons and CA1 pyramidal neurons to examine the effect of EGCG on LTP induction in both wild-type and Ts65Dn mouse. Two signal transduction pathways that I previously described as affecting LTP expression, as well as the inhibitory circuits were also investigated to explore the potential mechanisms of the effect.

Materials and Methods

Animals.

One- to four-month-old CD-1 and one to six-month-old Ts65Dn strains of mice and their littermates were used. The Ts65Dn mice were identified by PCR as previously described (Ramakrishna et al., 2005). For experiments involving Ts65Dn mice, a pair of age-matched animals (one Ts65Dn mouse and is normal littermate 2N) was always evaluated on the same day. All protocols for animal care and use were approved by the Animal Welfare Committees of the College of Staten Island, the City University of New York, and the New York State Institute for Basic Research in Developmental Disabilities. NIH guidelines were followed for all protocols.

Electrophysiological recordings.

Hippocampal slices were prepared and recorded as described in **Chapter 2** with the following modifications. The same LFS/HFS was applied to each slice except that the potentials after HFS application were followed for 30 min instead of 10 min. Paired-pulse inhibition (PPI) was induced by paired stimuli delivered in rapid succession (delay ranged from 6 to 12 msec) with the frequency of 0.03 Hz (Kleschevnikov et al., 2004). The amplitudes of both population spikes (PS1 and PS2) were recorded continuously from each slice starting from 10 min before and

80+ min after EGCG administration. The magnitude of PPI was expressed as the ratio between the amplitude of the population spikes recorded in response to the second (PS2) and the first (PS1) stimulus, respectively.

EGCG treatment.

EGCG was purchased from Sigma (cat. No. E4143) and used without further purification. EGCG was prepared as 10 mM stock solution in sodium acetate buffer (1 mM, pH 4.5) and stored at –20 ^{o}C. EGCG was diluted fresh in Ring's solution from stock solution on the day of use. Half of the prepared slices were randomly selected, transferred into a separate but adjacent holder containing EGCG/Ringer's solution, and incubated for 1 h before starting electrophysiological recordings. For EGCG-treated slices, the recording was performed in Ringer's solution supplemented with the same concentration of EGCG.

EGCG stability analysis.

Samples of EGCG / Ringer's solution (10 μM) were collected at 0, 10, 30, and 60 min. EGCG was first purified from 4 ml EGCG / Ringer's solution by passing it three times through a C18 Sep-Pak cartridge. Bound EGCG was eluted with 90% acetonitrile (with 1 mM sodium acetate, pH 4.5). This procedure consistently yielded acout 80% of the original input. After drying in a

speed-vacuum, the EGCG was dissolved in sodium acetate buffer (1 mM, pH 4.5) and was analyzed by reverse-phase HPLC similarly as described (Bronner and Beecher, 1998). The HPLC system consisted of a Hewlett-Packard AminoQuant system attached to a Varian 5 μm C18 Microsorb-MV column (4.6 mm X 25 cm). The chromatography was performed at ambient temperature with a 10-min 0.5 ml / min 5-40 % linear acetonitrile gradient (in 1 mM sodium acetate, pH 4.5) and was monitored continuously at wavelengths 200-450 nm by a diode array detector. The amount of sample analyzed in each chromatography was equivalent to 1.25 ml original EGCG/Ringer's solution. The area of EGCG elution peak obtained at a wavelength of 210 nm was used for relative amount calculation.

Slices extract preparation and immunoblotting.

Extracts from hippocampal slices were prepared as described (**Chapter 2**). Anti-p-CaMKIIa (Thr286) (Santa Cruz Biotech, cat. no.sc-12886) and anti-CaMKII (M-176) (Santa Cruz Biotech, cat. no. sc-9035) antibodies were used for detecting phospho- and total CaMKII, respectively. Phospho-ERK was detected by anti-phospho-ERK (T202/Y204) antibody (Cell Signaling Technlogy, cat. no. 9106), while anti-ERK2 antibody (Santa Cruz Biotech, cat. no. sc-154) was used to detect total ERK. The quantification of immunoblots was performed as described (**Chapter 2**).

Statistics.

For all experiments, data are presented as Mean ± SEM. n represented the number of slices. In the comparisons between two groups with equal n number, the student's t test was used. In all other comparisons, one-way ANOVA followed by a *post-hoc* multiple comparisons Student-Newman-Keuls test was used. When p value was less than 0.05, it was considered significant.

Results

EGCG enhances LTP induction in CD-1 mice.

The magnitude of LTP recorded from CD-1 mice was 130.5 ± 8.1% after HFS (n = 6 from 3 animals, $p < 0.01$ vs. pre-HFS) (**Figure 5.3 A and B**). The magnitude of LTP was greatly enhanced in the slices incubated with 10 μM EGCG for 60 min prior to the electrophysiological recordings (171.8 ± 25.0 %, n=6 from 3 animals, $p < 0.01$ vs. untreated slice, n = 6 from 3 animals). Over 75 % of all slices treated with 10 μM EGCG displayed a significant LTP enhancement. The effect of EGCG in LTP elevation required the combination of EGCG and HFS, as EGCG alone produced no measurable differences in recording potentials. In addition to the population spikes, the effect of EGCG on LTP was also evaluated as a change in excitatory postsynaptic potentials (EPSPs). LTP expressed either as the amplitude of the population spike, or the amplitudeof EPSP, was enhanced in a similar way. Interestingly, EGCG at a concentration of 5 μM had no effect on LTP induction, while EGCG applied at higher concentrations (20 and 40 μM) eliminated the ability of the slice to express LTP following HFS (**Figure 5.3 A**). None of the concentrations used (5, 10, 20, and 40 μM) had any effect on the population spikes evoked by low-frequency stimulation (0.03 Hz).

Effects of EGCG on LTP induction in Ts65Dn mice.

The analysis of the effects of EGCG was then extended to hippocampal slices prepared from the Ts65Dn mice. Breeding Ts65Dn mice inevitably produces diploid and partial chromosome 16 trisomic progeny on the same genetic background. These animals will be referred to as 2N and Ts65Dn, respectively.

Hippocampal slices prepared from 2N animals expressed LTP (123.7 ± 10.0%, n = 5 from 3 animals, $p < 0.05$ vs. pre-HFS) (**Figure 5.4 A and B**) upon HFS, while the same stimulation failed to evoke LTP in slices prepared from Ts65Dn mice (102.4 ± 10.2%, n = 6 from 3 animals, $p > 0.5$ vs. pre-HFS) (**Figure 5.5 A and B**). As observed in the slices prepared from CD-1 mice, EGCG (10 μM) enhanced the amplitude of LTP in 2N mice (**Figure 5.4 A and B**) (147.8 ± 11.2%, n = 5 from 3 animals, $p < 0.05$ vs. untreated slices, n = 5 from 3 animals). Similar to CD-1 slices, over 70 % of 2N slices treated with 10 μM EGCG displayed LTP enhancement.

The most striking effect of EGCG was observed on slices obtained from the Ts65Dn mice. While the slices from these animals normally do not express LTP, incubation with 10 μM EGCG resulted in the expression of LTP following HFS (**Figure 5.5 A and B**) (172.3 ± 28.9%, n = 6 from 3 animals, $p < 0.05$ vs. untreated slices, n = 6 from 3 animals). In fact, the level of LTP in the 2N and

Ts65Dn slices was indistinguishable following exposure to 10 μM EGCG. As in CD-1 slices, over 70 % of Ts65Dn slices treated with 10 μM EGCG expressed LTP.

The stability of EGCG during electrophysiological recording.

As an anti-oxidant reagent, EGCG is fairly unstable. The stability of EGCG is strongly influenced by light, pH, temperature, and oxygen (Sang et al., 2005). EGCG is more stable in a low pH, cool and less oxygenated environment. Since hippocampal slices were maintained at 33 ^{o}C and pH 7.4 with constant oxygenation, it was necessary to determine the stability of EGCG in such an environment. EGCG was found to have a half-life less of 10 min in oxygenated Ringer's solution. Thus, at the end of one hr of incubation, only a small fraction of the original EGCG remains (**Figure 5.6**).

Effects of EGCG on LTP-induced ERK1/2 and CaMKII phosphorylation.

To investigate the mechanism of EGCG's effect on LTP induction, ERK and CaMKII, two major signal transduction pathways involved in synaptic plasticity, were examined.

ERK1/2 phosphorylation at threonine-202 (T202) and tyrosine-204 (Y204) was measured as the indicator of ERK1/2 activation. Phosphorylation at

T202/Y204, which is prerequisite for ERK1/2 activation, has been correlated with LTP (Thomas and Huganir, 2004). I observed that LTP induction was accompanied by more than 2-fold increase in pT202/pY204 ERK1/2 (pERK1/2) in CD-1 hippocampal slices (2.34 ± 0.34, n = 6 from 4 animals, $p < 0.01$ vs. untreated slices without HFS) (**Figure 5.7 A and B**). However, EGCG treatment caused a reduction rather than an enhancement (**Figure 5.7 B**) in ERK phosphorylation (1.50 ± 0.33, n = 6 from 4 animals, $p < 0.05$ vs. untreated slices, n = 6 from 4 animals) even though the treatment raised the level of LTP expression (**Figure 5.3 A**). In Ts65Dn mice, HFS produced no significant elevation in ERK phosphorylation (1.47 ± 0.18, n = 5 from 2 animals; $p > 0.05$ vs. untreated slices without HFS). The level of ERK phosphorylation was essentially not changed by EGCG treatment (1.46 ± 0.31; n = 4 from 2 animals, $p > 0.5$ vs. untreated slices, n = 5 from 2 animals) (**Figure 5.7 B**).

Threonine-286 (T286) phosphorylation was used to monitor CaMKII activation as the phosphorylation at this site, an event induced by LTP, could render CaMKII independent of Ca^{2+}/calmodulin for activity (Lisman et al., 2002). A nearly 2-fold increase in pT286 CaMKII (pCaMKII) was observed in CD-1 hippocampal slices that expressed LTP (1.82 ± 0.22, n = 6 from 3 animals, $p < 0.05$ vs. untreated slices without HFS) (**Figure 5.8 A and B**). However, pre-incubating slices with 10 μM EGCG had little effect on the level of basal as well as LTP-induced pCaMKII (1.85 ± 0.51, n = 6 from 3 animals, $p > 0.5$ vs. untreated slices, n = 6 from 3 animals) (**Figure 5.8 B**). In addition, HFS, which did

not induce LTP in slices prepared from Ts65Dn mice, produced no significant change in the level of pCaMKII (1.41 ± 0.41, n = 4 from 2 animals; $p > 0.1$ vs. untreated slices without HFS) (**Figure 5.8 B**). EGCG treatment, which promotes LTP in Ts65Dn slices (**Figure 5.5 A**), caused a reduction in the level of pCaMKII upon exposure to HFS (0.32 ± 0.05, n = 4 from 2 animals, $p < 0.05$ vs. untreated slices, n = 4 from 2 animals) (**Figure 5.8 B**).

EGCG does not alter paired-pulse inhibition.

Activation of the pyramidal neurons could trigger inhibitory neurons, attenuating the response of pyramidal neurons to succeeding stimuli. This feedback inhibitory circuit is largely mediated by the hippocampal GABAergic system (Rock and Taylor, 1986; Kapur et al., 1989). In fact, the LTP deficit in Ts65Dn mice has been attributed to overactive GABAergic activity (Kleschevnikov et al., 2004; Costa and Grybko, 2005). Therefore, I examined whether the enhanced LTP by EGCG was mediated by suppressing the feedback inhibition circuit by measuring the effect of EGCG on PPI. Pairs of stimuli with an interstimulus interval ranging from 6-12 milliseconds were administrated to the Schaffer collateral, and the ratio of the response to the second stimulus over the response to the first stimulus was calculated as PPI. The results show that EGCG had no effect on the level of PPI regardless of whether the slices were prepared from CD-1 mice or Ts65Dn mice (**Figure 5.9**).

Discussion

The most striking finding in this study is that EGCG not only enhances LTP in normal mice but also induces expression of LTP in Ts65Dn mouse, which normally do not express LTP. Furthermore, the EGCG-induced enhancement of neuronal plasticity in normal and mutant mice did not correlate with the activation of two signaling pathways which are considered crucial for LTP expression nor did it equate with the modification of GABA-mediated synaptic inhibition.

The effects of EGCG on neuronal plasticity were tested by the standard paradigm of synaptic transmission involving the Schaffer collateral-CA1 of mouse hippocampus. EGCG at certain concentration (10 μM) was found to function as a positive modulator for LTP induction (**Figure 5.3-5**) in different mouse strains (CD1 and 2N). Most interestingly, Ts65Dn mouse which is deficit in LTP induction can express LTP as well as the 2N littermates following EGCG treatment. The fact that EGCG enhanced LTP expressed as both the amplitude of the population spike and the amplitude of EPSP suggests that it strengthens both synaptic transmission and the excitability of pyramidal neurons (Hogan et al., 2001). However, as LTP was followed for up to 30 min after HFS, it is still unclear how EGCG affects late phase of LTP.

The hippocampal slices obtained from Ts65Dn mice did not express LTP following application of HFS under my experimental conditions. This observation

is consistent with the findings of many others (Siarey et al., 1997; Kleschevnikov et al., 2004). Costa and Grybko, on the other hand, demonstrated that LTP could be induced in Ts65Dn mice by one train of 1-sec 100Hz HFS but not by Theta Burst Stimulation (Costa and Grybko, 2005). The difference in the HFS paradigm employed (three trains vs. one train 100 Hz pulse) for the LTP induction might explain the inconsistencies.

Although EGCG has a very short half-life in oxygenated Ringer's solution, slices with several hrs EGCG incubation in such environment still display the effect on LTP induction. Several mechanisms, either alone or in combination, may account for this observation. It is possible that EGCG effect is rapid and not easily reversible. This property would sustain the effect long after EGCG in the solution has been removed. On the other hand, the oxidation of EGCG doesn't necessarily mean the loss of function. If the primary EGCG oxidation products have the similar function as EGCG on LTP, a reduction in the amount of EGCG in Ringer's solution would not change the outcome. Furthermore, it is possible that the concentration required for triggering the effects is much lower than the administrated concentration. This would allow EGCG to achieve an effective concentration in hippocampal slices even though it is promptly degraded in oxygenated solution.

EGCG can promote LTP magnitude regardless of genetic backgrounds (**Figure 5.3-5**). This suggests that EGCG may influence common pathway(s)

leading to LTP induction. This is consistent with the findings that some LTP modulators are directly or indirectly affected by EGCG (Sweatt, 1999). Although both ERK and CaMKII were activated during LTP induction (**Figure 5.7-8**), there was no positive effect of EGCG on either pathway in this study. Therefore, it is unlikely that the LTP–promoting effect of EGCG involves these signal pathways directly. However, LTP is a complex phenomenon involving numerous other signal transduction pathways, such as cAMP-dependent protein kinase (PKA), phosphatidylinositol 3-kinase (PI3K), protein kinase M zeta, etc (Malenka and Bear, 2004). Many of these pathways are known to be affected by EGCG (Lin et al., 1999; Yang et al., 2002; Mandel et al., 2004). Therefore, it was no surprise that an EGCG "over-dose" (as with 20 μM EGCG and higher) inhibited LTP response. Some of these pathways affected by EGCG are also altered in the hippocampus of the Ts65Dn mouse (Siarey et al., 2006). This suggests some rational starting points to search for EGCG targets on LTP enhancement.

It should be emphasized that although EGCG appears to similarly affect both 2N and Ts65Dn mice, it may utilize different mechanisms for promoting LTP in 2N and Ts65Dn mice. Because the lack of LTP expression could be suppressed by the administration of the GABA receptor antagonist, picrotoxin, this LTP deficiency in Ts65Dn mice has been attributed to the overactive GABAergic system (Kleschevnikov et al., 2004; Costa and Grybko, 2005). EGCG incubation does not alter the level of PPI in CD-1 or Ts65Dn mice (**Figure 5.9**).

This result indicates that the LTP–promoting effect of EGCG is probably not mediated through restraining the inhibitory circuit of the GABAergic system.

This study, combining electrophysiological techniques with molecular biology approach, represents a first attempt to investigate further EGCG's benefits on the cognitive and memory enhancement. The rescue of LTP deficit in Ts65Dn mouse by EGCG, a potential Mnb/Dyrk1A inhibitor (Adayev et al., 2006) further connect Mnb/Dyrk1A to the DS, although the detailed mechanism(s) still need to be discovered. Further investigations whose aim is to identify these EGCG targets will not only broaden our understanding of the molecular mechanisms underlying LTP induction, but also provide more information about mental retardation in DS. More importantly, the results in this study, together with the finding with GABA antagonist (Kleschevnikov et al., 2004; Costa and Grybko, 2005; Fernandez et al., 2007), demonstrate that the LTP impairment and behavioral deficits in Ts65Dn mouse can be pharmacologically manipulated.

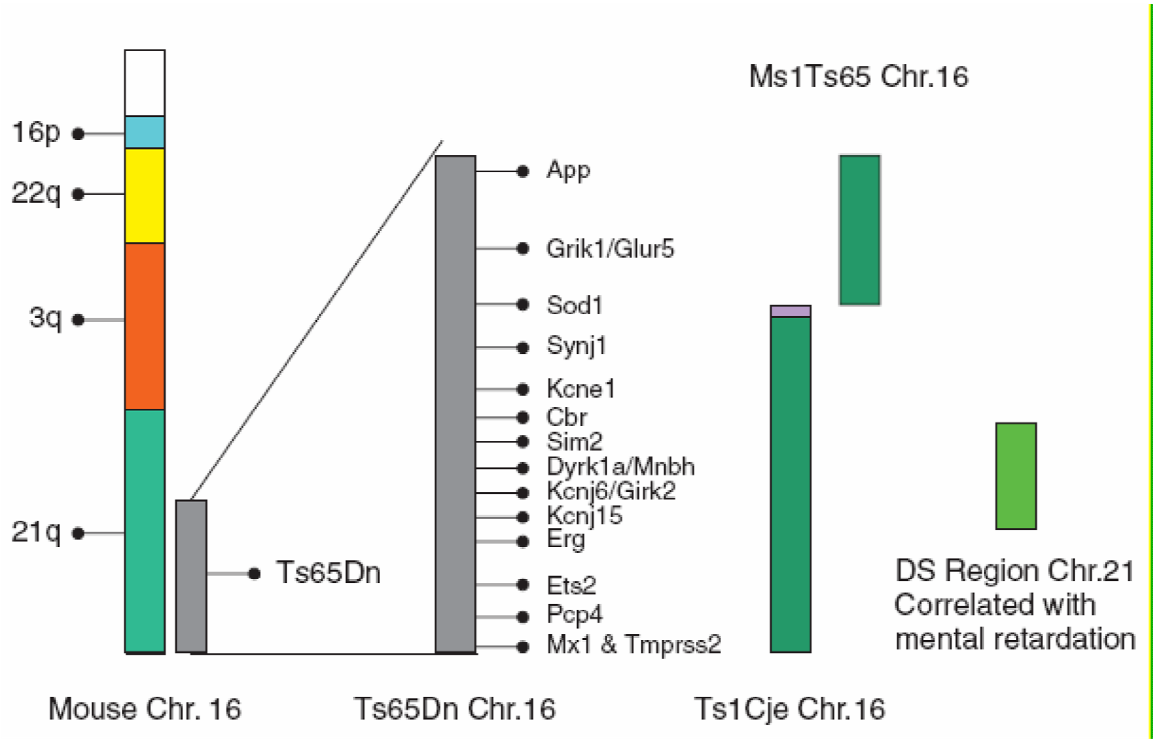

Figure 5.1 Schematic representation of mouse chromosome 16 fragments in some of the DS mouse models (Galdzicki and Siarey, 2003). Locations of chromosome fragments in several DS mouse model are shown. Various regions of MMU16 are syntenic to fragments of several human chromosomes (numbers on the left). Selected genes in the extra chromosome present of the Ts65Dn mouse genome corresponding to HSA21 homologous are shown. App, amyloid precursor protein; Girk1, glutamate receptor subunit 5; Sod1, superoxide dismutase-1; Cbr, carbonyl reductase; Sim2-single-minded 2; Kcnj6, potassium inwardly rectifying channel subfamily J member 6; Ets2, E26 avian leukemia oncogene 2, 30 domain; Pcp4, Purkinje cell protein 4; Mx1, myxovirus resistance-1, Tmprss2, transmembrane protease, serine 2.

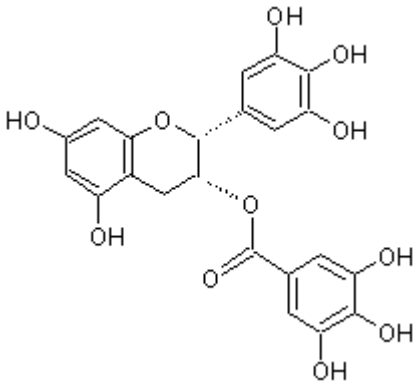

Figure 5.2 Chemical structure of EGCG.

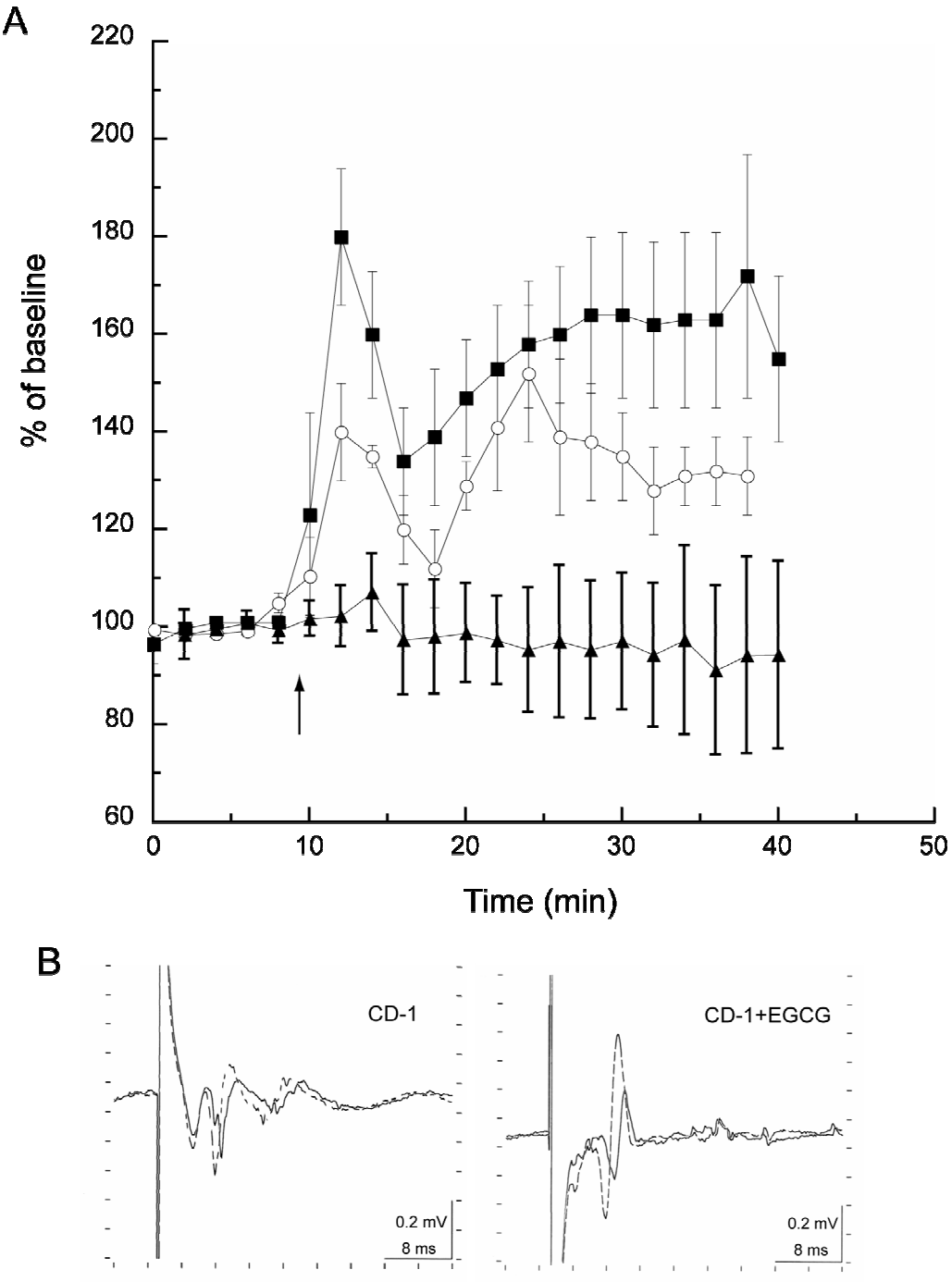

Figure 5.3 EGCG enhances LTP induction in CD-1 mice. A. *The amplitude of LTP*. A 10-min baseline (stimulated with 0.03–Hz pulse) recording was followed by the HFS (marked by an arrow) and the recording was continued for an

additional 30 min. Each point was the average of 2-min recording. The change in potentiation was plotted as the percentage of baseline (set as 100%) for the entire 40-min duration. The data represent the average (± SEM) of the total number of slices (n = 6 from 3 animals). (○), untreated group; (■), 10 μM EGCG-treated group; (▲), 20 μM EGCG-treated group. A significant difference was found between untreated and 10 μM EGCG-treated samples 30 min after the administration of HFS ($p < 0.01$). **B**. *Representative recordings*: potentials were recorded before (solid) and 30 min after (dash) HFS for CD-1 (left panel) and CD-1+EGCG (10 μM) (right panel) slices.

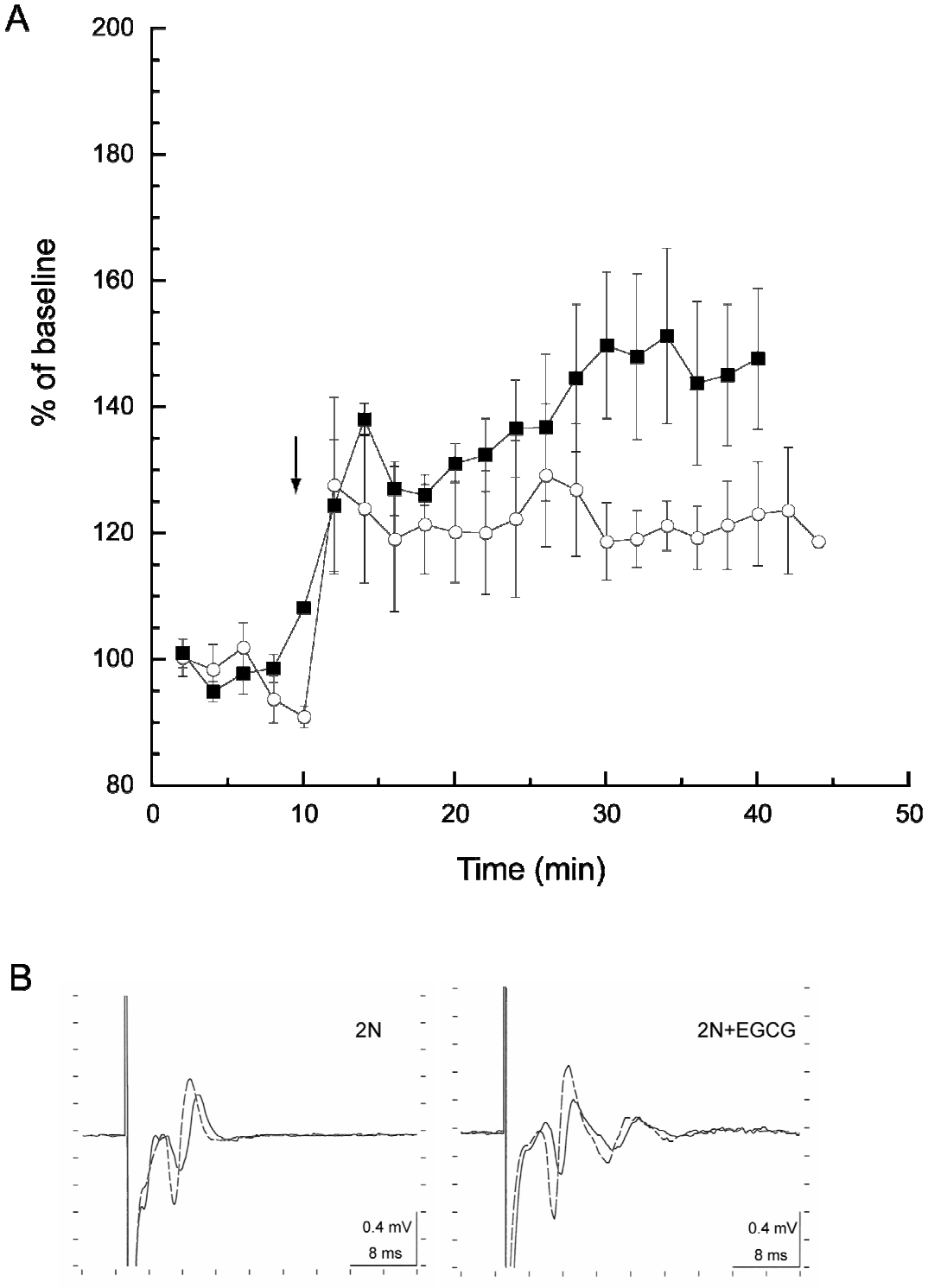

Figure 5.4 EGCG enhances LTP induction in 2N littermates of Ts65Dn mouse. **A**. *The amplitude of LTP*. The experiments were performed and recorded

similarly as described in **Figure 5.3**. The data represent the average (± SEM) of the total number of slices (n = 5 from 3 animals). (○), untreated group, and (■), 10 μM EGCG-treated group. A significant difference was found between control and EGCG-treated samples 30 min after the administration of HFS ($p < 0.05$). **B**. *Representative recordings*: potentials were recorded before (solid) and 30 min after (dash) HFS for 2N (left panel) and 2N+EGCG (10 μM) (right panel) slices.

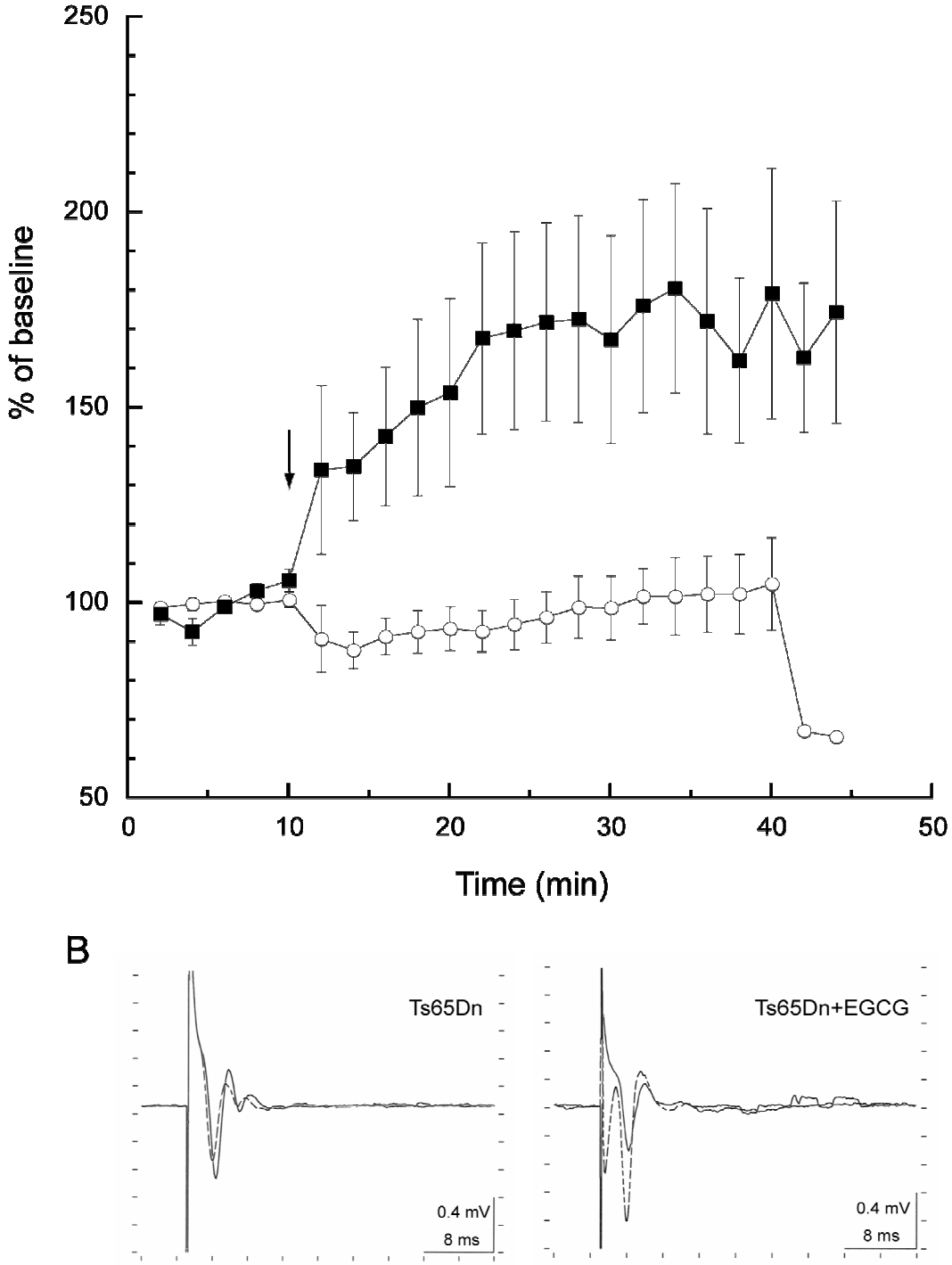

Figure 5.5 EGCG promotes LTP induction in Ts65Dn mice. **A**. *The amplitude of LTP*. The experiment was performed and recorded similarly as described in

Figure 5.3. The data represent the average (± SEM) of the total number of slices (n = 6 from 3 animals). (○), untreated group, and (■), 10 μM EGCG-treated group. A significant difference was found between control and EGCG-treated samples 30 min after the administration of HFS ($p < 0.001$). **B**. *Representative recordings*: potentials were recorded before (solid) and 30 min after (dash) HFS for Ts65Dn (left panel) and Ts65Dn+EGCG (10 μM) (right panel) slices.

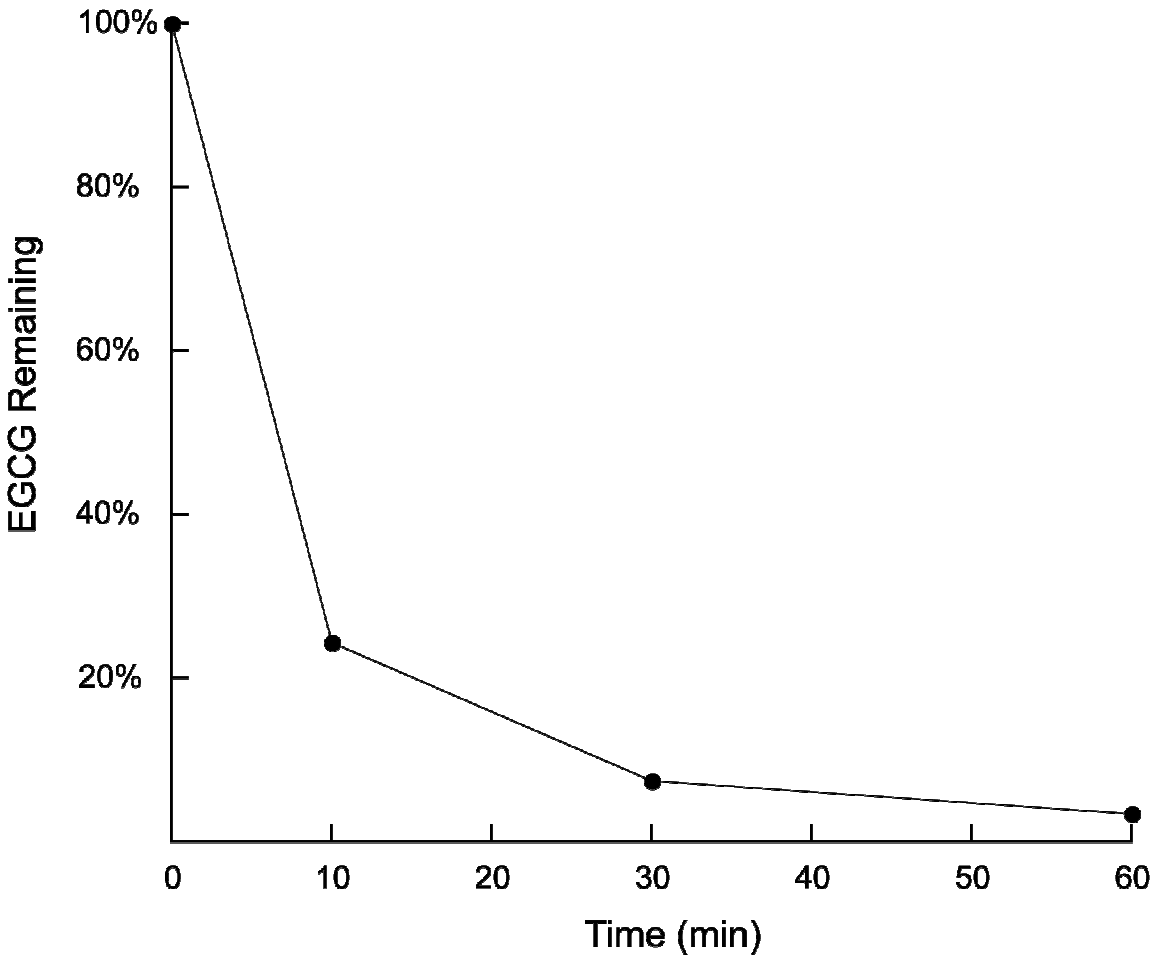

Figure 5.6 The stability of EGCG in Ringer's solution. 10 μM EGCG in Ringer's solution was incubated in the slice preparation chamber at 33 ^{o}C with constant oxygenation. EGCG in Ringer's solution was concentrated at different times (10, 30, 60 min) and analyzed by reverse-phase HPLC as described. The area of the EGCG elution peak was used as the amount in each sample. The relative amount of EGCG at each time point (●) was calculated as the percentage of the total amount of EGCG without incubation (sample at 0 min). Each point was the average of two independent trials. The results show a more than 80% reduction of EGCG with 10 min incubation.

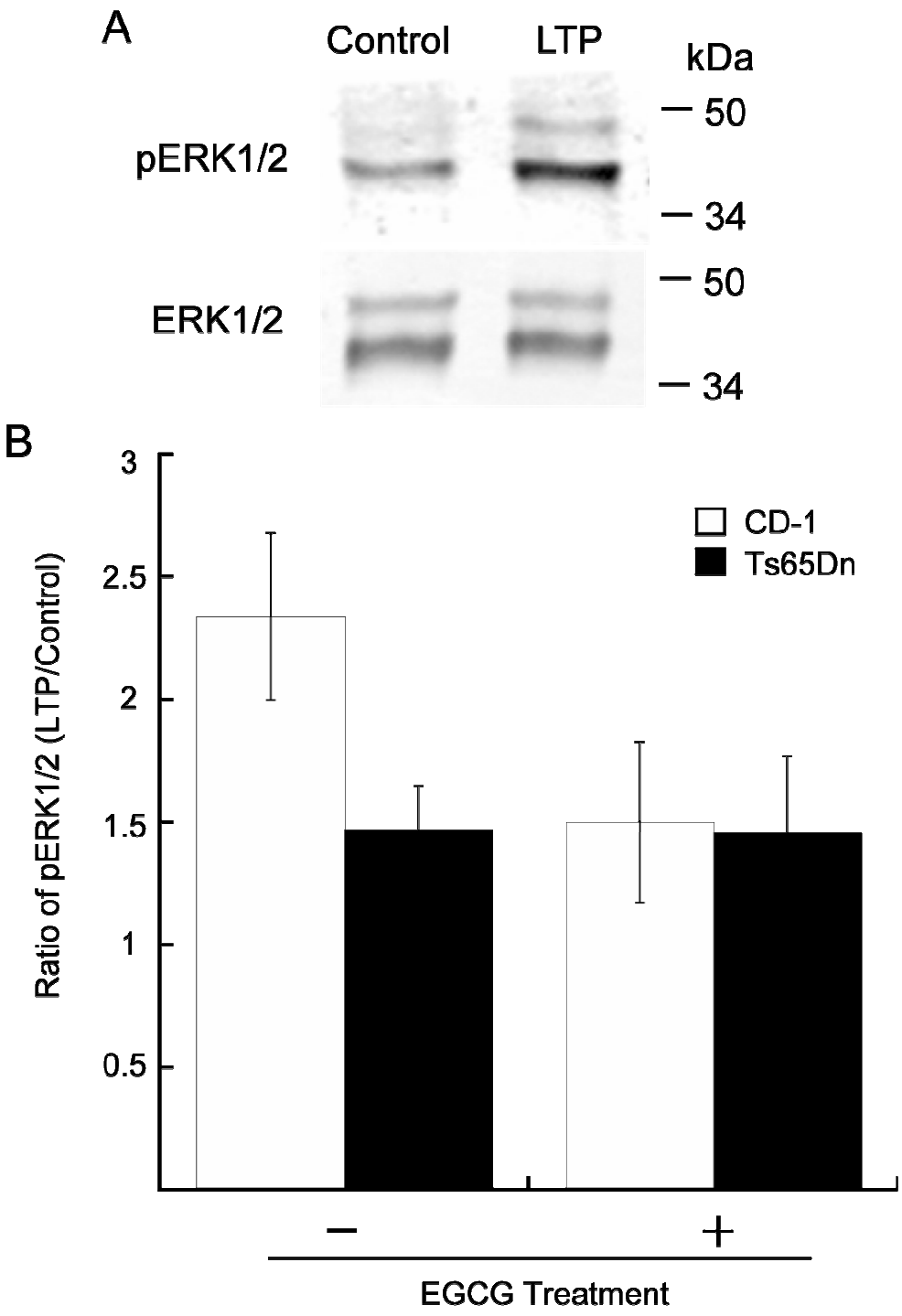

Figure 5.7 Effect of EGCG on LTP-induced ERK1/2 phosphorylation. **A**. *Determination of total and pT202/pY204 ERK1/2 (pERK1/2).* Hippocampal slices were stimulated and recorded for 30 min post–HFS to ensure LTP expression.

The slices were prepared and analyzed for pERK1/2 (upper panel) and total ERK (low panel) by immunoblotting as described. Representative blots obtained with the control (nonstimulated slices) and LTP-induced slices from the (EGCG) untreated CD-1 mouse group are shown. **B**. *LTP-induced changes in pERK of CD-1 and Ts65Dn hippocampal slices*. The ratio of pERK1/2 was calculated by dividing the level of pERK1/2 in the LTP-induced sample by that of the control sample and then corrected for the total amount of ERK1/2 used in the assay. For EGCG treatment, the slices were incubated with 10 μM EGCG for 60 min before experimenting. The data represent the average (± SEM) of the total number of slices (n). (–), untreated; (+), EGCG-treated; open bar, CD-1 (n = 6 from 3 animals); solid bar, Ts65Dn (n = 5 from 2 animals). A significant difference was found between the untreated and the EGCG-treated groups ($p < 0.05$) of CD-1 mice but no significant difference was found between untreated and EGCG-treated groups ($p > 0.5$) of Ts65Dn mice.

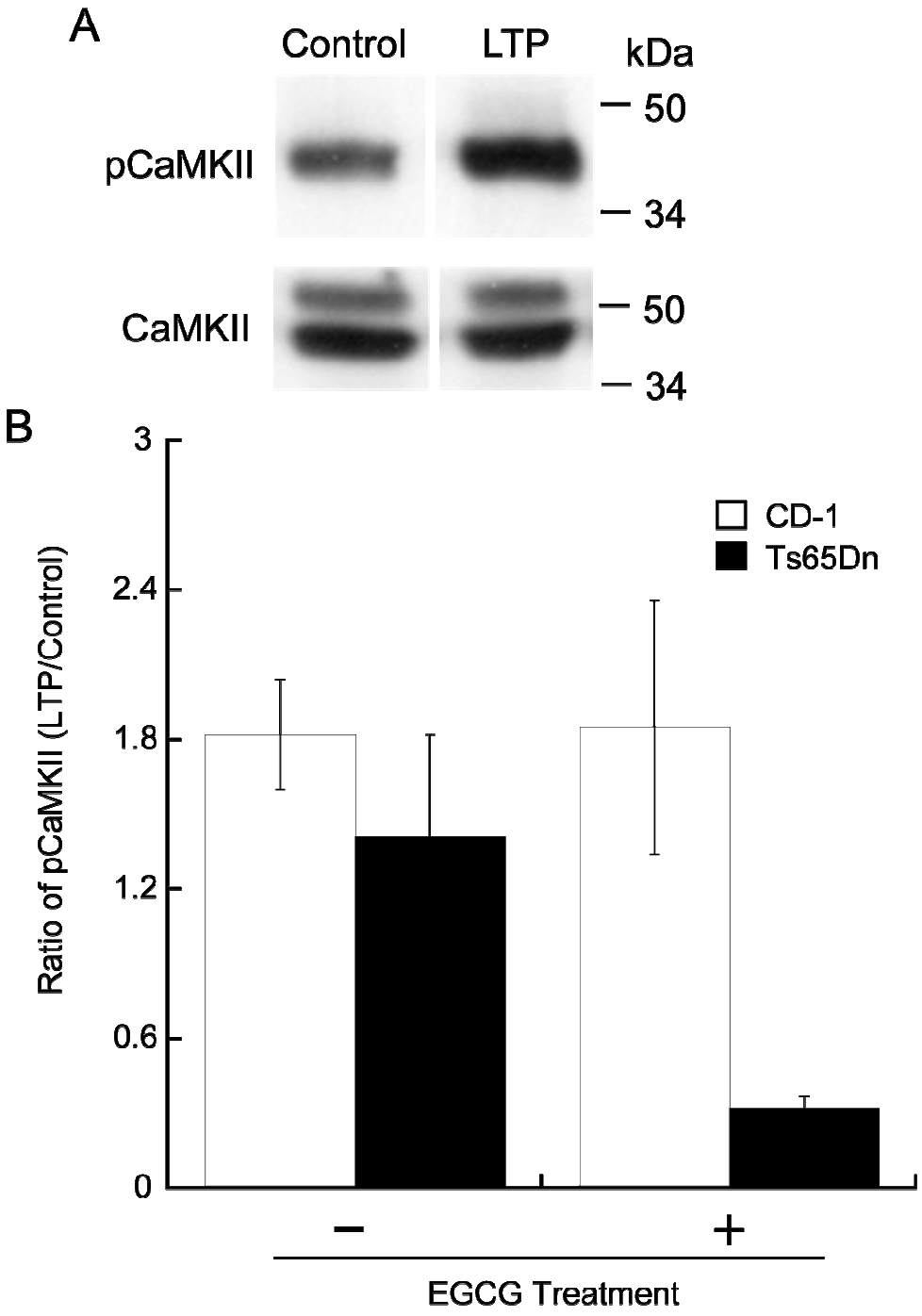

Figure 5.8 Effect of EGCG on LTP-induced CaMKII phosphorylation. **A**. *Determination of total and pT286 CaMKII (pCaMKII)*. Hippocampal slices were stimulated and recorded for 30 min post–HFS to ensure LTP expression. The

slices were processed and analyzed for pCaMKII (upper panel) and total CaMKII (low panel) by immunoblotting as described in **Figure 5.7**. Representative blots obtained with the control (nonstimulated slices) and LTP-induced slices from the (EGCG) untreated CD-1 mouse group are shown. **B**. *LTP-induced changes in pCaMKII of CD-1 and Ts65Dn hippocampal slices*. The ratio of pCaMKII was calculated by dividing the level of pCaMKII in LTP-induced sample by that of the control sample and then corrected for the total amount of CaMKII used in the assay. For EGCG treatment, the slices were incubated with 10 μM EGCG 60 min before experimenting. The data represent the average (± SEM) of the total number of slices (n). (–), untreated; (+), EGCG-treated; open bar, CD-1 (n = 6 from 3 animals); solid bar, Ts65Dn (n = 4 from 2 animals). No significant difference was found between the untreated and the EGCG-treated groups ($p > 0.5$) of CD-1 mice but a significant difference was found between untreated and EGCG-treated groups ($p < 0.05$) of Ts65Dn mice.

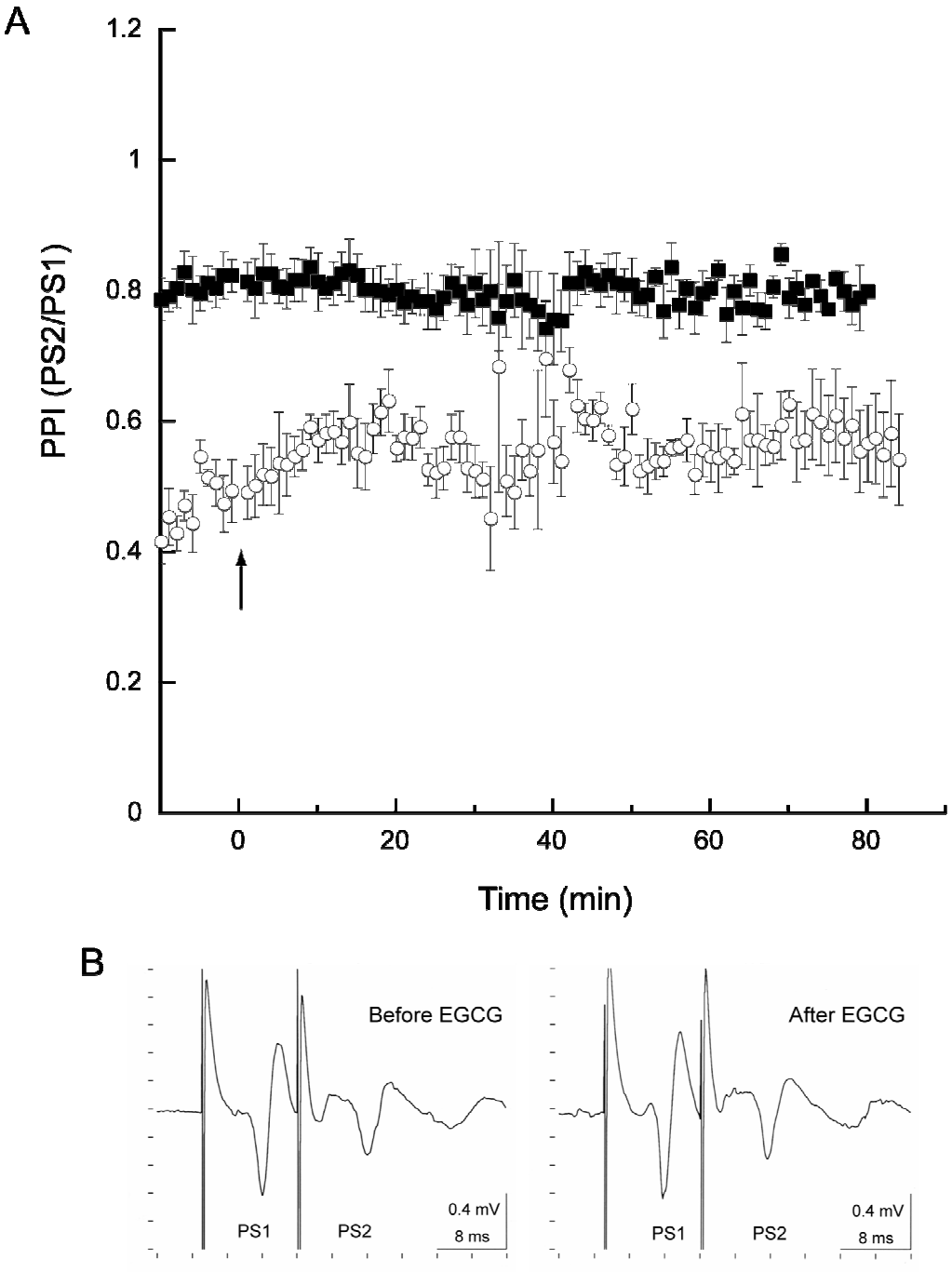

Figure 5.9 The effect of EGCG on PPI. A. *PPI recording*. PPI was measured as described, by recording continuously from the same slice first for 10 min without EGCG and then for 80+ min following EGCG application. The point of EGCG

addition (marked by an arrow) was set as time 0. The data represent the average (± SEM) of the total number of slices (n). (■), CD-1 slices (n = 4 from 4 animals); (○), Ts65Dn slices (n = 4 from 1 animals). **B**. *Representative potential from a Ts65Dn slice*. The synaptic response to a single paired-stimulus with an inter-stimulus interval of 11 millseconds was recorded. The response at approximately 5 min before (left panel) the addition of 10 μM EGCG and 70 min after (right panel) the addition of 10 μM EGCG are shown.

BIBLIOGRAPHY

Adayev T, Chen-Hwang MC, Murakami N, Wegiel J, Hwang YW (2006) Kinetic property of a MNB/DYRK1A mutant suitable for the elucidation of biochemical pathways. Biochemistry 45:12011-12019.

Ahn KJ, Jeong HK, Choi HS, Ryoo SR, Kim YJ, Goo JS, Choi SY, Han JS, Ha I, Song WJ (2006) DYRK1A BAC transgenic mice show altered synaptic plasticity with learning and memory defects. Neurobiol Dis.

Akeson EC, Lambert JP, Narayanswami S, Gardiner K, Bechtel LJ, Davisson MT (2001) Ts65Dn -- localization of the translocation breakpoint and trisomic gene content in a mouse model for Down syndrome. Cytogenet Cell Genet 93:270-276.

Alford S, Frenguelli BG, Schofield JG, Collingridge GL (1993) Characterization of Ca2+ signals induced in hippocampal CA1 neurones by the synaptic activation of NMDA receptors. J Physiol 469:693-716.

Alkon DL, Nelson TJ (1990) Specificity of molecular changes in neurons involved in memory storage. Faseb J 4:1567-1576.

Andrasfalvy BK, Magee JC (2004) Changes in AMPA receptor currents following LTP induction on rat CA1 pyramidal neurones. J Physiol 559:543-554.

Anggono V, Robinson PJ (2007) Syndapin I and endophilin I bind overlapping proline-rich regions of dynamin I: role in synaptic vesicle endocytosis. J Neurochem 102:931-943.

Anggono V, Smillie KJ, Graham ME, Valova VA, Cousin MA, Robinson PJ (2006) Syndapin I is the phosphorylation-regulated dynamin I partner in synaptic vesicle endocytosis. Nat Neurosci 9:752-760.

Antonarakis SE, Lyle R, Dermitzakis ET, Reymond A, Deutsch S (2004) Chromosome 21 and down syndrome: from genomics to pathophysiology. Nat Rev Genet 5:725-738.

Aravanis AM, Pyle JL, Tsien RW (2003) Single synaptic vesicles fusing transiently and successively without loss of identity. Nature 423:643-647.

Arron JR, Winslow MM, Polleri A, Chang CP, Wu H, Gao X, Neilson JR, Chen L, Heit JJ, Kim SK, Yamasaki N, Miyakawa T, Francke U, Graef IA, Crabtree GR (2006) NFAT dysregulation by increased dosage of DSCR1 and DYRK1A on chromosome 21. Nature 441:595-600.

Atwood HL, Karunanithi S (2002) Diversification of synaptic strength: presynaptic elements. Nat Rev Neurosci 3:497-516.

Bain J, McLauchlan H, Elliott M, Cohen P (2003) The specificities of protein kinase inhibitors: an update. Biochem J 371:199-204.

Banerjee P, Berry-Kravis E, Bonafede-Chhabra D, Dawson G (1993) Heterologous expression of the serotonin 5-HT1A receptor in neural and non-neural cell lines. Biochem Biophys Res Commun 192:104-110.

Baxter LL, Moran TH, Richtsmeier JT, Troncoso J, Reeves RH (2000) Discovery and genetic localization of Down syndrome cerebellar phenotypes using the Ts65Dn mouse. Hum Mol Genet 9:195-202.

Becker W, Joost HG (1999) Structural and functional characteristics of Dyrk, a novel subfamily of protein kinases with dual specificity. Prog Nucleic Acid Res Mol Biol 62:1-17.

Bekkers JM, Stevens CF (1990) Presynaptic mechanism for long-term potentiation in the hippocampus. Nature 346:724-729.

Benke TA, Luthi A, Isaac JT, Collingridge GL (1998) Modulation of AMPA receptor unitary conductance by synaptic activity. Nature 393:793-797.

Bliss TV, Lomo T (1973) Long-lasting potentiation of synaptic transmission in the dentate area of the anaesthetized rabbit following stimulation of the perforant path. J Physiol 232:331-356.

Bliss TV, Collingridge GL (1993) A synaptic model of memory: long-term potentiation in the hippocampus. Nature 361:31-39.

Bradford MM (1976) A rapid and sensitive method for the quantitation of microgram quantities of protein utilizing the principle of protein-dye binding. Anal Biochem 72:248-254.

Branchi I, Bichler Z, Minghetti L, Delabar JM, Malchiodi-Albedi F, Gonzalez MC, Chettouh Z, Nicolini A, Chabert C, Smith DJ, Rubin EM, Migliore-Samour D, Alleva E (2004) Transgenic mouse in vivo library of human Down syndrome critical region 1: association between DYRK1A overexpression, brain development abnormalities, and cell cycle protein alteration. J Neuropathol Exp Neurol 63:429-440.

Bredt DS, Nicoll RA (2003) AMPA receptor trafficking at excitatory synapses. Neuron 40:361-379.

Brodin L, Low P, Shupliakov O (2000) Sequential steps in clathrin-mediated synaptic vesicle endocytosis. Curr Opin Neurobiol 10:312-320.

Bronner WE, Beecher GR (1998) Method for determining the content of catechins in tea infusions by high-performance liquid chromatography. J Chromatogr A 805:137-142.

Cao H, Garcia F, McNiven MA (1998) Differential Distribution of Dynamin Isoforms in Mammalian Cells. Mol Biol Cell 9:2595-2609.

Carroll RC, Beattie EC, Xia H, Luscher C, Altschuler Y, Nicoll RA, Malenka RC, von Zastrow M (1999) Dynamin-dependent endocytosis of ionotropic glutamate receptors. Proc Natl Acad Sci U S A 96:14112-14117.

Castillo PE, Malenka RC, Nicoll RA (1997) Kainate receptors mediate a slow postsynaptic current in hippocampal CA3 neurons. Nature 388:182-186.

Caycho L, Gunn P, Siegal M (1991) Counting by children with Down syndrome. Am J Ment Retard 95:575-583.

Chang L, Karin M (2001) Mammalian MAP kinase signalling cascades. Nature 410:37-40.

Chen-Hwang MC, Chen HR, Elzinga M, Hwang YW (2002) Dynamin is a minibrain kinase/dual specificity Yak1-related kinase 1A substrate. J Biol Chem 277:17597-17604.

Chen H, Antonarakis SE (1997) Localisation of a human homologue of the Drosophila mnb and rat Dyrk genes to chromosome 21q22.2. Hum Genet 99:262-265.

Chittajallu R, Vignes M, Dev KK, Barnes JM, Collingridge GL, Henley JM (1996) Regulation of glutamate release by presynaptic kainate receptors in the hippocampus. Nature 379:78-81.

Clarke VR, Ballyk BA, Hoo KH, Mandelzys A, Pellizzari A, Bath CP, Thomas J, Sharpe EF, Davies CH, Ornstein PL, Schoepp DD, Kamboj RK, Collingridge GL, Lodge D, Bleakman D (1997) A hippocampal GluR5 kainate receptor regulating inhibitory synaptic transmission. Nature 389:599-603.

Collingridge GL, Isaac JT, Wang YT (2004) Receptor trafficking and synaptic plasticity. Nat Rev Neurosci 5:952-962.

Conner SD, Schmid SL (2003) Regulated portals of entry into the cell. Nature 422:37-44.

Costa AC, Grybko MJ (2005) Deficits in hippocampal CA1 LTP induced by TBS but not HFS in the Ts65Dn mouse: a model of Down syndrome. Neurosci Lett 382:317-322.

Cousin MA, Robinson PJ (2001) The dephosphins: dephosphorylation by calcineurin triggers synaptic vesicle endocytosis. Trends Neurosci 24:659-665.

Cousin MA, Tan TC, Robinson PJ (2001) Protein phosphorylation is required for endocytosis in nerve terminals: potential role for the dephosphins dynamin I and synaptojanin, but not AP180 or amphiphysin. J Neurochem 76:105-116.

de Graaf K, Czajkowska H, Rottmann S, Packman LC, Lilischkis R, Luscher B, Becker W (2006) The protein kinase DYRK1A phosphorylates the splicing factor SF3b1/SAP155 at Thr434, a novel in vivo phosphorylation site. BMC Biochem 7:7.

Dingledine R, Borges K, Bowie D, Traynelis SF (1999) The glutamate receptor ion channels. Pharmacol Rev 51:7-61.

Dolphin AC (2006) A short history of voltage-gated calcium channels. Br J Pharmacol 147 Suppl 1:S56-62.

Douglas RM (1977) Long lasting synaptic potentiation in the rat dentate gyrus following brief high frequency stimulation. Brain Res 126:361-365.

Dowjat WK, Adayev T, Kuchna I, Nowicki K, Palminiello S, Hwang YW, Wegiel J (2007) Trisomy-driven overexpression of DYRK1A kinase in the brain of subjects with Down syndrome. Neurosci Lett 413:77-81.

Earnest S, Khokhlatchev A, Albanesi JP, Barylko B (1996) Phosphorylation of dynamin by ERK2 inhibits the dynamin-microtubule interaction. FEBS Lett 396:62-66.

El-Sherif Y, Tesoriero J, Hogan MV, Wieraszko A (2003) Melatonin regulates neuronal plasticity in the hippocampus. J Neurosci Res 72:454-460.

English JD, Sweatt JD (1996) Activation of p42 mitogen-activated protein kinase in hippocampal long term potentiation. J Biol Chem 271:24329-24332.

Epstein CJ (1986) The consequences of chromosome imbalance:principles, mechanisms, and models. New York: Cambridge University Press.

Epstein CJ, Korenberg JR, Anneren G, Antonarakis SE, Ayme S, Courchesne E, Epstein LB, Fowler A, Groner Y, Huret JL, et al. (1991) Protocols to establish genotype-phenotype correlations in Down syndrome. Am J Hum Genet 49:207-235.

Escorihuela RM, Vallina IF, Martinez-Cue C, Baamonde C, Dierssen M, Tobena A, Florez J, Fernandez-Teruel A (1998) Impaired short- and long-term memory in Ts65Dn mice, a model for Down syndrome. Neurosci Lett 247:171-174.

Fernandez F, Morishita W, Zuniga E, Nguyen J, Blank M, Malenka RC, Garner CC (2007) Pharmacotherapy for cognitive impairment in a mouse model of Down syndrome. Nat Neurosci.

Fotaki V, Dierssen M, Alcantara S, Martinez S, Marti E, Casas C, Visa J, Soriano E, Estivill X, Arbones ML (2002) Dyrk1A haploinsufficiency affects viability and causes developmental delay and abnormal brain morphology in mice. Mol Cell Biol 22:6636-6647.

Frerking M, Malenka RC, Nicoll RA (1998) Synaptic activation of kainate receptors on hippocampal interneurons. Nat Neurosci 1:479-486.

Galceran J, de Graaf K, Tejedor FJ, Becker W (2003) The MNB/DYRK1A protein kinase: genetic and biochemical properties. J Neural Transm Suppl:139-148.

Galdzicki Z, Siarey RJ (2003) Understanding mental retardation in Down's syndrome using trisomy 16 mouse models. Genes Brain Behav 2:167-178.

Gandhi SP, Stevens CF (2003) Three modes of synaptic vesicular recycling revealed by single-vesicle imaging. Nature 423:607-613.

Geiger JR, Melcher T, Koh DS, Sakmann B, Seeburg PH, Jonas P, Monyer H (1995) Relative abundance of subunit mRNAs determines gating and Ca2+ permeability of AMPA receptors in principal neurons and interneurons in rat CNS. Neuron 15:193-204.

Giese KP, Fedorov NB, Filipkowski RK, Silva AJ (1998) Autophosphorylation at Thr286 of the alpha calcium-calmodulin kinase II in LTP and learning. Science 279:870-873.

Grabs D, Slepnev VI, Songyang Z, David C, Lynch M, Cantley LC, De Camilli P (1997) The SH3 domain of amphiphysin binds the proline-rich domain of dynamin at a single site that defines a new SH3 binding consensus sequence. J Biol Chem 272:13419-13425.

Graef IA, Chen F, Crabtree GR (2001) NFAT signaling in vertebrate development. Curr Opin Genet Dev 11:505-512.

Grover LM, Teyler TJ (1990) Two components of long-term potentiation induced by different patterns of afferent activation. Nature 347:477-479.

Gwack Y, Sharma S, Nardone J, Tanasa B, Iuga A, Srikanth S, Okamura H, Bolton D, Feske S, Hogan PG, Rao A (2006) A genome-wide Drosophila RNAi

screen identifies DYRK-family kinases as regulators of NFAT. Nature 441:646-650.

Hammerle B, Carnicero A, Elizalde C, Ceron J, Martinez S, Tejedor FJ (2003) Expression patterns and subcellular localization of the Down syndrome candidate protein MNB/DYRK1A suggest a role in late neuronal differentiation. Eur J Neurosci 17:2277-2286.

Hämmerle B, Vera-Samper E, Speicher S, Arencibia R, Martínez S, Tejedor FJ (2002) Mnb/Dyrk1A is transiently expressed and asymmetrically segregated in neural progenitor cells at the transition to neurogenic divisions. Dev Biol 246:259-273.

Haque AM, Hashimoto M, Katakura M, Tanabe Y, Hara Y, Shido O (2006) Long-term administration of green tea catechins improves spatial cognition learning ability in rats. J Nutr 136:1043-1047.

Harris CD, Ermak G, Davies KJ (2005) Multiple roles of the DSCR1 (Adapt78 or RCAN1) gene and its protein product calcipressin 1 (or RCAN1) in disease. Cell Mol Life Sci 62:2477-2486.

Hattori M, Fujiyama A, Taylor TD, Watanabe H, Yada T, Park HS, Toyoda A, Ishii K, Totoki Y, Choi DK, Groner Y, Soeda E, Ohki M, Takagi T, Sakaki Y, Taudien S, Blechschmidt K, Polley A, Menzel U, Delabar J, Kumpf K, Lehmann R, Patterson D, Reichwald K, Rump A, Schillhabel M, Schudy A, Zimmermann W, Rosenthal A, Kudoh J, Schibuya K, Kawasaki K, Asakawa S, Shintani A, Sasaki T, Nagamine K, Mitsuyama S, Antonarakis SE, Minoshima S, Shimizu N, Nordsiek G, Hornischer K, Brant P, Scharfe M, Schon O, Desario A, Reichelt J, Kauer G, Blocker H, Ramser J, Beck A, Klages S, Hennig S, Riesselmann L, Dagand E, Haaf T, Wehrmeyer S, Borzym K, Gardiner K, Nizetic D, Francis F, Lehrach H, Reinhardt R, Yaspo ML (2000) The DNA sequence of human chromosome 21. Nature 405:311-319.

Hebb D (1949) The Organization of Behavior. New York: Wiley.

Higdon JV, Frei B (2003) Tea catechins and polyphenols: health effects, metabolism, and antioxidant functions. Crit Rev Food Sci Nutr 43:89-143.

Himpel S, Tegge W, Frank R, Leder S, Joost HG, Becker W (2000) Specificity determinants of substrate recognition by the protein kinase DYRK1A. J Biol Chem 275:2431-2438.

Hogan MV, El-Sherif Y, Wieraszko A (2001) The modulation of neuronal activity by melatonin: in vitro studies on mouse hippocampal slices. J Pineal Res 30:87-96.

Hollmann M, Heinemann S (1994) Cloned glutamate receptors. Annu Rev Neurosci 17:31-108.

Hu JY, Glickman L, Wu F, Schacher S (2004) Serotonin regulates the secretion and autocrine action of a neuropeptide to activate MAPK required for long-term facilitation in Aplysia. Neuron 43:373-385.

Huang C, Sindic A, Hill CE, Hujer KM, Chan KW, Sassen M, Wu Z, Kurachi Y, Nielsen S, Romero MF, Miller RT (2007) Interaction of the Ca2+-sensing receptor with the inwardly rectifying potassium channels Kir4.1 and Kir4.2 results in inhibition of channel function. Am J Physiol Renal Physiol 292:F1073-1081.

Huang Y, Chen-Hwang MC, Dolios G, Murakami N, Padovan JC, Wang R, Hwang YW (2004) Mnb/Dyrk1A phosphorylation regulates the interaction of dynamin 1 with SH3 domain-containing proteins. Biochemistry 43:10173-10185.

Huang YY, Malenka RC (1993) Examination of TEA-induced synaptic enhancement in area CA1 of the hippocampus: the role of voltage-dependent Ca2+ channels in the induction of LTP. J Neurosci 13:568-576.

Huber KM, Mauk MD, Kelly PT (1995) LTP induced by activation of voltage-dependent Ca2+ channels requires protein kinase activity. Neuroreport 6:1281-1284.

Huettner JE (2003) Kainate receptors and synaptic transmission. Prog Neurobiol 70:387-407.

incidence Ds (2006) http://www.nichd.nih.gov/publications/pubs/downsyndrome.cfm#TheOccurrence. In.

Isaac JT (2003) Postsynaptic silent synapses: evidence and mechanisms. Neuropharmacology 45:450-460.

Jonas P, Racca C, Sakmann B, Seeburg PH, Monyer H (1994) Differences in Ca2+ permeability of AMPA-type glutamate receptor channels in neocortical neurons caused by differential GluR-B subunit expression. Neuron 12:1281-1289.

Kandel ER (1997) Genes, synapses, and long-term memory. J Cell Physiol 173:124-125.

Kapur J, Stringer JL, Lothman EW (1989) Evidence that repetitive seizures in the hippocampus cause a lasting reduction of GABAergic inhibition. J Neurophysiol 61:417-426.

Kelly PA, Rahmani Z (2005) DYRK1A enhances the mitogen-activated protein kinase cascade in PC12 cells by forming a complex with Ras, B-Raf, and MEK1. Mol Biol Cell 16:3562-3573.

Kennedy MB (1997) The postsynaptic density at glutamatergic synapses. Trends Neurosci 20:264-268.

Kentrup H, Becker W, Heukelbach J, Wilmes A, Schürmann A, Huppertz C, Kainulainen H, Joost HG (1996) Dyrk, a dual specificity protein kinase with unique structural features whose activity is dependent on tyrosine residues between subdomains VII and VIII. J Biol Chem 271:3488-3495.

Kimura R, Kamino K, Yamamoto M, Nuripa A, Kida T, Kazui H, Hashimoto R, Tanaka T, Kudo T, Yamagata H, Tabara Y, Miki T, Akatsu H, Kosaka K, Funakoshi E, Nishitomi K, Sakaguchi G, Kato A, Hattori H, Uema T, Takeda M (2007) The DYRK1A gene, encoded in chromosome 21 Down syndrome critical region, bridges between beta-amyloid production and tau phosphorylation in Alzheimer disease. Hum Mol Genet 16:15-23.

Kleschevnikov AM, Belichenko PV, Villar AJ, Epstein CJ, Malenka RC, Mobley WC (2004) Hippocampal long-term potentiation suppressed by increased inhibition in the Ts65Dn mouse, a genetic model of Down syndrome. J Neurosci 24:8153-8160.

Kranenburg O, Verlaan I, Moolenaar WH (1999) Dynamin is required for the activation of mitogen-activated protein (MAP) kinase by MAP kinase kinase. J Biol Chem 274:35301-35304.

Kuriyama S, Hozawa A, Ohmori K, Shimazu T, Matsui T, Ebihara S, Awata S, Nagatomi R, Arai H, Tsuji I (2006) Green tea consumption and cognitive function: a cross-sectional study from the Tsurugaya Project 1. Am J Clin Nutr 83:355-361.

Kwak YD, Brannen CL, Qu T, Kim HM, Dong X, Soba P, Majumdar A, Kaplan A, Beyreuther K, Sugaya K (2006) Amyloid precursor protein regulates differentiation of human neural stem cells. Stem Cells Dev 15:381-389.

Lai MM, Hong JJ, Ruggiero AM, Burnett PE, Slepnev VI, De Camilli P, Snyder SH (1999) The calcineurin-dynamin 1 complex as a calcium sensor for synaptic vesicle endocytosis. J Biol Chem 274:25963-25966.

Lejeune J, Gautier M, Turpin R (1959) Etude des chromosomes somatiques de neuf enfants mongoliens. CR AcadSci(Paris) 248:1721-1722.

Lin JK, Liang YC, Lin-Shiau SY (1999) Cancer chemoprevention by tea polyphenols through mitotic signal transduction blockade. Biochem Pharmacol 58:911-915.

Lisman J, Schulman H, Cline H (2002) The molecular basis of CaMKII function in synaptic and behavioural memory. Nat Rev Neurosci 3:175-190.

Little Z, Grover LM, Teyler TJ (1995) Metabotropic glutamate receptor antagonist, (R,S)-alpha-methyl-4-carboxyphenyglycine, blocks two distinct forms of long-term potentiation in area CA1 of rat hippocampus. Neurosci Lett 201:73-76.

Lu YM, Mansuy IM, Kandel ER, Roder J (2000) Calcineurin-mediated LTD of GABAergic inhibition underlies the increased excitability of CA1 neurons associated with LTP. Neuron 26:197-205.

Mainen ZF, Malinow R, Svoboda K (1999) Synaptic calcium transients in single spines indicate that NMDA receptors are not saturated. Nature 399:151-155.

Malenka RC, Nicoll RA (1999) Long-term potentiation--a decade of progress? Science 285:1870-1874.

Malenka RC, Bear MF (2004) LTP and LTD: an embarrassment of riches. Neuron 44:5-21.

Malinow R, Malenka RC (2002) AMPA receptor trafficking and synaptic plasticity. Annu Rev Neurosci 25:103-126.

Mandel S, Weinreb O, Amit T, Youdim MB (2004) Cell signaling pathways in the neuroprotective actions of the green tea polyphenol (-)-epigallocatechin-3-gallate: implications for neurodegenerative diseases. J Neurochem 88:1555-1569.

Mandel SA, Avramovich-Tirosh Y, Reznichenko L, Zheng H, Weinreb O, Amit T, Youdim MB (2005) Multifunctional activities of green tea catechins in neuroprotection. Modulation of cell survival genes, iron-dependent oxidative stress and PKC signaling pathway. Neurosignals 14:46-60.

Marti E, Altafaj X, Dierssen M, de la Luna S, Fotaki V, Alvarez M, Perez-Riba M, Ferrer I, Estivill X (2003) Dyrk1A expression pattern supports specific roles of this kinase in the adult central nervous system. Brain Res 964:250-263.

Martinez de Lagran M, Altafaj X, Gallego X, Marti E, Estivill X, Sahun I, Fillat C, Dierssen M (2004) Motor phenotypic alterations in TgDyrk1a transgenic mice implicate DYRK1A in Down syndrome motor dysfunction. Neurobiol Dis 15:132-142.

McClure SJ, Robinson PJ (1996) Dynamin, endocytosis and intracellular signalling (review). Mol Membr Biol 13:189-215.

McPherson PS, Kay BK, Hussain NK (2001) Signaling on the endocytic pathway. Traffic 2:375-384.

Moga DE, Shapiro ML, Morrison JH (2006) Bidirectional redistribution of AMPA but not NMDA receptors after perforant path simulation in the adult rat hippocampus in vivo. Hippocampus 16:990-1003.

Morioka M, Nagahiro S, Fukunaga K, Miyamoto E, Ushio Y (1997) Calcineurin in the adult rat hippocampus: different distribution in CA1 and CA3 subfields. Neuroscience 78:673-684.

Morita K, Lo Celso C, Spencer-Dene B, Zouboulis CC, Watt FM (2006) HAN11 binds mDia1 and controls GLI1 transcriptional activity. J Dermatol Sci 44:11-20.

Murakami N, Xie W, Lu RC, Chen-Hwang MC, Wieraszko A, Hwang YW (2006) Phosphorylation of amphiphysin I by minibrain kinase/dual-specificity tyrosine phosphorylation-regulated kinase, a kinase implicated in Down syndrome. J Biol Chem 281:23712-23724.

Muzzolini A, Bregola G, Bianchi C, Beani L, Simonato M (1997) Characterization of glutamate and [3H]D-aspartate outflow from various in vitro preparations of the rat hippocampus. Neurochem Int 31:113-124.

Nakata T, Takemura R, Hirokawa N (1993) A novel member of the dynamin family of GTP-binding proteins is expressed specifically in the testis. J Cell Sci 105:1-5.

Nicholson DA, Trana R, Katz Y, Kath WL, Spruston N, Geinisman Y (2006) Distance-dependent differences in synapse number and AMPA receptor expression in hippocampal CA1 pyramidal neurons. Neuron 50:431-442.

Petersen MB, Tranebjaerg L, McCormick MK, Michelsen N, Mikkelsen M, Antonarakis SE (1990) Clinical, cytogenetic, and molecular genetic characterization of two unrelated patients with different duplications of 21q. Am J Med Genet Suppl 7:104-109.

Plant K, Pelkey KA, Bortolotto ZA, Morita D, Terashima A, McBain CJ, Collingridge GL, Isaac JT (2006) Transient incorporation of native GluR2-lacking AMPA receptors during hippocampal long-term potentiation. Nat Neurosci 9:602-604.

Powell KA, Valova VA, Malladi CS, Jensen ON, Larsen MR, Robinson PJ (2000) Phosphorylation of dynamin I on Ser-795 by protein kinase C blocks its association with phospholipids. J Biol Chem 275:11610-11617.

Praefcke GJ, McMahon HT (2004) The dynamin superfamily: universal membrane tubulation and fission molecules? Nat Rev Mol Cell Biol 5:133-147.

Rachidi M, Lopes C, Charron G, Delezoide AL, Paly E, Bloch B, Delabar JM (2005) Spatial and temporal localization during embryonic and fetal human development of the transcription factor SIM2 in brain regions altered in Down syndrome. Int J Dev Neurosci 23:475-484.

Raich WB, Moorman C, Lacefield CO, Lehrer J, Bartsch D, Plasterk RH, Kandel ER, Hobert O (2003) Characterization of Caenorhabditis elegans Homologs of the Down Syndrome Candidate Gene DYRK1A. Genetics 163:571-580.

Ramakrishna N, Meeker C, Li S, Jenkins EC, Currie JR, Flory M, Lee B, Liu MS, Miller DL (2005) Polymerase chain reaction method to identify Down syndrome model segmentally trisomic mice. Anal Biochem 340:213-219.

Reeves RH, Irving NG, Moran TH, Wohn A, Kitt C, Sisodia SS, Schmidt C, Bronson RT, Davisson MT (1995) A mouse model for Down syndrome exhibits learning and behaviour deficits. Nat Genet 11:177-184.

Regehr WG, Tank DW (1992) Calcium concentration dynamics produced by synaptic activation of CA1 hippocampal pyramidal cells. J Neurosci 12:4202-4223.

Richtsmeier JT, Baxter LL, Reeves RH (2000) Parallels of craniofacial maldevelopment in Down syndrome and Ts65Dn mice. Dev Dyn 217:137-145.

Robinson PJ, Hauptschein R, Lovenberg W, Dunkley PR (1987) Dephosphorylation of synaptosomal proteins P96 and P139 is regulated by both depolarization and calcium, but not by a rise in cytosolic calcium alone. J Neurochem 48:187-195.

Rock DM, Taylor CP (1986) Effects of diazepam, pentobarbital, phenytoin and pentylenetetrazol on hippocampal paired-pulse inhibition in vivo. Neurosci Lett 65:265-270.

Rose CR, Konnerth A (2001) Stores not just for storage. intracellular calcium release and synaptic plasticity. Neuron 31:519-522.

Ryan TA (2003) Kiss-and-run, fuse-pinch-and-linger, fuse-and-collapse: the life and times of a neurosecretory granule. Proc Natl Acad Sci U S A 100:2171-2173.

Ryan TA (2006) A pre-synaptic to-do list for coupling exocytosis to endocytosis. Curr Opin Cell Biol 18:416-421.

Sang S, Lee MJ, Hou Z, Ho CT, Yang CS (2005) Stability of tea polyphenol (-)-epigallocatechin-3-gallate and formation of dimers and epimers under common experimental conditions. J Agric Food Chem 53:9478-9484.

Schmid SL, McNiven MA, De Camilli P (1998) Dynamin and its partners: a progress report. Curr Opin Cell Biol 10:504-512.

Schupf N, Sergievsky GH (2002) Genetic and host factors for dementia in Down's syndrome. Br J Psychiatry 180:405-410.

Scoville WB, Milner B (1957) Loss of recent memory after bilateral hippocampal lesions. J Neurol Neurosurg Psychiatry 20:11-21.

Selcher JC, Atkins CM, Trzaskos JM, Paylor R, Sweatt JD (1999) A necessity for MAP kinase activation in mammalian spatial learning. Learn Mem 6:478-490.

Selcher JC, Weeber EJ, Christian J, Nekrasova T, Landreth GE, Sweatt JD (2003) A role for ERK MAP kinase in physiologic temporal integration in hippocampal area CA1. Learn Mem 10:26-39.

Seregaza Z, Roubertoux PL, Jamon M, Soumireu-Mourat B (2006) Mouse models of cognitive disorders in trisomy 21: a review. Behav Genet 36:387-404.

Sever S, Damke H, Schmid SL (2000) Garrotes, springs, ratchets, and whips: putting dynamin models to the test. Traffic 5:385-392.

Shapiro BL (1999) The Down syndrome critical region. J Neural Transm Suppl 57:41-60.

Sheng M, Kim MJ (2002) Postsynaptic signaling and plasticity mechanisms. Science 298:776-780.

Shi SH, Hayashi Y, Petralia RS, Zaman SH, Wenthold RJ, Svoboda K, Malinow R (1999) Rapid spine delivery and redistribution of AMPA receptors after synaptic NMDA receptor activation. Science 284:1811-1816.

Siarey RJ, Stoll J, Rapoport SI, Galdzicki Z (1997) Altered long-term potentiation in the young and old Ts65Dn mouse, a model for Down Syndrome. Neuropharmacology 36:1549-1554.

Siarey RJ, Carlson EJ, Epstein CJ, Balbo A, Rapoport SI, Galdzicki Z (1999) Increased synaptic depression in the Ts65Dn mouse, a model for mental retardation in Down syndrome. Neuropharmacology 38:1917-1920.

Siarey RJ, Kline-Burgess A, Cho M, Balbo A, Best TK, Harashima C, Klann E, Galdzicki Z (2006) Altered signaling pathways underlying abnormal hippocampal synaptic plasticity in the Ts65Dn mouse model of Down syndrome. J Neurochem 98:1266-1277.

Soderling TR, Derkach VA (2000) Postsynaptic protein phosphorylation and LTP. Trends Neurosci 23:75-80.

Song BD, Schmid SL (2003) A molecular motor or a regulator? Dynamin's in a class of its own. Biochemistry 42:1369-1376.

Song WJ, Sternberg LR, Kasten-Sportes C, Keuren ML, Chung SH, Slack AC, Miller DE, Glover TW, Chiang PW, Lou L, Kurnit DM (1996) Isolation of human and murine homologues of the Drosophila minibrain gene: human homologue maps to 21q22.2 in the Down syndrome "critical region". Genomics 38:331-339.

Sontag JM, Fykse EM, Ushkaryov Y, Liu JP, Robinson PJ, Südhof TC (1994) Differential expression and regulation of multiple dynamins. J Biol Chem 269:4547-4554.

Sudhof TC (1995) The synaptic vesicle cycle: a cascade of protein-protein interactions. Nature 375:645-653.

Svoboda K, Mainen ZF (1999) Synaptic [Ca2+]: intracellular stores spill their guts. Neuron 22:427-430.

Sweatt JD (1999) Toward a molecular explanation for long-term potentiation. Learn Mem 6:399-416.

Tan TC, Valova VA, Malladi CS, Graham ME, Berven LA, Jupp OJ, Hansra G, McClure SJ, Sarcevic B, Boadle RA, Larsen MR, Cousin MA, Robinson PJ (2003) Cdk5 is essential for synaptic vesicle endocytosis. Nat Cell Biol 5:701-710.

Tassone F, Lucas R, Slavov D, Kavsan V, Crnic L, Gardiner K (1999) Gene expression relevant to Down syndrome: problems and approaches. J Neural Transm Suppl 57:179-195.

Tejedor F, Zhu XR, Kaltenbach E, Ackermann A, Baumann A, Canal I, Heisenberg M, Fischbach KF, Pongs O (1995) minibrain: a new protein kinase family involved in postembryonic neurogenesis in Drosophila. Neuron 14:287-301.

Thiery E, Thomas S, Vacher S, Delezoide AL, Delabar JM, Creau N (2003) Chromosome 21 KIR channels in brain development. J Neural Transm Suppl:105-115.

Thomas GM, Huganir RL (2004) MAPK cascade signalling and synaptic plasticity. Nat Rev Neurosci 5:173-183.

Thomas JB, Crews ST, Goodman CS (1988) Molecular genetics of the single-minded locus: a gene involved in the development of the Drosophila nervous system. Cell 52:133-141.

Tomizawa K, Sunada S, Lu YF, Oda Y, Kinuta M, Ohshima T, Saito T, Wei FY, Matsushita M, Li ST, Tsutsui K, Hisanaga S, Mikoshiba K, Takei K, Matsui H (2003) Cophosphorylation of amphiphysin I and dynamin I by Cdk5 regulates clathrin-mediated endocytosis of synaptic vesicles. J Cell Biol 163:813-824.

van den Heuvel S, Harlow E (1993) Distinct roles for cyclin-dependent kinases in cell cycle control. Science 262:2050-2054.

Wegiel J, Kuchna I, Nowicki K, Frackowiak J, Dowjat K, Silverman WP, Reisberg B, DeLeon M, Wisniewski T, Adayev T, Chen-Hwang MC, Hwang YW (2004) Cell type- and brain structure-specific patterns of distribution of minibrain kinase in human brain. Brain Res 1010:69-80.

Wigge P, Kohler K, Vallis Y, Doyle CA, Owen D, Hunt SP, McMahon HT (1997) Amphiphysin heterodimers: potential role in clathrin-mediated endocytosis. Mol Biol Cell 8:2003-2015.

Winder DG, Sweatt JD (2001) Roles of serine/threonine phosphatases in hippocampal synaptic plasticity. Nat Rev Neurosci 2:461-474.

Yang CS, Maliakal P, Meng X (2002) Inhibition of carcinogenesis by tea. Annu Rev Pharmacol Toxicol 42:25-54.

Yang EJ, Ahn YS, Chung KC (2001) Protein kinase Dyrk1 activates cAMP response element-binding protein during neuronal differentiation in hippocampal progenitor cells. J Biol Chem 276:39812-39824.

Yoshida Y, Takei K (2005) Stimulation of dynamin GTPase activity by amphiphysin. Methods Enzymol 404:528-537.